Geometric Constraint Based Range Free Localization Scheme For Wireless Sensor Networks (WSNs)

Munesh Singh

Department of Computer Science and Engineering
National Institute of Technology Rourkela

Geometric Constraint Based Range Free Localization Scheme For Wireless Sensor Networks (WSNs)

Dissertation submitted in partial fulfillment

of the requirements of the degree of

Doctor of Philosophy

in

Computer Science and Engineering

by

Munesh Singh

(Roll Number: 512cs1017)

based on research carried out

under the supervision of

Prof. Pabitra Mohan Khilar

April, 2016

Department of Computer Science and Engineering

National Institute of Technology Rourkela

Department of Computer Science and Engineering
National Institute of Technology Rourkela

April 20, 2016

Certificate of Examination

Roll Number: *512cs1017*
Name: *Munesh Singh*
Title of Dissertation: *Geometric Constraint Based Range Free Localization Scheme For Wireless Sensor Networks (WSNs)*

We the below signed, after checking the dissertation mentioned above and the official record book (s) of the student, hereby state our approval of the dissertation submitted in partial fulfillment of the requirements of the degree of *Doctor of Philosophy* in *Computer Science and Engineering* at *National Institute of Technology Rourkela*. We are satisfied with the volume, quality, correctness, and originality of the work.

Pabitra Mohan Khilar
Principal Supervisor

Banshidhar Majhi
Member, DSC

Dayal Ramakrushna Parhi
Member, DSC

Santanu Kumar Behera
Member, DSC

External Examiner

Dugra Prasad Mohapatra
Chairperson, DSC

Dugra Prasad Mohapatra
Head of the Department

Department of Computer Science and Engineering
National Institute of Technology Rourkela

Prof. Pabitra Mohan Khilar
Assistant Professor

April 20, 2016

Supervisor's Certificate

This is to certify that the work presented in the dissertation entitled *Geometric Constraint Based Range Free Localization Scheme For Wireless Sensor Networks (WSNs)* submitted by *Munesh Singh*, Roll Number 512cs1017, is a record of original research carried out by him under my supervision and guidance in partial fulfillment of the requirements of the degree of *Doctor of Philosophy* in *Computer Science and Engineering*. Neither this dissertation nor any part of it has been submitted earlier for any degree or diploma to any institute or university in India or abroad.

_____
Pabitra Mohan Khilar

Dedication

I want to dedicate this thesis to my family with love.

Munesh Singh

Declaration of Originality

I, *Munesh Singh*, Roll Number *512cs1017* hereby declare that this dissertation entitled *Geometric Constraint Based Range Free Localization Scheme For Wireless Sensor Networks (WSNs)* presents my original work carried out as a doctoral student of NIT Rourkela and, to the best of my knowledge, contains no material previously published or written by another person, nor any material presented by me for the award of any degree or diploma of NIT Rourkela or any other institution. Any contribution made to this research by others, with whom I have worked at NIT Rourkela or elsewhere, is explicitly acknowledged in the dissertation. Works of other authors cited in this dissertation have been duly acknowledged under the sections ‘‘Reference’’ or ‘‘Bibliography’’. I have also submitted my original research records to the scrutiny committee for evaluation of my dissertation.

I am fully aware that in case of any non-compliance detected in future, the Senate of NIT Rourkela may withdraw the degree awarded to me on the basis of the present dissertation.

April 20, 2016
NIT Rourkela

Munesh Singh

Acknowledgment

''The will of God will never take you where Grace of God will not protect you." Thank you God for showing me the path…

I owe deep gratitude to the ones who have contributed greatly in completion of this thesis.

Foremost, I would like to express my sincere gratitude to my advisor, Prof. Pabitra Mohan Khilar for providing me with a platform to work on challenging areas of localizationin WSNs. His profound insights and attention to details have been true inspirations to my research.

I am thankful to Prof. S. K. Rath, Prof. B. Majhi of Computer Science and Engineering Department and Prof. D.R. Parhi of Mechanical Engineering Department for extending their valuable suggestions and help whenever I approached them.

It is my great pleasure to show indebtedness to my friends for their support during my research work. I acknowledge all staff, research scholars, juniors and seniors of CSE Department, NIT Rourkela, India for helping me during my research work. I am grateful to NIT Rourkela, India for providing me adequate infrastructure to carry out the present investigations.

I take this opportunity to express my regards and obligation to my family members whose support and encouragement I can never forget in my life. I wish to thank all faculty members and secretarial staff of the CSE Department for their sympathetic cooperation.

Munesh Singh

Abstract

Localization of the wireless sensor networks (WSNs) is an emerging area of research. The accurate localization is essential to support extended network lifetime, better covering, geographical routing, and congested free network. In this thesis, we proposed four distributed range-free localization schemes. The proposed schemes are based on the analytical geometry, where an arc is used as the geometric primitive shape. The simulation and experimental validation are performed to evaluate the performance of the proposed schemes.

First, we have proposed a mobile beacon based range-free localization scheme (MBBRFLS). The proposed scheme resolved the two underlying problems of the constraint area based localization: (i) localization accuracy depends on the size of the constraint area, and (2) the localization using the constraint area averaging. In this scheme, the constraint area is used to derive the geometric property of an arc. The localization begins with an approximation of the arc parameters. Later, the approximated parameters are used to generate the chords. The perpendicular bisector of the chords estimate the candidate positions of the sensor node. The valid position of the sensor node is identified using the logarithmic path loss model. The performance of proposed scheme is compared with Ssu and Galstyan schemes. From the results, it is observed that the proposed scheme at varying DOI shows 20.7% and 11.6% less localization error than Ssu and Galstyan schemes respectively. Similarly, at the varying beacon broadcasting interval the proposed scheme shows 18.8% and 8.3% less localization error than Ssu and Galstyan schemes respectively. Besides, at the varying communication range, the proposed scheme shows 18% and 9.2% less localization error than Ssu and Galstyan schemes respectively.

To further enhance the localization accuracy, we have proposed MBBRFLS using an optimized beacon points selection (OBPS). In MBBRFLS-OBPS, the optimized beacon points minimized the constraint area of the sensor node. Later, the reduced constraint area is used to differentiate the valid or invalid estimated positions of the sensor node. In this scheme, we have only considered the sagitta of a minor arc for generating the chords. Therefore, the complexity of geometric calculations in MBBRFLS-OBPS is lesser than MBBRFLS. For localization, the MBBRFLS-OBPS use the perpendicular bisector of the chords (corresponding to the sagitta of minor arc) and the approximated radius. The performance of the proposed MBBRFLS-OBPS is compared with Ssu, Galstyan, and Singh schemes. From the results, it is observed that the proposed scheme using CIRCLE,

SPIRAL, HILBERT, and S-CURVE trajectories shows 74.68%, 78.3%, 73.9%, and 70.3% less localization error than Ssu, Galstyan, and Singh schemes respectively.

Next, we have proposed MBBRFLS using an optimized residence area formation (ORAF). The proposed MBBRFLS-ORAF further improves the localization accuracy. In this scheme, we have used the adaptive mechanism corresponding to the different size of the constraint area. The adaptive mechanism defines the number of random points required for the different size of the constraint area. In this scheme, we have improved the approximation accuracy of the arc parameters even at the larger size of the constraint area. Therefore, the localization accuracy is improved. The previous scheme MBBRFLS-OBPS use the residence area of the two beacon points for approximation. Therefore, the larger size of the constraint area degrades the approximation accuracy. In the MBBRFLS-ORAF, we have considered the residence area of the three non-collinear beacon points, which further improves the localization accuracy. The performance of the proposed scheme is compared with Ssu, Lee, Xiao, and Singh schemes. From the results, it is observed that the proposed MBBRFLS-ORAF at varying communication range shows 73.2%, 48.7%, 33.2%, and 20.7% less localization error than Ssu, Lee, Xiao, and Singh schemes respectively. Similarly, at the different beacon broadcasting intervals the proposed MBBRFLS-ORAF shows 75%, 53%, 38%, and 25% less localization error than Ssu, Lee, Xiao, and Singh schemes respectively. Besides, at the varying DOI the proposed MBBRFLS-ORAF shows 76.3%, 56.8%, 52%, and 35% less localization error than Ssu, Lee, Xiao, and Singh schemes respectively.

Finally, we have proposed a localization scheme for unpredictable radio environment (LSURE). In this work, we have focused on the radio propagation irregularity and its impact on the localization accuracy. The most of the geometric constraint-based localization schemes suffer from the radio propagation irregularity. To demonstrate its impact, we have designed an experimental testbed for the real indoor environment. In the experimental testbed, the three static anchor nodes assist a sensor node to perform its localization. The impact of radio propagation irregularity is represented on the constraint areas of the sensor node. The communication range (estimated distance) of the anchor node is derived using the logarithmic regression model of RSSI-distance relationship. The additional error in the estimated distances, and the different placement of the anchor nodes generates the different size of the constraint areas. To improve the localization accuracy, we have used the dynamic circle expansion technique. The performance of the proposed LSURE is compared with APIT and Weighted Centroid schemes using the various deployment scenarios of the anchor nodes. From the results, it is observed that the proposed LSURE at different deployment scenarios of anchor nodes shows 65.94% and 73.54% less localization error than APIT and Weighted Centroid schemes.

***Keywords*: *Geometric Constraint*; *WSNs*; *Mobile Beacon*; *RSSI*; *Range Free*; *Localization*.**

Contents

List of Figures

List of Tables

List of Abbreviations

WSN	Wireless Sensor Network
RSSI	Received Signal Strength Indicator
TOA	Time of Arrival
TDOA	Time Difference of Arrival
AOA	Angle of Arrival
DOI	Degree of irregularity
ROI	Region of interest
RWP	Random Way Point
GPS	Global Positioning System
RSS	Received Signal Strength
RMSE	Root mean square error
QOS	Quality of Service
SPI	Serial Peripheral Interface
VSP	Variance of Sending Power
3-D	Three Dimensional
MBBRFLS	Mobile Beacon Based Range Free Localization Scheme
MBBRFLS-OBPS	MBBRFLS using Optimized Beacon Points Selection
MBBRFLS-ORAF	MBBRFLS using Optimized Residence Area Formation
LSURE	Localization Scheme for Unpredictable Radio Environment

List of Symbols

S	Sensor Node
K	Path Loss Coefficient
N	Number of the Sensor Nodes
P	Power
η	Path Loss Exponent
d	Distance
X_σ	Gaussian Random Variable
E	Euclidean Distance
U	Random Normal Distribution
R	Random Points
Rand	Random Point Generating Function
H	Sagitta of an arc
k	Number of Generated Random Points
C	Half Chord Length

Chapter 1

Introduction

We are living in the world, where technology revolutionized the living society in many ways. Today, we use varieties of the sensors to monitor the dangerous places, where the human accessibility is hazardous [1, 2]. A sensor is a tiny, inexpensive device that can work as a single entity with multiple attributes such as communication, sensing, processing, and storing [3]. In wireless sensor networks (WSNs), these tiny, inexpensive sensors work together in organized ways. The organized way defines the multiple operations performed by the sensors such as sensing, routing, communications, energy saving, and maintaining the topology. However, these many useful operations cannot be performed efficiently without the localization of WSNs. The localization provides the meaningful sense to any sensor data. The recorded actuating event without a significant geographical location has no use. In this thesis, we have addressed the various issues and challenges to provide simple, inexpensive, and accurate localization schemes.

1.1 Introduction

Wireless sensor networks (WSNs) have many research possibilities that attract researchers around the globe [3]. To resolve the various issues of WSNs, the researcher primarily focused on localization [4]. The sensor node without the localization can not make the intelligent decision of data forwarding, topology maintaining, and efficient covering of the network. All the major functions that performed by the sensor nodes are linked with location. Therefore, localization is essential for any WSNs. In WSNs, the sensor nodes are worked together to perform a critical task associated with risk. The critical tasks are the sudden rise in humidity, temperature, pressure, fire eruption, and radiation leak [5, 6], as shown in Fig.1.1. However, the sensed information without the geographical location is meaningless [7–10]. Since, the global positioning system (GPS) brought to WSNs, the sensor nodes identify its location more precisely than ever. However, the GPS have limitations such as cost, energy inefficient, and work only in outdoor environment [11]. Besides, sensors are a tiny, inexpensive device with low power, short communication, and low processing ability. Therefore, the GPS is not preferred as the liable solution for each sensor nodes. To provide an energy efficient localization, the researcher proposed a novel ideal based on the different

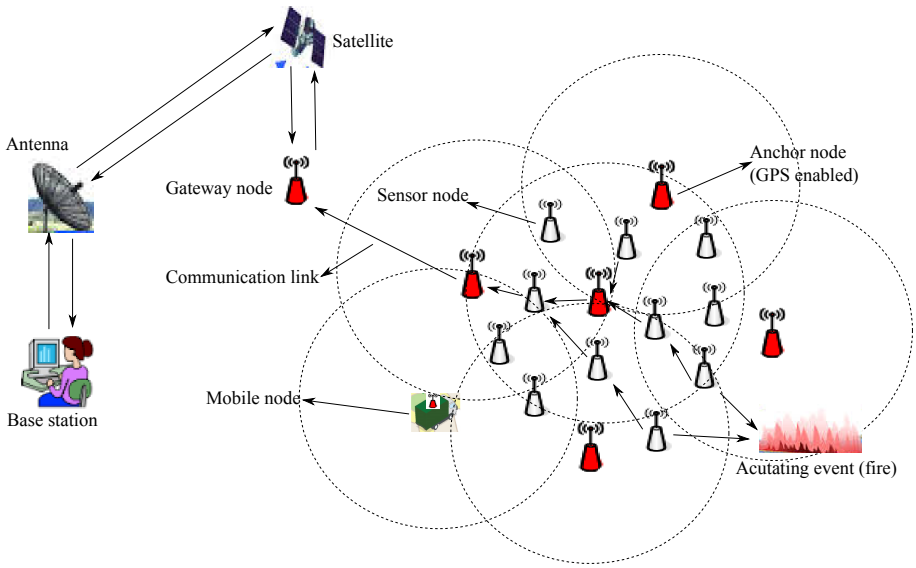

Figure 1.1: Overview of Localization in WSNs

deployment scenarios. The idea suggests the few sensor nodes with GPS capability assist the other sensor nodes to perform its localization. Based on this idea, the various localization schemes are proposed to provide the accurate, cost effective and simple localization [12, 13]. In this work, we have focused on geometric constraint-based range-free localization scheme. The geometric schemes are simple, energy efficient, and cost effective.

The remaining part of this chapter are as follows. In Section 1.2, discussed the issues and challenges of WSNs. Section 1.3, discuss the motivation of the work. Section 1.4, discuss the objective of the work. Section 1.5 presents the thesis contribution. Section 1.6 presents the thesis organization. Section 1.7, presents the summary.

1.1.1 Applications of WSNs

In WSNs, the sensor nodes are worked together to perform a critical task associated with risks. Today, we have used varieties of sensors and their organized network to solve the various real world problems [14, 15].

- Application of WSNs are categorized into:

    1. **Area Surveillance:** The sensors are placed in a hostile inaccessibility environment to monitor the movements; for instance monitoring the battlefield , locating the landlines, and for efficient battle planning.
    2. **Environmental Monitoring:** Sensor nodes are used to gather the actuating response of the environment such as forest fire, volcano eruption, earthquakes, etc. Hence, these missions critical operations of a sensor network can prevent the massive damages and loss of lives [5, 6].

3. **Industrial Monitoring:** In industries, the sensor nodes are used for various tracking and sensing. The primary function is to track the malfunction in the production lines [16]. Any anomaly without tracking has a significant impact on the production and the revenue.
4. **Medical and Health care Monitoring:** In a medical field, the sensors perform lifesaving tasks such monitoring the patients blood pressures, blood sugar level, reviews ECG and do some critical surgical operations [17].
5. **Traffic Control System:** Sensors within the cities are used to maintain the traffic flow and prevent the congestion and collisions [16]. The sensor network within the entire cities also used to monitor the dangerous driving events.
6. **Underwater Acoustic Sensor Networks:** Sensors within the acoustic environment monitoring the marine life, water pollutant, mixed minerals, and explore hidden undersea oil fields [16].

These applications without the locations can not provide the meaningful information. Therefore, the localization is essential to extend the functionality of WSNs.

1.2 Localization Issues and Challenges in WSNs

Localization of WSNs has the following issues and challenges:

- High localization error
- Vulnerable to radio propagation irregularity
- Energy inefficiency
- High communication overhead
- High localization error at longer communication range
- High localization error at longer beacon broadcasting interval
- Cost and complexity of the scheme

Designing an efficient localization scheme is a critical requirement for any WSNs, where the energy efficiency, less localization error, and minimum overhead are prominent. In this work, we have addressed some issues and challenges that influence the accuracy of any localization schemes. These issues and challenges are detailed as given below:

- Localization scheme has certain limitation such as sensor inefficiency to measure physical distances or angles from other location aware sensors, which lead most of the localization schemes to high localization error.

- Ideally, radio signal in a real environment suffers from scattering, diffusion, multipath, reflection, refraction, and shadowing. Therefore, most of the localization scheme are vulnerable to radio propagation irregularity.
- Some schemes require high information exchange to perform localization. Therefore, the number of collisions and high energy expense affect the performance of the network.
- Most of the schemes show high localization error at high communication range.
- The longer beacon broadcasting interval of a mobile beacon degrades the localization accuracy and localization percentage of the sensor node.
- Some localization schemes use the range determining hardware to gather the physical distance between the nodes. Hence, their schemes are costly, energy inefficient, and complex.

1.3 Motivation of the Work

The localization of WSNs is essential to extend the network services along with network lifetime. To enhance the functionality of WSNs, we have outlined the following motivation of our work:

- The basic necessity of any WSNs is to provide their services for longer period [1–3]. Therefore, a localized WSNs is essential to extend the network lifetime along with other network fundamental services such as meaning sensing, efficient routing, and the less congested network.
- The localization schemes are broadly classified into two categories called range based and range free. In range-based schemes, the localization is performed using the node to node distance or angle information. Besides, the range free schemes localized the sensor node using the connectivity of proximity information [4, 7]. Therefore, the range free schemes are simple, energy efficient, and less costly. In this work, we have used the range free scheme for localization of WSNs.
- In WSNs, the primary mode of communication between the sensors is the radio. Ideally, the radio signal suffers from various environmental obstruction and noise. Therefore, the radio propagation irregularity is an another major issue that influences the localization accuracy of the WSNs.
- The most of the localization schemes provide the better localization accuracy at the higher density of the reference nodes. However, the higher density increased the deployment cost and degraded the network lifetime and through [8, 16].

- The lack of the experimental validation using the real sensor in the real environment.
- A localized WSNs have wide variety of applications [1–3].

1.4 Objective of the Work

Motivation by the need of an efficient localization scheme, the following objectives are undertaken:

- To design a mobile beacon based range-free localization scheme (MBBRFLS), that resolve the two underlying problems: (i) constraint area size dependent accuracy, and (ii) high localization error through constraint area averaging.
- To design MBBRFLS using an optimized beacon points selection (OBPS), that further improves the localization accuracy using the constraint area based differentiation.
- To design MBBRFLS using an optimized residence area formation (ORAF), that minimizes the approximation accuracy using the adaptive mechanism for varying size of the residence area.
- To design a localization scheme for unpredictable radio environment (LSURE), that performs localization even in the worst scenario of radio propagation irregularity.
- To analyze the performance of proposed schemes using simulation and experimental validation.

1.5 Thesis Contribution

In this section, we have presented the chapters contribution of proposed schemes.

- **Chapter 3** The proposed MBBRFLS resolved two underlying problems of the constraint area based localization schemes: (1) constraint area size dependent accuracy, and (2) high localization error through constraint area averaging. In proposed MBBRFLS, the constraint area is used to derive the geometric property of an arc. The localization begins with an approximation of the arc parameters (radius, half length of the chord, and sagitta of an arc (height)). Later, the approximated parameters are used to generate the chords. The perpendicular bisector of the chords estimates the candidate positions of the sensor nodes. To differentiate the valid position, we have used the logarithmic path loss model. In this work, the constraint area is used for approximation rather than localization. Therefore, the localization accuracy is improved even at the larger size of the constraint area. From the simulation results, it is observed that the proposed MBBRFLS shows better localization accuracy.

- **Chapter 4** To further enhance the localization accuracy, we have proposed an another MBBRFLS using an optimized beacon points selection (OBPS). In this work, we have replaced the logarithmic path loss model based differentiation through constraint area of the optimized beacon points. The constraint area of optimized beacon points minimizes the invalid decision for the valid estimated position of the sensor node. Therefore, the increased localization error in MBBRFLS is further minimized in proposed MBBRFLS-OBPS. In this work, we have only considered the sagitta of the minor arc to generate the chord, which reduced the complex geometric calculation in proposed MBBRFLS-OBPS. For localization, we have used the perpendicular bisector of the chords and the approximated radius. The performance of the proposed scheme is evaluated using the simulation.

- **Chapter 5** Next, we have proposed MBBRFLS using an optimized residence area formation (ORAF). In this scheme, we have used the adaptive mechanism corresponding to the different size of the constraint area. The adaptive mechanism defines the number of the random points for the different size of the constraint area. The mechanism improves the approximation accuracy of arc parameters even at the larger size of the constraint area. In this scheme, we have used the residence area of the three non-collinear beacon points, which further minimizes the residence area and improves the approximation accuracy. The smaller size of the residence area along with adaptive mechanism improves the localization accuracy. The performance of the proposed MBBRFLS-ORAF is evaluated using simulation as well as experimental validation.

- **Chapter 6** Finally, we have proposed a localization scheme for unpredictable radio environment (LSURE). The proposed LSURE localizes the sensor nodes even in the worst scenario of radio propagation irregularity. In this scheme, we have taken the static sensor and static anchor based deployment scenario. The objective of this work is to validate the proposed LSURE in the real indoor environment. For validation, we have designed a prototype experimental testbed. In the experimental testbed, the different scenario of radio propagation irregularity is modeled using the additional error in the estimated distance (derived from the logarithmic regression model of RSSI-distance relationship), and by changing the positions of the anchor nodes. To improve the localization accuracy in the worst scenario of radio propagation irregularity, we have used the dynamic circle expansion technique. From the experimental results, it is observed that the proposed scheme provides better localization even in an unpredictable radio environment.

1.6 Thesis Organization

The rest of the thesis is organized as follows:

Chapter 2 In this chapter, we review the localization schemes based on geometric formulation. Firstly, we review the classification of localization schemes based on deployment scenarios. Secondly, we further classify the localization schemes based on the technique used to perform localization. Finally, we classified the trajectories of a mobile beacon and discussed their impact on localization accuracy.

Chapter 3 In this chapter, we have proposed a mobile beacon based range-free localization scheme (MBBRFLS) for WSNs. The proposed MBBRFLS relies on the analytical geometry, where an arc is used as the geometric primitive shape. The localization begins with an approximation of the arc parameters. Later, the approximated arc parameters are used to estimate the chords. The perpendicular bisector of the generated chord determines the position of the sensor node. To differentiate the valid position of the sensor node, we have used the logarithmic path loss model. In this scheme, the generated chords are corresponding to the sagitta of the minor arc and major arc.

Chapter 4 In this chapter, we have proposed MBBRFLS using an optimized beacon points selection (OBPS). The MBBRFLS-OBPS localizes the sensor nodes using the perpendicular bisector of the chord and the approximated radius. The proposed scheme minimized the localization error using the constraint area based differentiation technique. In this scheme, we have considered the sagitta of the minor arc to generated the chord. Therefore, the complex geometric calculation is further minimized in proposed MBBRFLS-OBPS. To evaluate the performance of the proposed MBBRFLS-OBPS, we have performed the simulation using the various trajectory of a mobile beacon.

Chapter 5 In this chapter, we have proposed MBBRFLS using an optimized residence area formation (ORAF). The scheme utilized the adaptive mechanism corresponding to varying size of the constraint area. Besides, we have used the minimized residence area of the three non-collinear beacon points. The both techniques improve the approximation accuracy of the arc parameters, which further minimizes the localization error in MBBRFLS-ORAF. To validate the proposed MBBRFLS-ORAF, we have used the simulation as well as the experimental testbed.

Chapter 6 In this chapter, we have proposed a localization scheme for unpredictable radio environment (LSURE). The applicability of LSURE in the real indoor environment is validated using a prototype experimental testbed. In the experimental scenario, the static anchors assist the static sensor to perform its localization. The communication range used to create the constraint area is derived through logarithmic regression model of RSSI-distance relationship. The different scenarios of radio propagation irregularity are modeled using the additional error in the estimated distances, and the different placement of the anchors. To improve the localization accuracy in worst scenario of radio propagation irregularity, we

have proposed a dynamic circle expansion technique.

Chapter 7 we outline the conclusion of the work and future research scope.

1.7 Summary

WSNs have wide varieties of applications, among them; the event tracking is essential. The event monitoring is necessary to understand the event behavior and its consequence. In WSNs, the sensor nodes are usually deployed in a hostile environment to monitor the actuating events such as floods, volcanic eruptions, earthquake, tsunamis, and other geological processes. Therefore, the actuating event geographical location is essential. The localization in WSNs is used to map the actuating even with an exact geographic location. In this chapter, we discussed various issues and challenges that impact the localization accuracy. We outline the motivation of our work to implement an efficient localization schemes. The objective of our work is to provide a simple, cost-effective, and computational inexpensive localization scheme. Finally, the chapter organization and work detailing are highlighted in this chapter. In next chapter, we review the various localization scheme based on geometric constraint and range free techniques.

Chapter 2

Literature Survey

In this chapter, we have reviewed the various localization scheme. First, we examined the localization schemes based on the deployment scenarios. Later, the further classification divides the localization schemes into two categories called range based and range free. The each category of localization schemes are reviewed along with their merits and demerits. Finally, we have classified the various trajectories of the mobile beacon and examined their impacts on the localization accuracy.

2.1 Introduction

Localization has become a pervasive issue in wireless sensor networks. In recent years, various types of localization schemes have been evolved. They are broadly classified into four groups based on their deployment scenarios: (i) static anchors and static sensors [18, 19] (ii) static anchors and mobile sensors [20, 21] (ii) mobile anchors and static sensors [22, 23] (iv) mobile anchors and mobile sensors [14, 24], as shown in Fig. 2.1. The further classification of localization schemes is on the techniques used to perform the localization such as range based and range free [4]. In this chapter, we briefly reviewed the localization schemes of each category.

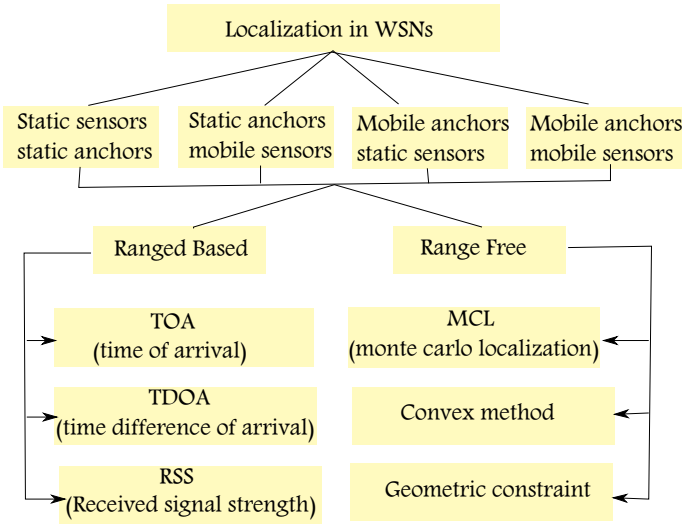

Figure 2.1: Classification of localization schemes

The remaining part of this chapter are as follows. In Section 2.2, reviewed the localization scheme based on different deployment scenarios. Section 2.3, presents the classification of localization scheme based technique. Section 2.4, reviewed the classification of mobile trajectories. Section 2.5, presents the summary.

2.2 Different Deployment Scenario

In this section, we have reviewed the localization schemes categorized based on the different deployment scenarios.

2.2.1 Static Anchors and Static Sensors

In WSNs, the static anchors and static sensors based deployment scenarios are more common. Besides, it is widely preferred among other three categories of deployment scenarios. In this group of localization schemes, the sensor nodes along with few anchors are randomly deployed in a sensing area. The anchor nodes are location aware (either manual or through GPS), while sensor nodes are unaware of its location. The localization of this category is performed using the broadcast messages of the anchor nodes. For localization, these schemes can use either range based or range free techniques. The localization schemes of this categories are simple, inexpensive and accurate.

The few localization schemes of this category are as follows:

- He et al. [25] proposed an algorithm called APIT (Approximation Point in Triangle), which is a triangular geometric based scheme. In APIT, each sensor constructs its triangular regions by combining all possible sets of anchors within its hearing range. The centroid of all the intersection points of the triangles is used to estimates the position of the sensor node. However, the scheme performed better at higher deployment density with more neighboring information exchange. The high communication overhead degrade the performance of the proposed scheme.

- Doherty et al. [26]] proposed a centralized convex optimization algorithm, which is based on the bounding box (rectangle) geometric constraint. The localization is performed using the proximity or connectivity information of all nodes. In this scheme, the accuracy of localization depends on the size of the constraint area.

- Vivekanandan et al. [27] proposed a concentric anchor beacon (CAB) based localization scheme for WSNs. In CAB, the anchors transmit the beacon at the varying power levels. From the information of the beacon messages, the sensor node creates its constraint area within the concentric rings, which are corresponding to the varying transmit power levels. The localization is performed using the average of the constraint area intersection points. However, the accuracy of the proposed scheme depends on the high density of the anchor nodes deployment.

- Liu et al. [28] proposed a localization scheme called ROCRSSI (Ring overlapping based on Comparison of Received Signal Strength Indicator). In this scheme, the position of the sensor node is constraint within the rings (represented using the RSSI). The presence of the sensor node within the rings is determined using the RSSI of the beacon messages. The localization is performed using the average of all the intersection points belongs to the valid intersection area. However, the scheme is vulnerable to the radio propagation irregularity.

- Mihail et al. [29] proposed a localization scheme based on the varying transmit power levels. In this scheme, the constraint area of the sensor node is created using the explicitly considered inaccurate range measurements. The localization is performed using the constraint area averaging. However, the localization accuracy of the proposed scheme depends on the high information exchange.

- Liu et al. [30, 31], proposed an optimization ROCRSSI, where the range information is modeled using the RSSI. The accuracy of the proposed scheme depends on the high neighboring information exchange with grid based deployment. Similarly, the localization schemes [32, 33] are based on the restricted area. In this schemes, the constrained area of the sensor node is created using the intersection of symmetric communication circles with known radius. However, the practicality of modeling the circular communication pattern is not realistic and does not hold in practice.

2.2.2 Static Anchors and Mobile Sensors

The localization schemes of this categories use the static anchors to localize the mobile sensors. The most generic applications of these category are used for tracking the employees in an office or animals within a farm. In these schemes, the anchors are deployed in an unobstructed area such as ceiling or wall. The traditional schemes of this category are RADAR [34] and Dynamic Triangular (DTN) [35]. For localization, these schemes use the fingerprinting method, which has two phases: offline phase and online phase. In offline phase, the RSSI mapping is performed at various covering zone of the anchors. Later, the recorded RSSI of various location is used for localization in online phase. The localization of the mobile sensor nodes is performed by mapping the received RSSI with the recorded RSSI of the different location. The best match determines the position of the mobile sensor nodes. Similarly, an another scheme [36] using an artificial neural network based classifier further improves the localization accuracy. In this scheme, the artificial neural network is used to trained the network from the recorded RSSI data set of the different location. Later, in online phase the artificial neural network based classifier localize the mobile sensors. The best mapping determines the position of the mobile sensors. Besides, an another scheme [37]] based on the same terminology of artificial neural network is used to localized the

mobile sensor in different noisy environments. However, the localization schemes of these categories are energy inefficient, computationally expensive, and complex.

2.2.3 Mobile Anchors and Static Sensors

The schemes of this category use a mobile beacon to assist the static sensors to perform its localization. In these schemes, the mobile beacon provides the efficient covering along with better localization accuracy. However, these schemes are vulnerable to radio propagation irregularity, longer communication range, and longer beacon broadcasting intervals. The work in this thesis belongs to this category.

In this section, we have reviewed the range-free localization schemes based on a mobile beacon.

- Ssu et al. [38] proposed a range-free localization scheme using the geometric conjecture perpendicualr bisector of the chords. In this scheme, the chords are derived using the beacon points of the mobile beacon. The selected beacon points are assumed on the communication range of the sensor node. Later, the line segment between the selected anchor points is represented as the chords. The perpendicular bisector of the chords estimates the position of the sensor node. The major drawback of this scheme is its long execution time, high communication overhead, and vulnerable to radio propagation irregularity.

- To further improve the Ssu scheme, Lee et al. [39] proposed a geometric constraint-based range-free localization scheme. In this scheme, the possible positions of the sensor node are delimited within the areas obtained from the pre-arrival and post-departure points of the mobile beacon. However, the scheme fails to identify the valid position of the sensor node within the generated delimited areas, which leads to high localization error. Besides, the scheme shows high localization error at longer communication range.

- Galstyan et al. [40] proposed a constraint-based distributed localization scheme, where the delimited areas of the sensor node are created by using the two reference points. In this scheme, the localization is performed using all possible intersection areas of the selected two reference points. The main drawback of this scheme is less number of the delimited areas, which leads the scheme to high localization error.

- Xiao et al. [41] proposed a range-free localization using a mobile beacon. In this scheme, the position of the sensor node is constraint within the overlapping area of pre-arrival and post-arrival intersection with the pre-departure and the post-departure points of the mobile anchor. The possible position of the sensor node identified within the different overlapping areas. However, the scheme is computationally expensive and vulnerable to radio propagation irregularity.

- Guerrero et al. [42] proposed a range free method based on mobile beacons (ADAL). In this scheme, the mobile beacon is enabled with a rotatory directional antenna, which periodically transmits the beacon messages in a determined azimuth. Each sensor node estimates its position by taking the centroid of all intersection created by the circular sector of varying azimuth. The proposed scheme is expensive and complicated. Besides, intersection points of the circular sector at varying azimuth may not always provide the small delimited area, which leads to high localization error.

- Dong et al. [43] proposed an iterative localization scheme, where a sensor node makes an initial guess of its position using Levenberg-Marquardt method, and then iteratively refine its new position based on the Gauss-Newton method and using the newly-acquired beacon points. However, initial guess determines the accuracy of the localization, where a wrong guess may lead to high localization error.

- Singh et al. [44] proposed a range-free localization scheme using a mobile beacon. The localization is performed using the analytical geometry, where an arc is used as the geometric primitive shape. In this scheme, the localization begins with the approximation of the arc parameters. Later, the approximated arc parameters are used to generate the chord points. The perpendicular bisector of the chord between the generated chord points and approximated radius are used to localize the sensor node. The main drawback of this scheme is its lack of differentiation capability to identify the valid or invalid position of the sensor node. Besides, scheme shows high localization error at longer communication range with less number of beacon points.

2.2.4 Mobile Anchors and Mobile Sensors

This group of localization schemes uses the mobile anchors and mobile sensors. Due to the mobility of both sensors and anchors , the localization schemes requires more frequent information exchange, which increases the energy consumption and communication overheads. Therefore, the localization schemes of this category are more complex and computationally expensive. The general application of this category is found in mining [45] and urban cities [46]. The most traditional localization scheme of this category is Monte Carlo Localization (MCL) [24, 47]. In MCL, the possible location of a mobile sensor is represented using a set of weighted samples and which is recursively updated in time using Monte Carlo approximation method. The other schemes of this categories [48] and [49], where the localization is performed using the RSSI and fuzzy based logic.

2.3 Classification of Localization Technique

The methods employed to achieve the localization are further categories into range based and range free techniques.

2.3.1 Range Based Localization Scheme

In the range-based localization schemes, the sensors require the node to node distance or angle information. Later using triangulation or other geometric technique, sensor node estimates its location. The basic idea for distance estimation is performed using the Received Signal Strength Indicator (RSSI), Time of Arrival (ToA), and Time Difference of Arrival (TDoA) [50].

Localization based on ToA

The time of arrival (ToA) metric is used to estimate the distance between the sender and receiver. The signal travel time determines the distance between the sender and receiver. However, the lack of synchronized clock of the sender and receiver and the environmental noise and obstruction impacts the accuracy of distance estimation. Therefore, the localization schemes using the time of arrival metric fails to improve the localization accuracy [51–54]. The ToA measurement for distance estimation is performed as follows: The distance between the anchor node and sensor node is estimated using the time of flight delay of the radio signal, as shown in Fig. 2.2. The distance between the anchor node and

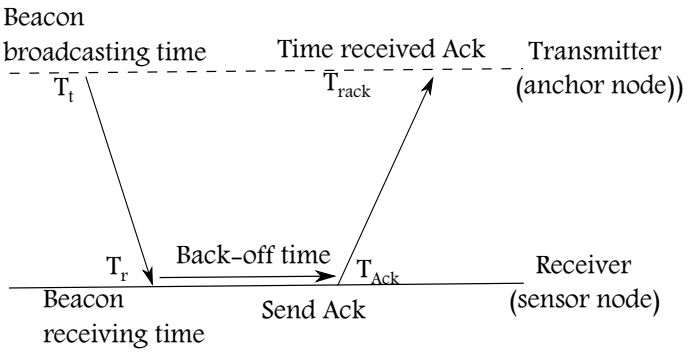

Figure 2.2: An example of ToA ranging technique

sensor node is represented as $d_t = c(T_r^2 - T_t^2)$. Similarly, distance between sensor node and anchor node is represented as $d_r = c(T_{Ack}^2 - T_{rAck}^2)$. To calculate the distance, we have combined both the estimated distances as follows:

$$\frac{d_t + d_r}{2} = \frac{c}{2}[(T_r^2 - T_t^2) - (T_{Ack}^2 - T_{rAck}^2)], \tag{2.1}$$

where c is the speed of light, T_t time to broadcast the beacon message, T_r is the time to receive the beacon signal, T_{Ack} is time to send an acknowledgment (Ack), and T_{rAck} is time to receive the Ack.

Localization based on TDoA

The time difference of arrival (TDoA) is an extension of ToA measurement, where time difference of two different signals is used to approximate the distance between the sender

and the receiver. In TDoA measurement, the anchor node transmits two separate signals one using the radio transceiver and other after a short interval using the ultrasonic transducer, as shown in Fig. 2.3. The sensor node receives the signal from RF and ultrasonic transducer, the time difference of arrival of RF and ultrasonic signals are used to compute the distance. the popular localization schemes of this category are [55, 56].

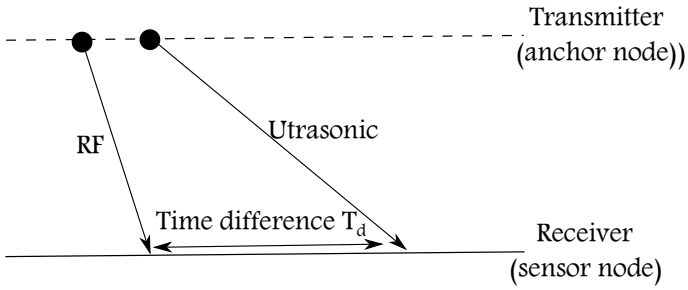

Figure 2.3: An example of TDoA ranging technique

Localization based on RSSI

Among all ranging technique, the RSSI based ranging is most popular and widely preferred. However, the RSSI based ranging is unpredictable in nature and easily affected by noise and obstruction, which leads to inaccurate distance estimation. The most widely preferred method for distance estimation using the RSSI is the logarithm path loss model, as follows:

$$P_R(d) = P_T - P_L(d_0) - 10 * n * log_{10}\frac{d}{d_0}, \tag{2.2}$$

where parameter P_T described the maximum power that an anchor node can transmit. Parameter P_R received signal power, and $P_L(d_0)$ is the path loss measured at reference distance of $d_0.n$ is the path loss exponent. The localization schemes of these categories are [57–61].

2.3.2 Range Free Based Localization Scheme

In the range-free localization scheme, the sensor node estimates its location using the connectivity or proximity information. Therefore, the range-free localization schemes are simple, inexpensive, and energy efficient. In this thesis, we have used the geometric approach for localization of WSNs. Hence, few schemes familiar of this categories are given in Tab. 2.1.

2.4 Mobile Trajectories

The mobile trajectories have a significant impact on the localization accuracy of WSNs [66]. The mobile beacon trajectories have been classified into two categories: deterministic and non-deterministic, as shown in Fig. 2.4.

Table 2.1: Geometric constraint area based localization schemes

Authors	Proposed geometric scheme	Deployment scenario	Demetris	Accuracy
Ssu et al. [38] (2005)	Localization using the perpendicular bisector of the chords	Static sensors and mobile anchors	Vulnerable to radio propagation irregularity,	Low
Vivekanandan et al. [27] (2007)	Concentric circle based constraint area for localization	Static sensors and Static anchors	Constraint area size dependent accuracy, localization performed using constraint area averaging	Average
Xiao et al. [41] (2008)	Overlapping constraint area based localization	Static sensors and mobile anchor	Vulnerable to radio propagation irregularity and computational costly	Average
Lee et al. [39] (2009)	Geometric constraint area based localization	Static sensors and mobile anchor	Vulnerable to radio propagation irregularity	Average
Yu et al. [62] (2007)	localization using perpendicular bisector of the chords in noisy environment	Static sensors and mobile anchors	Vulnerable to radio propagation irregularity	Average
Guo et al. [63] (2010)	Geometric relationship of a perpendicular intersection for localization	Static sensors and mobile anchors	Vulnerable to radio propagation irregularity,	Average
Wang et al. [64] (2008)	Dual restricted area based localization using the perpendicular bisector of the chords	Static sensors and mobile anchors	Vulnerable to radio propagation irregularity	Low
Shen et al. [65] (2015)	Single chord based localization	Static sensors and mobile anchors	Vulnerable to radio propagation irregularity	Average

2.4.1 Deterministic trajectories of mobile beacon

An efficient trajectory of the mobile beacon provides the better covering of the network along with less energy consumption and communication overhead. Koutsonikolas et al. [67] present a survey on localization schemes using a mobile beacon. Similarly, the Mao et al. [4] survey on localization issues and challenges in an unpredictable environment. Koutsonikolas et al. [67], discussed the deterministic trajectories of a mobile beacon called SCAN and HILBERT. The mobile beacon using the SCAN trajectory moves along one dimension either x-axis or y-axis. Besides, the mobile beacon using the HILBERT trajectory moves in a geometric pattern, where the nonlinear movements are more. The nonlinear movement pattern increases the energy consumption due to larger traveling path length. To minimize the traveling path length, Huang et al. [68] proposed a deterministic static path planning scheme for a mobile beacon. The proposed path planning schemes called CIRCLE and S-CURVE. The CIRCLE and S-CURVE trajectories provide the non-collinear movement that reduces the traveling pathlength and provides the better covering of the networks. However, the CIRCLE and S-CURVE trajectory do not provide an efficient covering at the boundary of the networks. Similarly, Han et al. [69] proposed an efficient deterministic mobile beacon trajectory called LMAT. The LMAT trajectories provide the short path length along with better coverage of the network. Besides, Hu et al. [70] proposed a deterministic SPIRAL

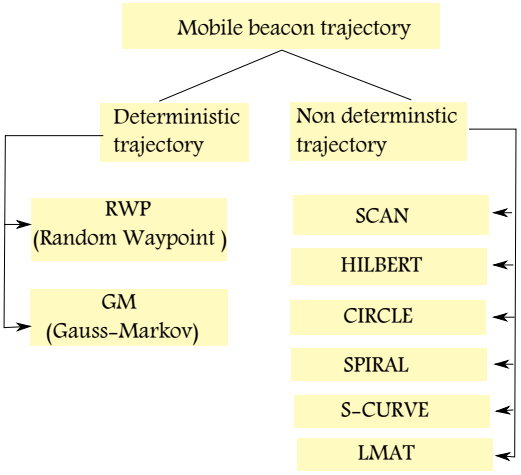

Figure 2.4: Classification of mobile trajectories

trajectory for a mobile beacon. The mobile beacon using SPIRAL trajectories further reduces the movement and provides the better covering of the network.

2.4.2 Non-deterministic trajectories of mobile beacon

In the non-deterministic trajectories, the destination of the mobile beacon is randomly chosen. The most popular mobility model of this category is random waypoints (RWP) mobility model [71]. In RWP, the mobile anchor starts from a random source and moves towards a random destination. The main drawback of RWP model is the non-uniform covering of the network and may follow the visited path repeatably. Besides, the GM Mobility model [72] is more realistic as seen in the practical world.

2.5 Summary

In this chapter, we have reviewed the various localization schemes. First, we reviewed the localization scheme of each category based on deployment scenarios. Later, the further classification divides the localization schemes into two categories called range based and range free. The each category of localization schemes are reviewed along with their merits and demerits. Finally, we have classified the various trajectories of the mobile beacon and examined their impacts on the localization accuracy.

Chapter 3

Mobile Beacon Based Range Free Localization Scheme (MBBRFLS)

In this chapter, we have proposed a mobile beacon based range free localization scheme (MBBRFLS). The proposed scheme is based on the analytical geometry, where arc is used as the primitive geometric shape. The localization begins with approximation of the arc parameters (radius, half length of the chord, and sgaitta of an arc). Later, the approximated parameters are used to generate the chords on the assumed circle. The perpendicular bisector of the chords estimate the candidate positions of the sensor node. To identify the valid position, we have used the logarithmic path loss model. The performance of the proposed MBBRFLS is evaluated using simulation.

3.1 Introduction

Most of the localization algorithms use the fixed infrastructure, where the sensor nodes along with few anchor nodes are randomly deployed in the sensing area. However, the fixed infrastructure requires the higher density of the anchor deployment to gain the acceptable accuracy [1–4, 7, 8]. Therefore, to overcome the limitation (density dependent precision) of the fixed infrastructure, we have utilized the GPS-enabled mobile beacon. The mobile beacon navigates the sensing field and periodically broadcast the beacon messages [38–44]. From the collected beacon information, the sensor node estimates its position. In the proposed MBBRFLS, we have use the geometric property of an arc to estimate the position of the sensor node. The localization begins with approximation of the arc parameters using the residence area of the sensor node. The residence area is created using the communication range of the selected three non-collinear mobile beacon points. The approximated arc parameters included the radius, half length of the chord, and Sagitta of an arc (major arc and minor arc). These approximated parameters belongs to a assumed circle of the sensor node. Later, the approximated parameters are used to generate the chords on the assumed circle. The perpendicular bisector [73] of the chords estimate the candidate positions of the sensor node. To identify the valid position, we have used the logarithmic path loss

model. In the proposed MBBRFLS, we have use the Sagitta of minor arc and major arc for generating the chords on the assumed circle. For performance evaluation, we have performed the simulation using various performance evaluating metrics such as communication range, beacon broadcasting interval, degree of irregularity (DOI), and mobile trajectories.

The remaining part of this chapter are as follows. Section 3.2, presents the mobile beacon based assumption and radio propagation model. Section 3.3, presents the proposed MBBRFLS geometric method for localization. Section 3.4, presents the simulation and results. Section 3.5, presents the summary.

3.2 Mobile Beacon Based Assumption And Radio Propagation Model

In this section, we present the proposed MBBRFLS and underlying assumption corresponding to a mobile beacon.

3.2.1 Mobile Beacon Trajectory Based Assumptions

The mobile beacon traverses the sensing field and periodically broadcast its current location coordinate. We assume that the sensor node listens to the beacon messages, as mobile beacon enters the communication range of the sensor node. We define two states for each sensor node as follows:

1. ***Inside:*** The sensor node within the broadcasting range of the mobile beacon.
2. ***Outside:*** The sensor node out of the broadcasting range of the mobile beacon.

We also define the transitions between the above two states as follows:

1. ***Arrival:*** Once the sensor node receives the beacon messages from the mobile beacon, the sensor node resets its status from *Outside* to *Inside*.
2. ***Departure:*** Once the mobile beacon departs the communication range of the sensor node, the sensor node resets its status from *Inside* to *Outside*.

The proposed MBBRFLS is based on the restricted area, where these two transitions are useful to create the residence area of the sensor node. The accuracy of the position estimation depends on the minimized residence area of the sensor node. As shown in Fig. 3.1, the sensor node needs to retain the following beacon points to minimize its residence area: (1) the beacon point B, where the sensor node listen to the first beacon message and (2) the beacon point C, where the sensor node listen to the last beacon message. However, due to radio propagation irregularity, there is a possibility that the sensor node can miss the beacon messages transmitted from the beacon position B and C.

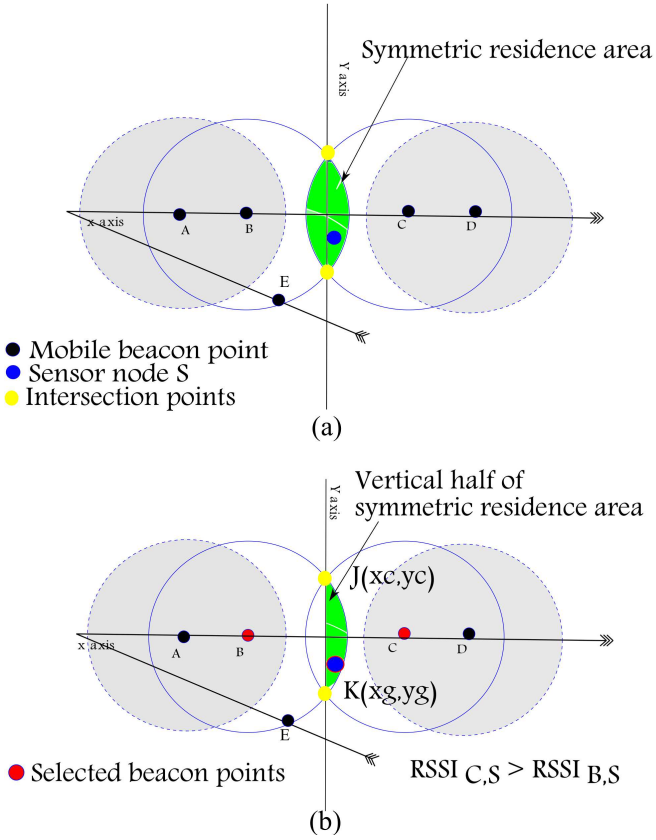

Figure 3.1: Steps describing the residence area formation. (a) Sensor node creating its residence area under the communication range intersection of two farthest beacon points B and C. (b) Based on RSSI, sensor node identifies its residence area, which is adjacent to the nearest anchor node C.

3.2.2 Radio Propagation Model

To simulate the radio propagation irregularity, we have used a Radio Irregularity Model (RIM) [25]. The model represents the radio propagation irregularity as degree of irregularity (DOI), where DOI defines the path loss variation per unit degree change in direction. The radio propagation irregularity is modeled as follows:

$$K_i = \begin{cases} 1, & i = 0, \\ K_{i-1} \pm Rand * DOI, & 0 < i < 360, i \in N, \end{cases} \tag{3.1}$$

where $|K_0 - K_{359}| \leq DOI$, K_i represents the coefficient that defines the per unit degree change in path loss from 0 to 360 degrees. Fig. 3.2 shows the varying DOI corresponding radio patterns. The RIM model adjusts the value of path loss model based on the DOI values as follows:

$$P_R = P_T - P_{DOI} + P_F, \tag{3.2}$$

where P_F defines the fading exponent, P_{DOI} defines the signal power loss, P_T defines the transmission power, and P_R defines the received power. P_{DOI}=$\eta * K_i$, where η defines the path loss exponent. The propagation of the radio signal depends on the distance, as distance

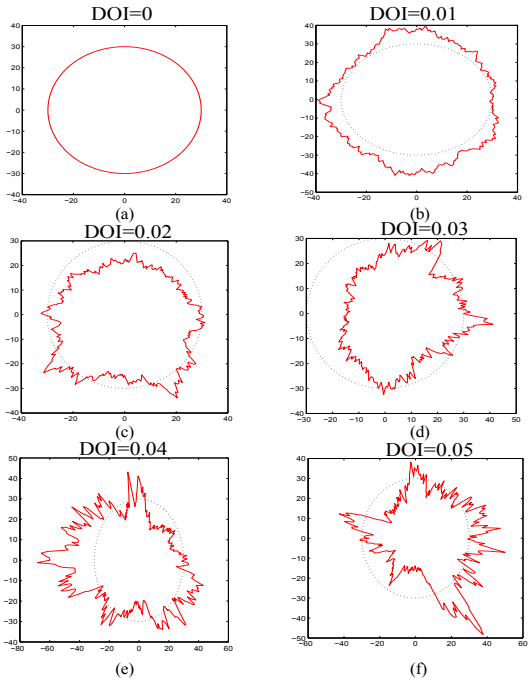

Figure 3.2: Radio propagation pattern at different values of DOI.

increases the signal strength decreases. In logarithmic path loss model, we can predict the signal strength at any particular distance. The path loss model is defined as follows:

$$P_R(d) = P_T - P_L(d_0) - 10 * \eta * log_{10}\frac{d}{d_0} + X_\sigma, \tag{3.3}$$

where $P_L(d_0)$ is the path loss at a reference distance d_0 and $X_\sigma \sim N(0, \sigma^2)$ represents the Gaussian random variable with zero mean and standard deviation σ, which is used to express the logarithmic shadowing effect. Usually, the maximum radio propagation irregularity is found at the boundary of the maximum radio range. Therefore, we divide the communication range into upper bound and lower bound. The upper limit defines the maximum radio range r, and the lower limit is defined as $r \times (1 - DOI)$. The division of the communication range may rise three conditions as follows:

1. If $E_d > r$, then the probability P of receiving the beacon message is P=0, where E_d is the euclidean distance between the sensor node and mobile beacon. If this condition occurs, sensor node fails to localize itself.

2. If $E_d < r \times (1 - DOI)$, than the probability P of receiving the beacon message is P=1. If this condition occurs, the sensor node can localize itself.

3. If $r \times (1 - DOI) \leq E_d \leq r$, the probability of receiving the beacon message is randomly distributed within $U(0, 1)$. If this condition occurs, localization of the sensor node is uncertain.

To satisfy the probability $P = 1$ of successful receiving of the beacon message. The sensor node has to select the beacon points whose path loss corresponding to the distance E_d are less than the path loss corresponding to the DOI (0 to 360 degree). In this type of selection, the sensor node sometimes fails to distinguish whether the selected beacon points are nearer or farther. Therefore, the size of the residence area corresponding to selected beacon points is larger, which leads to high localization error.

3.3 MBBRFLS Geometric Method for Localization

Geometry has various primitive shapes such as triangle, circle, rectangle, and rings, which are used in various range-free localization methods [25–28]. The proposed MBBRFLS use the analytical geometry of an arc [73]. According to analytical geometry, if any line segment joining any two points on the circumference of the circle, actually divides the circle into two halves called major arc and minor arc, as shown in Fig. 3.3. An arc have Sagitta (height), half chord length, and radius, which are used in this scheme to estimate the position of the sensor node.

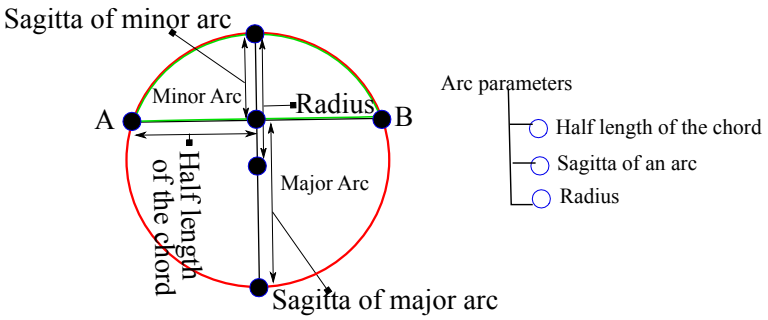

Figure 3.3: Arc of the circle.

The proposed MBBRFLS have five phases. In the first phase, the sensor node identifies its location within vertical half of the symmetric residence area. In the second phase, the sensor node randomly approximates the radius and half chord length. In the third phase, the sensor node estimates the Sagitta of an arc using the unknown criterion (radius and half chord length). In the fourth phase, the sensor node uses the perpendicular bisector of the chord to estimate its position. In the final phase, the sensor node identifies its location within the horizontal half of the residence area.

3.3.1 Finding the Vertical Half of the Symmetric Residence Area

The residence area of the sensor node is symmetric along the x-axis and y-axis, which is vertically and horizontally divided into two halves along the y-axis and x-axis, as shown in Fig. 3.1(a). Sensor node S is inside the vertical half of the symmetric residence area of beacon points B and C as shown in Fig. 3.1(b). The recent work [74] shows that even in obstacle environment using the power scanning techniques, we can know the sensor node

positions either nearer or farther. Accordingly, if $RSSI_{C,S} > RSSI_{B,S}$ then the sensor S concludes that it is in the vertical half of B, otherwise it is in the vertical half of C. Later, the sensor node identified its location within the horizontal half, which is symmetric along the x-axis horizontally.

3.3.2 Random Approximation of Radius and Half Chord Length

In the previous section, based on the comparison of RSSI ($RSSI_{C,S} > RSSI_{B,S}$), the sensor node concludes that B is the distant beacon point. The farthest beacon B is chosen as first chord point on the assumed circle of the sensor node. After acquiring first chord point, the sensor node approximate other two more chord points using the analytical geometry of an arc. The sensor node randomly generates few points (3 to 5) on the line segment BC. The generated points reside inside the residence area of the sensor node. Later, the sensor node calculates the euclidean distance between the generated points and beacon point B. Among the calculated euclidean distances, sensor node selects few of them as the radius and half chord length. According to the geometric relation, the selected distances as the radius should be greater than or equal to the distances as the half chord length.

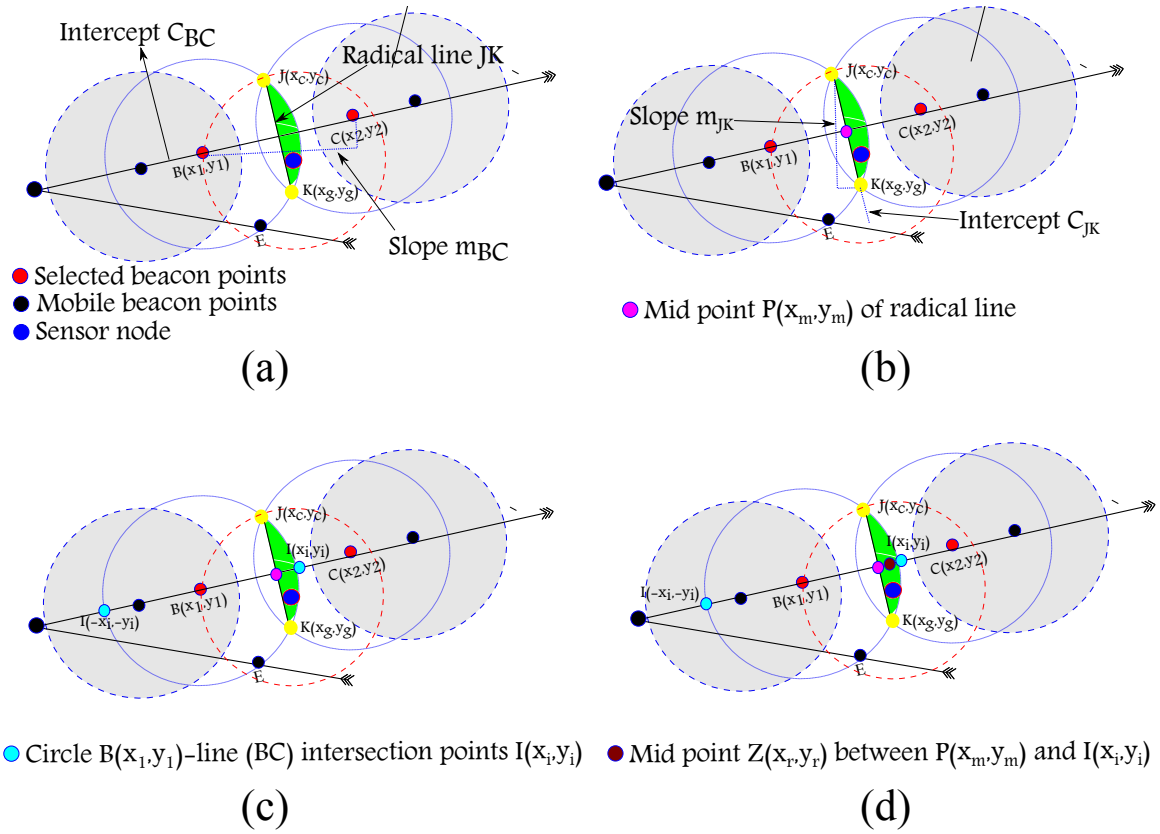

Figure 3.4: Estimated parameters for approximation range

The following input parameters are required to set the random approximation range for the radius and half chord length, as shown in Fig. 3.4. The beacon points B and C are considered as the center of the circle and their communication range as radius r.

- Fig. 3.4(a) shows the slope m_{BC} and intercept c_{BC} of the line segment between the beacon points $B(x_1, y_1)$ and $C(x_2, y_2)$.

- Fig. 3.4(b) shows the mid point $P(x_m, y_m)$ of radical line, which is calculated as $P(x_m = (x_c + x_g)/2, y_m = (y_c + y_g)/2)$ using the two intersecting points $J(x_c, y_c)$ and $K(x_g, y_g)$.

- The circle-line intersection point $I(x_i, y_i)$ is generated on the line segment BC through the intersection of the communication range of $B(x_1, y_1)$. The generated intersection points $I(x_i, y_i)$ and $I(-x_i, -y_i)$ are shown in Fig. 3.4(c). To choose the valid point either $I(x_i, y_i)$ or $I(-x_i, -y_i)$, the sensor node calculates the euclidean distance between $P(x_m, y_m)$ and $I(\pm x_i, \pm y_i)$ as E_p and E_n respectively. Based on the comparison between E_p and E_n as $(E_p < E_n)?(-x_i, -y_i) : (x_i, y_i)$, sensor node selects the root which is nearer to $P(x_m, y_m)$. Let $I(x_i, y_i)$ be the circle-line intersection coordinate.

- Fig. 3.4(d) shows the mid point $Z(x_r, y_r)$ of the residence area, which is calculated as $Z(x_r = (x_m + x_i), y_r = (y_m + y_i))$ using coordinates $P(x_m, y_m)$ and $I(x_i, y_i)$. From the earlier estimated coordinates, $P(x_m, y_m)$, $I(x_i, y_i)$, and $Z(x_r, y_r)$, we derive the euclidean distances E_{PI}, E_{PZ}, and E_{AZ} respectively. The estimated euclidean distances E_{PI}, E_{PZ}, and E_{AZ} are used to set the random approximation range for the radius and half chord length.

- The end point coordinates of the radical line JK are $J(x_c, y_c)$ and $K(x_g, y_g)$. Its slope $m_{JK} = \frac{y_c - y_g}{x_c - x_g}$ and intercept $c_{JK} = -(m_{JK} * x_c) + y_c$ are later used to approximate the Sagitta (height) of an arc.

All the earlier estimated parameters are successively applied to approximate the radius and half chord length, as shown in Fig. 3.5. The relation given below, randomly approximate the radius within the range specified as follows:

$$r_1 = E_{AZ} + E_{PI} \tag{3.4}$$

$$r_2 = E_{AZ} - E_{PZ} \tag{3.5}$$

$$R = (r_2 - r_1) * rand(k, 1) + r_1,\ k = 1, 2, ..., k_n, \tag{3.6}$$

where r_1 and r_2 are the random approximation range and R represents the random point generating function. Each random value R (R_1, R_2, R_3,...,R_n) within the range r_1 and r_2 are considered as the radius, as shown in Fig. 3.5(b). Each circle drawn against the radius r (corresponding to R) with center $B(x_1, y_1)$, intersects the lines BC and JK. Then the corresponding intersection coordinates of the circle with lines BC and JK are designated as $Q(\pm x_e, \pm y_e)$ and $F(\pm x_t, \pm y_t)$ respectively. The intersection coordinates $Q(\pm x_e, \pm y_e)$

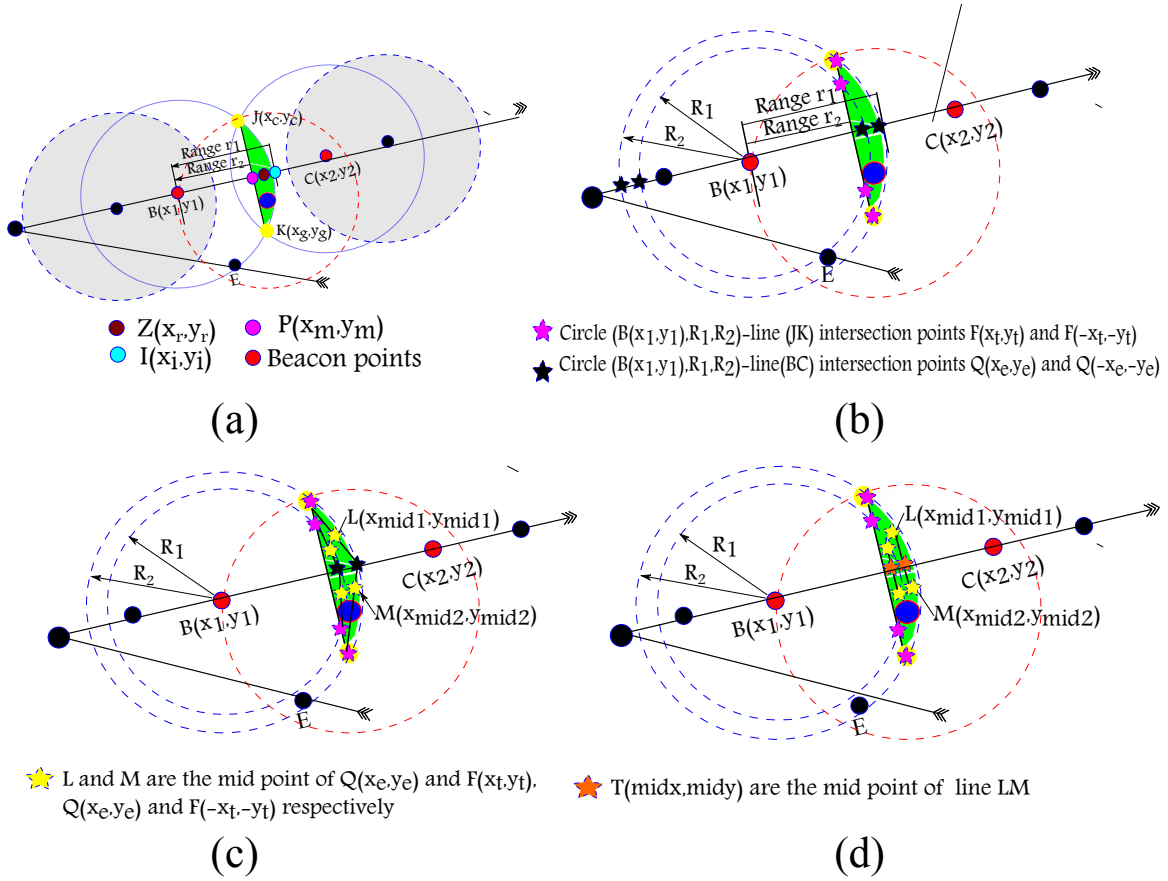

Figure 3.5: Random approximation of radius and half chord length.

and $F(\pm x_t,\pm y_t)$ are later used to approximate the half chord length. The equation of the circle with center $B(x_1, y_1)$ and the radius corresponding to the random values R (R_1, R_2, R_3,...,R_n) is shown in Eq. (3.7). After solving the Eq. (3.7) using quadratic equation, the two roots of the circle-line intersection coordinates are generated as $Q(x_e, y_e)$ or $Q(-x_e, -y_e)$.

$$(x_e - x_1)^2 + (y_e - y_1)^2 = (R)^2 \, , R = R_1, R_2, R_3, ..., R_n \tag{3.7}$$

To choose the valid root either $Q(x_e, y_e)$ or $Q(-x_e, -y_e)$, the sensor node calculates the euclidean distance between $P(x_m, y_m)$ and $Q(\pm x_e,\pm y_e)$ as E_p and E_n. Based on the comparison between E_p and E_n as $(E_p < E_n)?(-x_e, -y_e) : (x_e, y_e)$, the sensor node selects the root which is nearer to $P(x_m, y_m)$, as shown in Fig. 3.5(c). Let $Q(x_e, y_e)$ be the circle-line intersection coordinate.

To find the other intersection coordinates $F(\pm x_t,\pm y_t)$ on a radical line JK, let relabel the input coefficients of Eq. (3.7) as x_e to x_t. After rebelling the coefficients, the circle line intersection points $F(\pm x_t,\pm y_t)$ are calculated using quadratic equation. The generated two roots $F(\pm x_e,\pm y_e)$ are shown in Fig. 3.5(b). The mid point of the line segment between $Q(x_e, y_e)$ and $F(x_t, y_t)$, and $Q(x_e, y_e)$ and $F(-x_t, -y_t)$ are $L(x_{mid1} = \frac{xe+x_t}{2}, y_{mid1} = \frac{ye-x_t}{2})$ and $M(x_{mid2} = \frac{xe+x_t}{2}, y_{mid2} = \frac{ye-x_t}{2})$ respectively, as shown in Fig. 3.5(c). The slope m_{LM} and intercept c_{LM} of the line segment between the points $L(x_{mid1}, y_{mid1})$ and

$M(x_{mid2}, y_{mid2})$ are used to approximate the point on the circumference of the assumed circle, as shown in Fig. 3.5(d). The euclidean distance between the mid point $T(mid_x, mid_y)$ of the line segment LM and beacon point $B(x_1, y_1)$ estimates the half chord length E_{xy} as follows:

$$E_{xy} = \sqrt{(x_1 - mid_x)^2 + (y_1 - mid_y)^2} \tag{3.8}$$

3.3.3 Approximation of Sagitta

From the previous calculation, we have half chord length E_{xy}, the midpoint of the chord $T(mid_x, mid_y)$, and the radius corresponding to each random values R. The approximated parameters are used to estimate the Sagitta of an arc. The Sagitta [73] is the vertical line from the midpoint of the chord to the arc itself, as shown in Fig. 3.3. The half chord length, Sagitta, and radius of the arc are inter-related, and if we know any two of them, then we can calculate the third. Each generated random values of R and measured half-length of the chord E_{xy} are used to derive the Sagitta of an arc as follows:

$$H = \left(\frac{\sum_{i=1}^{k} R(i)}{k}\right) \pm \sqrt{\left(\frac{\sum_{i=1}^{k} R(i)}{k}\right) - E_{xy}^2)} \tag{3.9}$$

Then we approximate the points on the circumference of the assumed circle corresponding to Sagitta $\pm H$ (major and minor) of an arc. Using the quadratic equation, the sensor node generate the points $N(\pm\ x_{c(1)}(k), \pm\ y_{c(1)}(k))$ on the circumference of the assumed circle, when Sagitta of major arc $(+H)$ is considered. The other point $V(\pm\ x_{c(2)}(k), \pm\ y_{c(2)}(k))$ is generated on the circumference of the assumed circle, when Sagitta of minor arc $(-H)$ is considered.

3.3.4 Position Estimation

From Fig. 3.6(a), each Sagitta $\pm H$ (major arc and minor arc) corresponding estimated points are $N(\pm x_{c(1)}(k), \pm y_{c(1)}(k))$ and $V(\pm x_{c(2)}(k), \pm y_{c(2)}(k))$ respectively. From Fig. 3.6(b) and Table. 3.1, the combination of beacon points $B(x_1, y_1)$, $N(\pm x_{c(1)}(k), \pm y_{c(1)}(k))$, and $V(\pm x_{c(2)}(k), \pm y_{c(2)}(k))$ generates two different chords $\overline{BN}$ and $\overline{BV}$. Consider the lines L_{BN} and L_{BV} as the corresponding perpendicular bisectors of the chords $\overline{BN}$ and

Table 3.1: Generated all combination of chord points

All combination of chord points		
Chord point 1	**Chord point 2**	**Chord point 3**
$B(x_1, y_1)$	$N(x_{c(1)}(k), y_{c(1)}(k))$	$V(x_{c(2)}(k), y_{c(2)}(k))$
$B(x_1, y_1)$	$N(-x_{c(1)}(k), -y_{c(1)}(k))$	$V(-x_{c(2)}(k), -y_{c(2)}(k))$
$B(x_1, y_1)$	$N(-x_{c(1)}(k), -y_{c(1)}(k))$	$V(x_{c(2)}(k), y_{c(2)}(k))$
$B(x_1, y_1)$	$N(x_{c(1)}(k), y_{c(1)}(k))$	$V(-x_{c(2)}(k), -y_{c(2)}(k))$

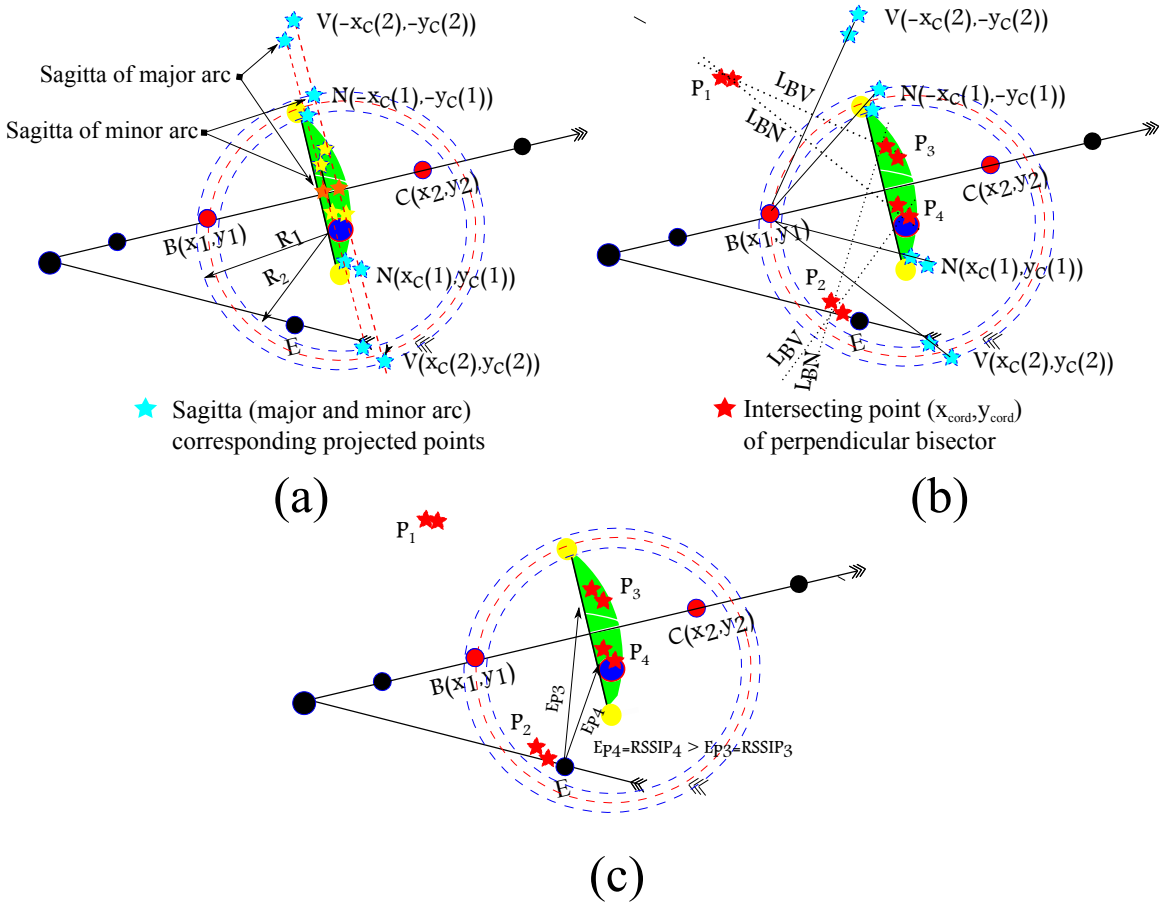

Figure 3.6: Final position estimation and differentiation. (a) Approximated Sagitta $\pm H$ (major arc and minor arc) corresponding generated beacon points. (b) Apply the perpendicular bisectors of the chords on the generated beacon points. (c) Final position is differentiated using path loss model.

$\overline{BV}$ respectively. Based on the $Cramer's\ rule$, the intersection point of the perpendicular bisectors L_{BN} and L_{BV} of the chords $\overline{BN}$ and $\overline{BV}$ generates four candidate positions of the sensor node, as shown in Fig. 3.6(b). The relation given below estimates the perpendicular bisectors of the chords corresponding to all input combination of the beacon points, as shown in Table. 3.1.

$$a_{BN} = x_{c(1)}(k) - x_1 \tag{3.10}$$

$$a_{BV} = x_1 - x_{c(2)}(k) \tag{3.11}$$

$$b_{BN} = y_{c(1)}(k) - y_1 \tag{3.12}$$

$$b_{BV} = y_1 - y_{c(2)}(k) \tag{3.13}$$

$$c_{BN} = (x_{c(1)}(k) - x_1)((x_1 + x_{c(1)}(k))/2) + 3(y_{c(1)}(k) - y_1)(y_1 + y_{c(1)}(k))/2) \tag{3.14}$$

$$c_{BN} = (x_1 - x_{c(2)}(k))((x_{c(2)}(k) + x_1)/2) + (y_1 - y_{c(2)}(k))((y_{c(2)}(k) + y_1)/2) \tag{3.15}$$

$$x_{cod} = (c_{BN} * b_{BV} - c_{BV} * b_{BN})/(a_{BN} * b_{BV} - a_{BV} * b_{BN}) \tag{3.16}$$

$$y_{cod} = (a_{BN} * c_{BV} - a_{BV} * c_{BN})/(a_{BN} * b_{BV} - a_{BV} * b_{BN}) \tag{3.17}$$

Fig. 3.6(b) presents the estimated positions (P_1, P_2, P_3, and P_4) of the sensor node, generated using the perpendicular bisectors of the chords. From the four estimated positions (P_1, P_2, P_3, and P_4), the two of them resides within the residence area of sensor node, as shown in Fig. 3.6(c). However, to differentiate the valid candidate position of the sensor node within the residence area, the sensor node use the logarithmic path-loss model.

3.3.5 Final Position Differentiation

The valid position of the sensor node is identified using RSSI of the received beacon points. The valid position of the sensor node resides within the residence area. As shown in Fig. 3.6(c), the sensor node selects that beacon point through which it receives maximum RSSI. Then the sensor node calculates the euclidean distance E_{P3} and E_{P4} between the selected beacon point and the estimated positions P_3 and P_4 respectively. Using Eq. (3.3), the sensor node estimates the received power $RSSI_{P_3}$ and $RSSI_{P_4}$ corresponding to the euclidean distances E_{P3} and E_{P4}. Based on the small difference between the received RSSI from the selected beacon point and estimated RSSI ($RSSI_{P_3}$ and $RSSI_{P_4}$), the sensor node estimated its position either P_3 or P_4. However, the radio propagation irregularity may affect the valid differentiation of the sensor node position. Although, if sensor node made the invalid decision, the maximum localization error can not go beyond the size of the residence area. The final position of the sensor node is taken as the average of all the positions generated corresponding to the each random value of R. The average of these positions are stored in x_p and y_p as follows:

$$x_p = \left(\frac{\sum_{i=1}^{k} x_{pos(i)}}{k} \right) \tag{3.18}$$

$$y_p = \left(\frac{\sum_{i=1}^{k} y_{pos(i)}}{k} \right), \tag{3.19}$$

where k is the number of the generated random values $R = R_1, R_2, R_3, ..., R_k$.

3.4 Simulation And Results

The simulation is performed using MATLAB R2013a (8.1.0.604). MATLAB is an efficient tool to perform analytical computation and modeling of any mathematical model based on complex geometry. All the necessary modules related to WSNs is modeled in MATLAB. Table. 3.2 shows the simulation environment. The performance of the proposed MBBRFLS is evaluated at various influencing parameters such beacon broadcasting interval, communication range and degree of irregularity (DOI). Besides, we have shown the impact of RSSI differentiation and mobile trajectories on the localization accuracy.

Table 3.2: Simulation parameters and values

Parameters	Values
Network size (m^2)	100×100
Number of unknown nodes	100, 200, 300
Number of the mobile beacon	1
Beacon broadcasting intervals	3 m, 5 m, 7 m, 9 m
Communication range (r)	20, 30, 40, 50
DOI	0.01, 0.02, 0.03, 0.04, 0.05

3.4.1 Performance Evaluation At Varying DOI and Communication Range

The performance of the proposed MBBRFLS is evaluated at a network area of size 100×100 m^2, where a mobile beacon traverse the sensing field using random way-point mobility model (RWP). For simulation, we have used the varying communication range (20 m - 50 m), beacon broadcasting interval of 5 m, and DOI varying from 0-0.05. From Fig. 3.7, it is observed that as DOI is increased localization error also increased. At high DOI, the sensor node fails to differentiate whether the selected beacon points are nearer or farther. Therefore, the size of the residence area corresponding to the selected beacon points is larger, which leads to high localization error. Besides, the communication range is an another parameter that influences the size of the residence area. At longer communication range and inadequate

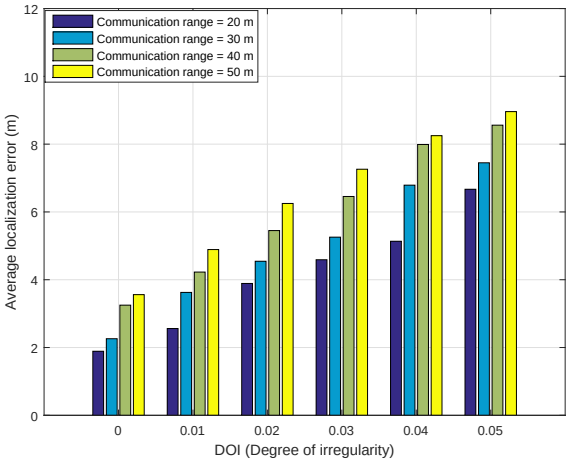

Figure 3.7: Performance at varying DOI versus average localization error on varying communication range.

density of anchor nodes, the size of the residence area and localization error are increased. From Fig. 3.7, it is observed that the average localization error at a communication range of 20 m and DOI of 0.05 is 25.5 % less than at DOI of 0.05 and communication range of 50 m. The average localization error at DOI of 0.05 for communication range 20 m, 30 m, 40 m, and 50 m are 6.6 m, 7.45 m, 8.56 m, and 8.96 m respectively.

3.4.2 Performance Evaluation At Varying DOI and Beacon Broadcasting Interval

In Fig. 3.8, we compare the performance of the proposed MBBRFLS at varying beacon broadcasting intervals (5 m, 7 m, 9 m). The simulation comparison is performed at the network areas of size 100×100 m^2, where the DOI is varying, and communication range of the mobile beacon is fixed at 30 m. The beacon broadcasting interval defines the density

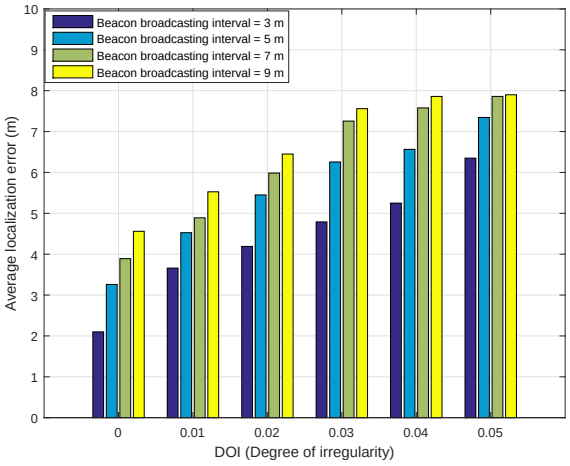

Figure 3.8: Performance at varying DOI versus average localization error on varying beacon broadcasting intervals.

of the beacon points. At the longer beacon broadcasting interval the quantity of the beacon point is less, resulting schemes based on constraint area or residence area generally shows high localization error. The lesser quantity of beacon points reduces the options for the sensor nodes to minimization its residence area, which leads to high localization error. Similarly, the DOI influence the differentiation (nearer or farther) capability of the sensor nodes, which further leads to high localization error. From the result, it is observed that as the beacon broadcasting interval is increased the localization error is also increased. From Fig. 3.8, it is observed that at a beacon broadcasting interval of 5 m and DOI of 0.05, the average localization error is 12.65 % less than at a beacon broadcasting interval of 9 m and DOI of 0.05. The beacon broadcasting interval and varying DOI affect the localization accuracy of the proposed MBBRFLS. However, at closer beacon broadcasting interval the effect of DOI is negligible.

3.4.3 Impact of RSSI Based Differentiation

In the proposed MBBRFLS, the valid position of the sensor node is differentiated using the maximal RSSI of beacon points. Due to the various environmental noise and obstruction, the RSSI based differentiation is very unpredictable. Therefore, the sensor node valid candidate position differentiation may not always be accurate, resulting the average localization error

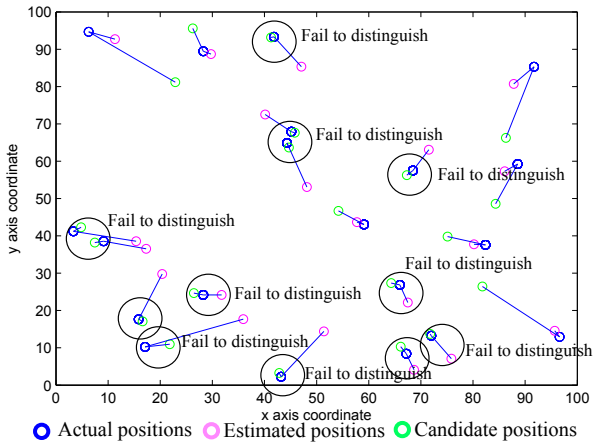

Figure 3.9: Impact of RSSI on sensor node candidate position differentiation.

is increased. To show its impact, we have performed a simulation using the communication range of 20 m, beacon broadcasting interval of 5 m, and DOI of 0.05 along with deployed density of 20 sensor nodes. The lesser deployed density of the sensor node helps to recognize the failure of RSSI-based differentiation and its impact on the average localization accuracy. From Fig. 3.9, we can observed the failure of the sensor node to differentiate its valid positions, which leads the proposed MBBRFLS to high localization error. However, the invalid differentiation can not leads the maximum localization error beyond the size of the residence area.

3.4.4 Impact of Density on Localization Accuracy

In Fig. 3.10, we have shown the influence of deployed density on the localization accuracy. The different deployed density along with longer beacon broadcasting interval and high DOI

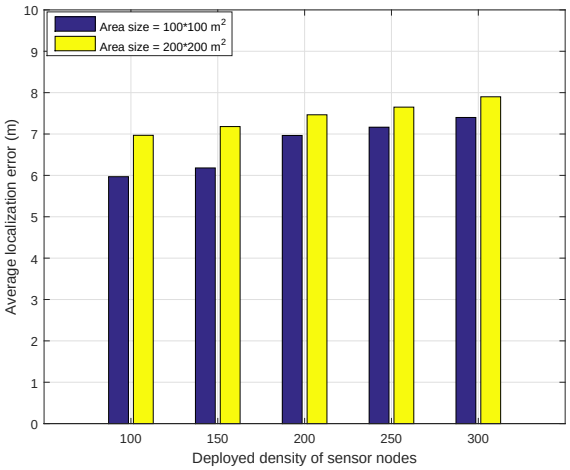

Figure 3.10: Performance at deployed density versus average localization error.

are used to evaluate the performance of the proposed MBBRFLS. To show is impact, we

have considered the two different network size. The longer beacon broadcasting interval reduced the density of the beacon points, resulting the few sensor node have the less options to minimize its residence area. Similarly, the high DOI influence the regular distribution of the radio signal, resulting few sensor nodes fails to acquire enough beacon points to minimize its residence area. These two parameters along with different deployment density affect the localization accuracy. From Fig. 3.10, it is observed that at the network area of size 100×100 m^2 and the deployment density of 300, the average localization error is 6.3 % less than network area of size 200×200 m^2. From the results, it is observed that the network size has a minor influence on the localization accuracy even considered the different deployment density.

3.4.5 Impact of Communication Range and Beacon Broadcasting Interval on Localization Percentage

Fig. 3.11 shows the impact of varying communication range on the localization percentage. The longer communication range improves the localization percentage, because the sensor

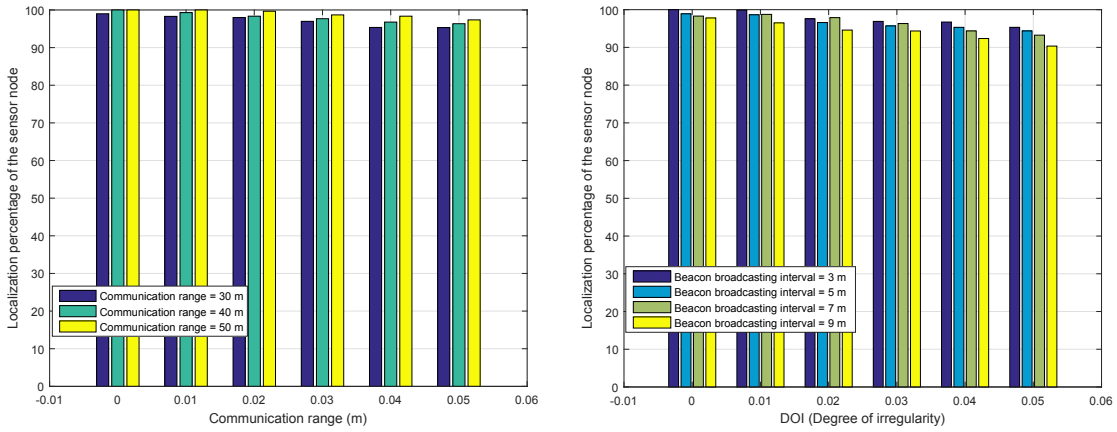

Figure 3.11: Localization percentage. (a) Varying communication range versus localization percentage. (b) Varying beacon broadcasting interval versus localization percentage

nodes lying at the corner of the network can also receive the beacon information. From Fig. 3.11 (a), it is observed that at beacon broadcasting interval of 5 m and varying DOI, the average localization percentage is above 97%. However, the longer communication range along with longer beacon broadcasting intervals sometimes affect the localization percentage. Similarly, the longer beacon broadcasting without longer communication range affect the localization percentage. From Fig. 3.11 (b), it is observed that at the longer beacon broadcasting interval and the high DOI, the localization percentage is reduced. At a beacon broadcasting interval of 5 m and DOI of 0.03, the localization percentage is 5.58 % greater than the DOI of 0.05 and beacon broadcasting interval of 9 m. The average localization percentage at varying DOI and varying beacon broadcasting interval is greater than 96 %.

3.4.6 Impact of Mobile Beacon Trajectories

The trajectories of the mobile beacon have a significant impact on the localization accuracy. Different trajectories have different shapes, which are primarily used to resolved the various network issues such as inefficient covering, localization, topology control, and energy inefficiency. To evaluate the performance, we have used various trajectories of mobile

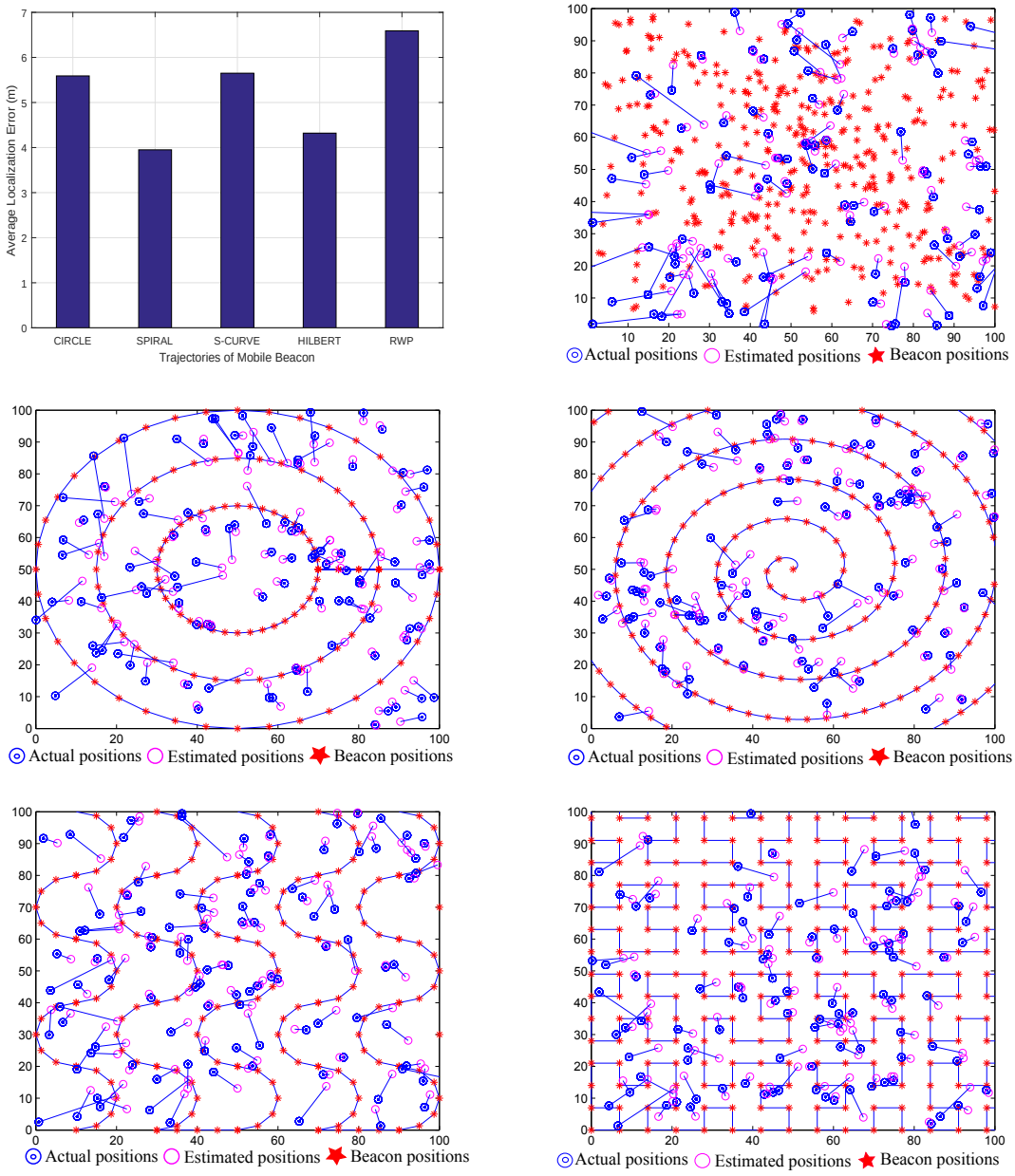

Figure 3.12: Simulation outcome of the proposed MBBRFLS using RWP, CIRCLE, SPIRAL, S-CURVE, and HILBERT trajectories

beacon such as CIRCLE, SPIRAL, HILBERT, S-CURVE, and RWP. The simulation is performed using the communication range of 20 m, beacon broadcasting interval of 5 m, and DOI of 0.05. From the results, it is observed that the mobile beacon using different trajectories influence the localization accuracy. The mobile beacon using the SPIRAL

trajectory improves the 27.1 % localization accuracy than any other trajectory. From Fig. 3.12, the average localization error using CIRCLE, SPIRAL, HILBERT, S-CURVE, and RWP trajectories are 5.59 m, 3.95 m, 5.65 m, 4.32 m, 6.59 m, respectively.

3.4.7 Performance Comparison with Ssu and Galstyan Schemes

In this section, we compare the performance of the proposed MBBRFLS with Ssu [38] and Galstyan [40] schemes. The performance is evaluated at varying degree of irregularity (DOI), where the mobile beacon uses the RWP trajectory with a communication range of 30 m and beacon broadcasting interval of 5 m.. From Fig. 3.13, it is observed that as the DOI

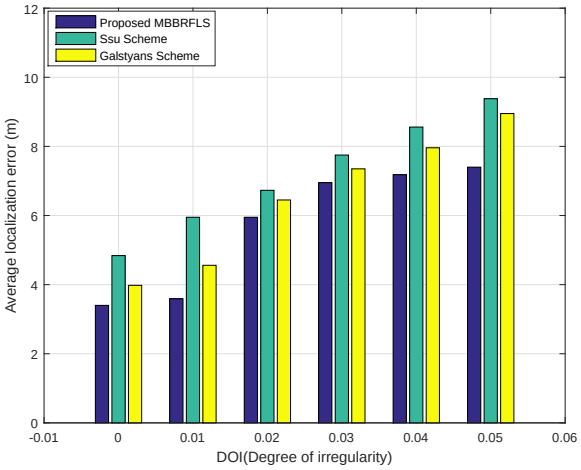

Figure 3.13: Performance comparison at varying DOI between the proposed MBBRFLS, Galstyan [40], and Ssu [38] schemes.

is increased the localization error is also increased. In Ssu scheme, the average localization error is increased at the varying DOI. The DOI influence the uniform distribution of the radio signal, which results sensors fails to distinguish the near far relationship between the received beacon points. Therefore, the selected beacon points of a mobile beacon are not exactly resided on the communication range of the sensor node. Therefore, the perpendicular bisector of the chords corresponding to the selected beacon points leads the Ssu scheme to high localization error. Similarly, the invalid selection of beacon points creates the larger size of the delimited, which leads the Galstyan scheme to high localization error. The less number of the delimited areas is another factor that influence the localization accuracy of Galstyan scheme. However, the Galstyan scheme at a DOI of 0.05 shows 4.58 % less localization error than Ssu scheme. Besides, the proposed MBBRFLS outperforms even at the varying DOI. The average localization error obtained at the DOI of 0.05 in the proposed MBBRFLS, Ssu, and Galstyan schemes are 7.4 m, 9.38 m, and 8.95 m respectively.

In Fig. 3.14, we have compared the performance at varying communication range along with beacon broadcasting interval of 5 m and DOI of 0.05. From the result, it is observed that the proposed MBBRFLS is vulnerable at longer communication range. However, its

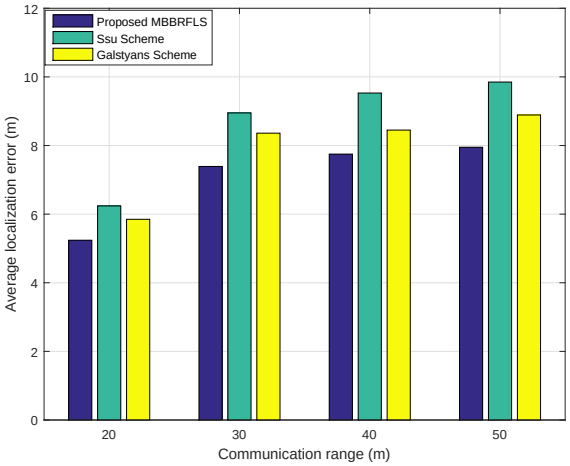

Figure 3.14: Performance comparison at varying communication range between the proposed MBBRFLS, Galstyan [40], and Ssu [38] schemes.

impact is only significant at the insufficient quantity of beacon points. Besides, the longer communication range the DOI influence the optimal selection of the beacon points, which further leads to high localization error. The proposed MBBRFLS and Galystan schemes at a DOI of 0.05 fails to minimize its residence area, which leads the schemes to high localization error. In Ssu scheme, the longer communication range has no effect rather DOI affects the selection of beacon points. Although, even at high DOI, the proposed MBBRFLS shows less localization error than Ssu and Galstyan scheme. From the result, it is observed that at the communication range of 50 m the average localization error in the proposed MBBRFLS, Ssu, and Galystan schemes are 6.25 m, 8.85 m, and 6.39 m respectively.

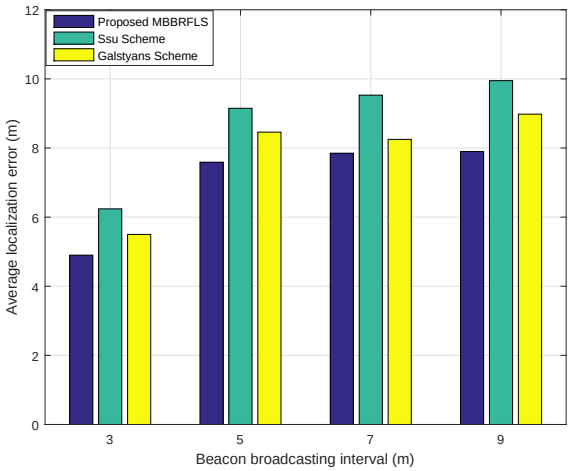

Figure 3.15: Performance comparison at varying beacon broadcasting interval between the proposed MBBRFLS, Galstyan [40], and Ssu [38] schemes

In Fig. 3.15, we have performed the comparison at varying beacon broadcasting intervals along with communication range of 30 m and DOI of 0.05. From the result, its is observed

that as the beacon broadcasting interval is increased the localization error is also increased. In Ssu scheme, the longer beacon broadcasting interval affects the optimal selection of the beacon points. Therefore, the perpendicular bisector of the chords corresponding to the selected beacon points leads to high localization error. Besides, the Galystan and the proposed MBBRFLS schemes at longer beacon broadcasting fails to minimized the residence area of the sensor node. The longer broadcasting interval reduces the number of the beacon points, which results the sensor node have lesser options for minimization of its residence area. From the results, it is observed that the average localization error at the beacon broadcasting interval of 9 m in the proposed MBBRFLS, Ssu, and Galystan schemes are 7.55 m, 8.85 m, and 8.58 m respectively.

3.5 Comparative Strength And Weakness

In this section, we have taken the different types of overhead to compare the strength and weakness of the proposed scheme with other schemes. The overhead includes the computation and communication cost, number of anchor nodes, scalability, and energy consumption. The performance comparison of the proposed MBBRFLS with other schemes is given in Table. 3.3. Where N designate the total number of the beacon points.

Table 3.3: Comparative strength and weakness

Performance parameters	MBBRFLS	Ssu [38]	Galystan [40]
Accuracy	Fair	Fair	Fair
Node Density	>0	>0	>0
Beacon Heard	>2	>3	>3
DOI	Good	Fair	Fair
GPS error	Good	Good	Good
Scalability	Fair	Good	Fair
Communication Overhead	N	N	N
Time Complexity	O(N^2)	O(N^2)	O(N^2)
Energy efficiency	Fair	Good	Fair

3.6 Analysis of Robustness and Efficiency

To analyse the robustness and efficiency of the proposed scheme with other schemes, we have taken the worst case scenarios in terms of worst performance evaluating parameters. The worst performance evaluating parameters are longer beacon broadcasting interval, longer communication range, and radio propagation irregularity.

3.6.1 Longer beacon broadcasting interval

The longer beacon broadcasting interval of mobile beacon reduces the number of beacon points, which results the sensor node can have less options to choose appropriate beacon points.

Robustness

Unlike Ssu [38] and Galystan [40] schemes, the proposed scheme gives less localization error even in the inappropriate selection of the beacon points. The inappropriate selection largely effect the size of the constraint area, and size of constraint area directly propositional to the accuracy of localization. In proposed scheme, the size of constraint area effect the approximation accuracy of arc parameters. Due to the random approximation in proposed scheme, the large error in approximation accuracy can not static for each sensor. Hence, the average localization error in the proposed scheme is much lower than the Ssu [38] and Galystan [40] schemes.

Efficiency

Due to less options of appropriate beacon points, the proposed scheme still manage to localize the sensor node with maximum localization error within the constraint limit. Besides, the Ssu [38] and Galystan [40] schemes fails to minimize the localization error even the certain limit.

3.6.2 Communication range

The longer communication range definitely improves the covering of the network. However, longer communication range can not provide the smaller constraint area when the obstacle and noise in the environment effect the appropriate selection of beacon points.

Robustness

The proposed scheme with longer communication range and less number of beacon points localize the maximum number of the sensor nodes, where Ssu [38] and Galystan [40] schemes fails to achieve such percentage of localization.

Efficiency

The longer communication range with inappropriate selection of beacon points increases the size of the constraint area, which may gives high approximation error in proposed scheme. However, the proposed scheme use the random points for approximation, and it is vary for each sensor nodes. Hence, the localization error for each sensor node is vary, where some times it gives less estimation error and sometimes more. Therefore, the average localization error is lesser than the Ssu [38] and Galystan [40] schemes.

3.6.3 Degree of Irregularity

The degree of irregularity in the radio propagation impact on both the localization accuracy and localization percentage. It also impact on the proper selection of the beacon points,

which results the selected beacon points communication range may not be intersect to form a constraint area.

Robustness

In the proposed scheme, the degree of irregularity has a impact on localization accuracy and localization percentage. However, the proposed scheme still mange to gives better localization accuracy and localization percentage than Ssu [38] and Galystan [40]. The robustness of the proposed scheme lies on the beginning of localization using only two beacon points, while other schemes required minimum three beacon points.

Efficiency

The high degree of irregularity impact on the appropriate selection of beacon points, which may sometimes gives overlap region and sometimes not. Still, the proposed scheme manage to localize the maximum number of sensor node with maximum localization error within the constraint limit. Besides, the Ssu [38] and Galystan [40] does not have any constraint limit to restrict the localization error. The proposed scheme only need two beacon points at the beginning to generate the candidate positions of the sensor node, while the Ssu [38] and Galystan [40] scheme demands more. Even the proposed scheme may not gives correct identification of the candidate position, the localization error can not go beyond the limit of constraint area.

The comparative results of worst case scenarios are given in the Table. 3.4. From

Table 3.4: Comparative results of worst case scenarios

Comparative Parameters	Worst Scenario of Performance Parameters	Proposed MBBRFLS		Ssu [38]		Galstyan [40]	
		Average Location Error (m)	Average Localized (%)	Average Location Error (m)	Average Localized (%)	Average Location Error (m)	Average Localized (%)
Longer Beacon Broadcasting Interval	9 m	<8 & >7	>90	<10 & >9	>85	<9 & >8	>89
Longer Communication Range	50 m	<8 & >7	>95	<10 & >9	>94	<10 & >9	>93
High Degree of Irregularity	0.05	<8 & >7	>98	<10 & >9	>96	<9 & >8	>97

the results, it is observed that the proposed scheme shows better localization accuracy and localization percentage. However, the comparison results of proposed scheme with other schemes are not far better. In the next chapter, we have proposed an another localization scheme MBBRFLS-OBPS that further improve the localization accuracy, and avoid uncertainty of differentiation using RSSI in proposed MBBRFLS.

3.7 Summary

In this chapter, we have proposed a mobile beacon based range free localization scheme (MBBRFLS). The proposed scheme is based on the analytical geometry, where arc is used as the primitive geometric shape. In this scheme, the localization begins with approximation of the arc parameters. Later, the approximated arc parameters are used to generated the chords.

The perpendicular bisector of the chords estimate the candidate positions of the sensor node. To identify the valid position, we have used the logarithmic path loss model. The lack of the differentiation capability of logarithmic path loss model leads the proposed scheme to high localization error. To enhance the localization accuracy, we have proposed another mobile beacon based range free localization scheme (MBBRFLS) using an optimized beacon points selection (OBPS). The proposed MBBRFLS-OBPS replace the demerits of logarithmic path loss based differentiation with optimized constraint area of the beacon points.

Chapter 4

MBBRFLS Using Optimized Beacon Points Selection (MBBRFLS-OBPS)

In this chapter, we have proposed a mobile beacon based range free localization scheme (MBBRFLS) using an optimized beacon points selection (OBPS). The proposed MBBRFLS-OBPS begins its localization with the selection of beacon points, that can create a differentiating residence area. Later, the differentiating residence area is used to identify the valid estimated position of the sensor node. The residence area based differentiation improves the localization accuracy. For localization, the proposed MBBRFLS-OBPS use the perpendicular bisector of chords and the approximated radius. In this scheme, we have only consider the Sagitta of an minor arc for generating the chords. Therefore, the complexity of geometric calculation is further reduced than the proposed MBBRFLS. The performance of the proposed MBBRFLS-OBPS is evaluated using simulation.

4.1 Introduction

The existing restricted area based localization scheme identify the valid estimated position of the sensor node using the restricted area [21, 27, 39, 44]. Therefore, the size of the restricted area is essential to improve the localization accuracy. In the previous proposed MBBRFLS, we have identified the valid estimated positions of the sensor node by comparing the received RSSI and RSSI derived through logarithmic path loss model. However, the unpredictability of RSSI sometimes make the invalid decision, which leads the proposed MBBRFLS to high localization error. In the proposed MBBRFLS-OBPS, we initially choose the optimal beacon points that can create a differentiating residence area. The differentiating residence area minimizes the localization error that was more in the proposed MBBRFLS. In the proposed MBBRFLS-OBPS, the localization begins with approximation of arc parameters. The approximated arc parameters includes the radius, half chord length, and Sagitta of minor arc. These approximated parameters are belongs to a assumed circle of the sensor node, which are used to generate a chord on the assumed circle. Later, the localization is performed using the geometric property, where perpendicular bisector of the chord and the approximated radius

are used to determined the center coordinate. In this scheme, we have generated the chord corresponding to the Sagitta of minor arc. Therefore, the complex of geometric calculation is further minimized. The performance of the proposed MBBRFLS-OBPS is evaluated using the different trajectories of mobile beacon (SCAN, CIRCLE, S-CURVE, SPIRAL) [66–68].

The remaining part of this chapter are as follows. Section 4.2, presents the proposed MBBRFLS using optimized beacon points selection. Section 4.3, presents the simulation and results. Section 4.4, presents the summary.

4.2 Mobile Beacon Based Range Free Localization Scheme

In this section, we have proposed a range-free localization method based on geometric formulation. Geometry has various primitive shapes such as triangle, circle, rectangle, and rings, which are used in different range-free localization methods [25–28]. In the proposed MBBRFLS-OBPS, we have used the analytical geometry, where arc is the primitive geometric shape.

The proposed MBBRFLS-OBPS have four phases. In the first phase, the sensor node estimates its residence area. In the second phase, the sensor node randomly approximates the radius and half chord length. In the third phase, the sensor node estimates the Sagitta of an arc using the approximated radius and half chord length. In the fourth phase, the sensor node estimates its position using the approximated radius, half chord length, and Sagitta of an arc.

4.2.1 Sensor Node Residence Area Formation

This the first phase of the proposed MBBRFLS-OBPS. In this phase, we have used the beacon points to create the residence area of the sensor node. The mobile beacon traverses the sensing field and periodically broadcast its current location coordinate. We assume that sensor node receives the beacon messages, once the mobile beacon enters the communication range of the sensor node. Sensor node maintains the list of the received beacon messages. Each beacon message holds the necessary information such as its current location coordinate, communication range, and transmission power level. From the information of the beacon message, the sensor node selects the three distant beacon points. Initially, the sensor node choose two distant beacon points to create the primary residence area of the sensor node, as shown in Fig. 4.1. The third distant beacon point is later used by the sensor node for differentiation purpose, as shown in Fig. 4.2.

Let L=$A, B, C, ..., n$ be the list of the beacon points recorded by the sensor node with its communication range r. To select the two distant beacon points, the sensor node calculates the euclidean distance E = $E_{AB}, E_{AC}, E_{BC}..., E_{An}, E_{Bn}$ between each beacon point of the list L. As shown in Fig. 4.1, the sensor node selects the maximum euclidean distance corresponding beacon points $B(x1, y1)$ and $C(x_2, y_2)$. The intersection of two distant

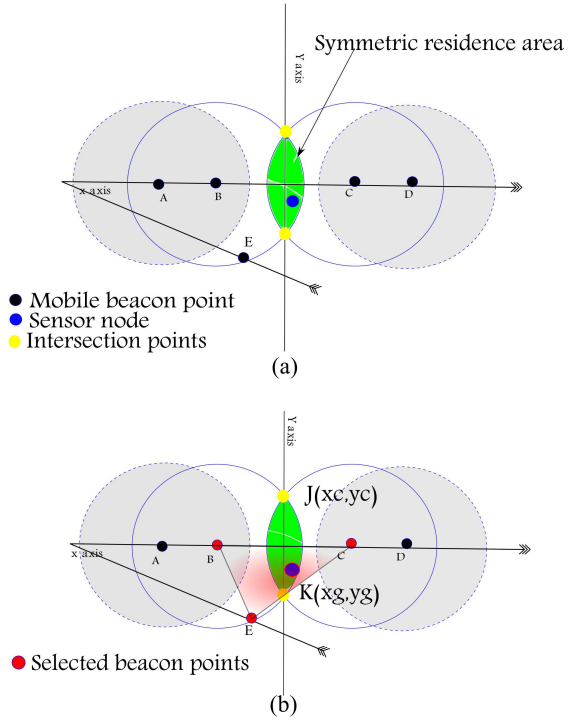

Figure 4.1: Residence area formation. (a) Primary residence area of the sensor node. (b) Optimized selection of the beacon points.

beacon point $B(x1, y1)$ and $C(x_2, y_2)$ communication range, creates the primary residence area of the sensor node, as shown in Fig 4.1(a).

$$\Delta x = x_2 - x_1 \tag{4.1}$$

$$\Delta y = y_2 - y_1 \tag{4.2}$$

$$D = \sqrt{\Delta x^2 + \Delta y^2} \tag{4.3}$$

$$D_{CL} = (D^2 + r^2 - r^2)/(2 * D) \tag{4.4}$$

$$x_c = x_1 + (\Delta x * D_{CL})/D + (\Delta y/D) * sqrt(r^2 - D_{CL}^2) \tag{4.5}$$

$$y_c = y_1 + (\Delta y * D_{CL})/D - (\Delta x/D) * sqrt(r^2 - D_{CL}^2) \tag{4.6}$$

$$x_g = x_1 + (\Delta x * D_{CL})/D - (\Delta y/D) * sqrt(r^2 - D_{CL}^2) \tag{4.7}$$

$$y_g = y_1 + (\Delta y * D_{CL})/D + (\Delta x/D) * sqrt(r^2 - D_{CL}^2), \tag{4.8}$$

where (x_c,y_c) and (x_g,y_g) be the intersection points of their communication range. The intersection coordinate (x_c,y_c) and (x_g,y_g) are designated as $J(x_c, y_c)$ and $K(x_g, y_g)$, as shown in Fig. 4.2. The line segment joining the intersection point J and K is called radical line JK.

4.2.2 Random Approximation of Radius and Half Chord Length

This is the second phase of the proposed MBBRFLS-OBPS. In this phase, we have approximated the arc parameters (radius and half length of the chord). According to the

geometry, the radius and two chord points on the circle are known, then the center coordinate of the circle can be determine. To apply the geometric property, the sensor node assumed a circle whose circumference resides on the any one the beacon point (earlier used for primary residence area formation). The other points on the assumed circle are generated using the geometry property of an arc. To approximate the two points on the circumference of the circle, we have used the analytical geometry of an arc. As shown in Fig. 4.2, a line

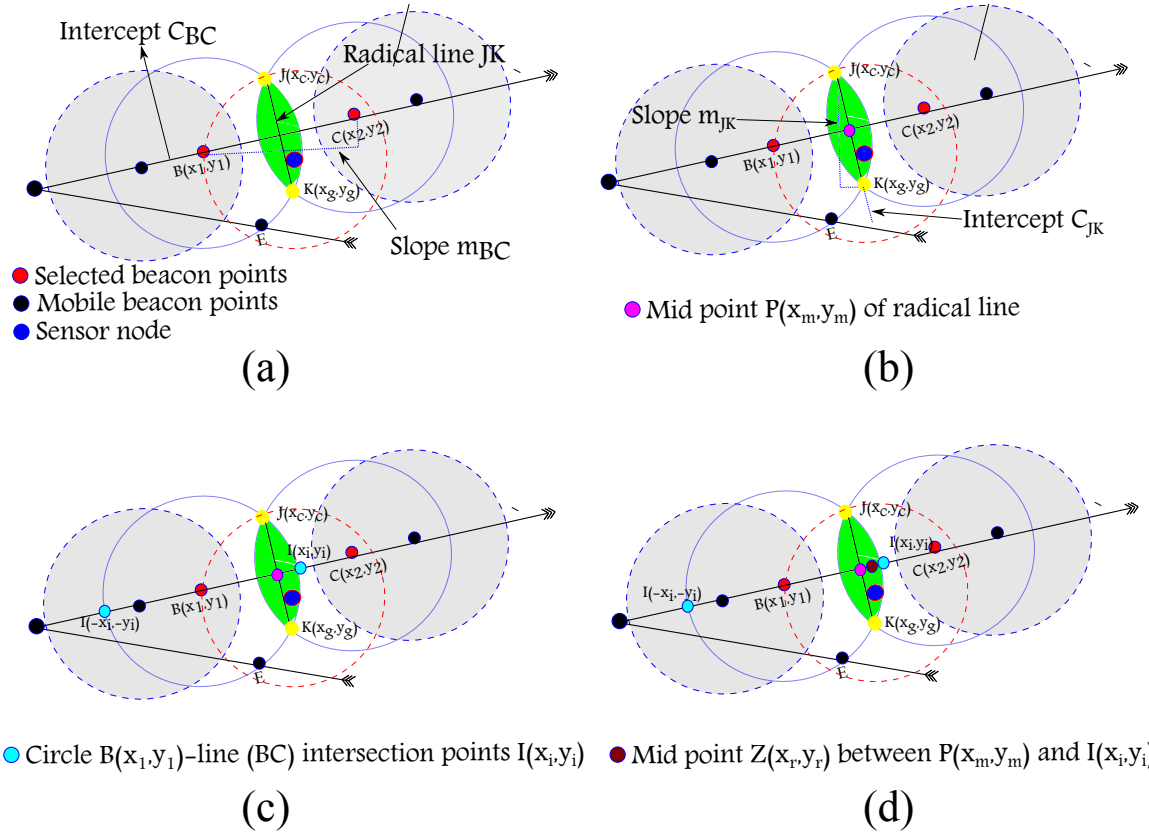

Figure 4.2: Setting the approximation range for radius and half length of the chord chord.

segment between the two distant beacon points B and C, divides the assumed circle into two consecutive arcs (major arc and minor arc). In-fact, the line segment joining the beacon points B and C is not a complete chord of the assumed circle. Rather, it has enough length to be used to estimate the radius and half chord length. For an approximation of radius and the half chord length, the sensor node randomly generates few points on the line segment BC. The generated points must be resides within the primary residence area of the sensor node. To ensure that the generated points resides within the residence area, we have required the following input parameters to set the random approximation range for radius and the half chord length.

1. Given two beacon points B(x_1,y_1) and C(x_2,y_2) as shown in Fig. 4.2(a), the slope and intercept of line BC are calculated as $m_{BC} = \frac{y_1 - y_2}{x_1 - x_2}$ and intercept $c_{BC} = -(m_{BC} * x_1) + y_1$ respectively.

2. The mid point P(x_m,y_m) of radical line is calculated as P($x_m = (x_c + x_g)/2$, $y_m = (y_c+y_g)/2$) using two intersecting points J(x_c,y_c) and K(x_g,y_g) as shown in Fig. 4.2(b).

3. The circle-line intersection point $I(x_i, y_i)$ is generated on the line segment BC through the intersection of the communication range of $B(x_1, y_1)$. The generated intersection points $I(x_i, y_i)$ and $I(-x_i, -y_i)$ are shown in Fig. 4.2(c). To choose the valid point either $I(x_i, y_i)$ or $I(-x_i, -y_i)$, the sensor node calculates the euclidean distance between $P(x_m, y_m)$ and $I(\pm x_i,\pm y_i)$ as E_p and E_n respectively. Based on the comparison between E_p and E_n as $(E_p < E_n)?(-x_i, -y_i) : (x_i, y_i)$, the sensor node selects the root which is nearer to $P(x_m, y_m)$. Let $I(x_i, y_i)$ be the circle-line intersection coordinate.

4. Fig. 4.2(d) shows the mid point $Z(x_r, y_r)$ of the residence area, which is calculated as $Z(x_r = (x_m + x_i), y_r = (y_m + y_i))$ using coordinates $P(x_m, y_m)$ and $I(x_i, y_i)$. From the earlier estimated coordinates, $P(x_m, y_m)$, $I(x_i, y_i)$, and $Z(x_r, y_r)$, we derive the euclidean distances E_{PI}, E_{PZ}, and E_{AZ} respectively. Estimated distances E_{PI}, E_{PZ}, and E_{AZ} are used to set the random approximation range for the radius and half chord length.

5. The end point coordinates of the radical line JK are $J(x_c, y_c)$ and $K(x_g, y_g)$. Its slope $m_{JK} = \frac{y_c - y_g}{x_c - x_g}$ and intercept $c_{JK} = -(m_{JK} * x_c) + y_c$ are later used to approximate the Sagitta (height) of an arc.

The distances between the generated random points and the beacon point on the assumed circle are used to represent the radius and half chord length. The geometric relation differentiate the distances as the radius and the half length of the chord. According to the geometric relation, the radius should be larger than or equal to the half length of the chord. All the earlier estimated parameters are successively applied to approximate the radius and half chord length, as shown in Fig. 4.3. The relation given below, randomly approximate the radius within the range specified as follows:

$$r_1 = E_{AZ} + E_{PI} \tag{4.9}$$

$$r_2 = E_{AZ} - E_{PZ} \tag{4.10}$$

$$R = (r_2 - r_1) * rand(k, 1) + r_1,\ k = 1, 2, ..., k_n, \tag{4.11}$$

where r_1 and r_2 are the random approximation range and R represents the random point generating function. Each random value R (R_1, R_2, R_3,...,R_n) within the range r_1 and r_2 are considered as the radius, as shown in Fig. 4.3(b). The each circle drawn against the radius r (corresponding to R) with center $B(x_1, y_1)$, intersects the lines BC and JK. Then the corresponding intersection coordinates of the circle with lines BC and JK are designated as $Q(\pm x_e,\pm y_e)$ and $F(\pm x_t,\pm y_t)$ respectively. The intersection coordinates $Q(\pm x_e,\pm y_e)$

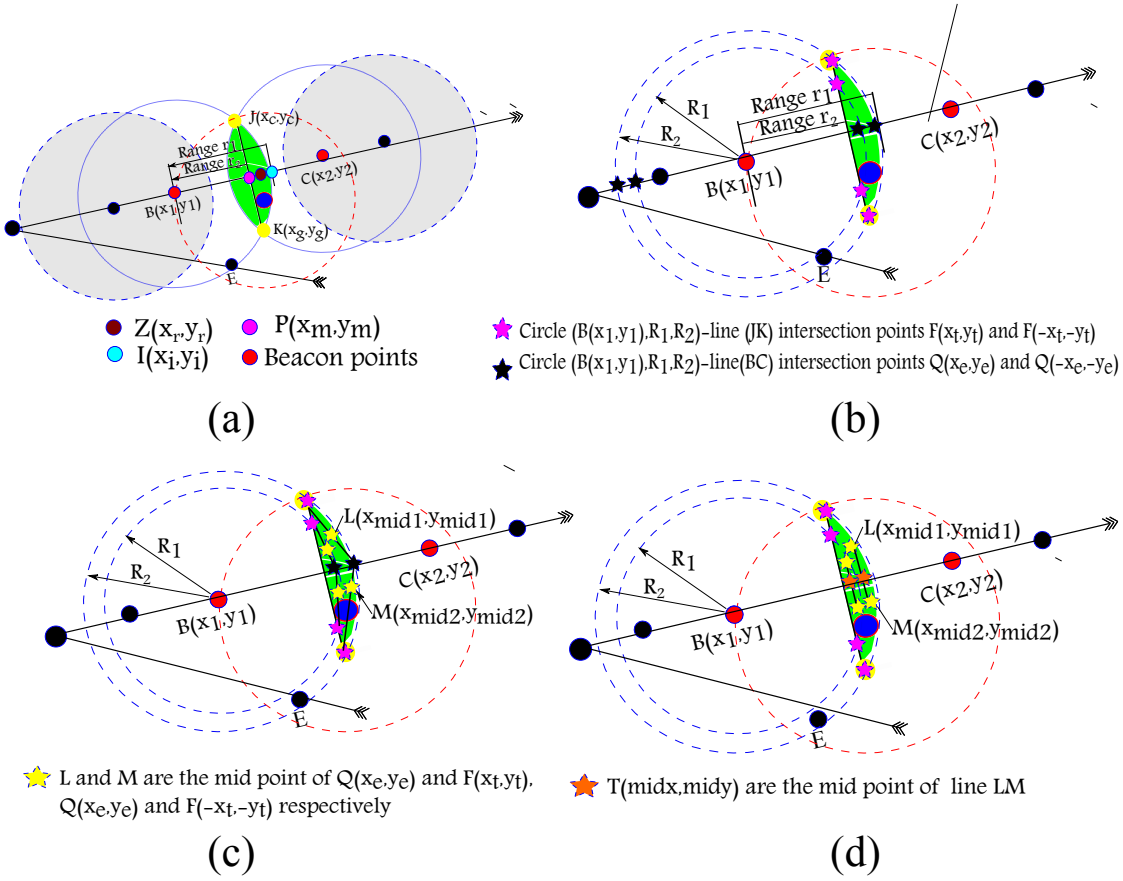

Figure 4.3: Random approximation of radius and half chord length.

and $F(\pm x_t,\pm y_t)$ are later used to approximate the half chord length. The equation of the circle with center $B(x_1, y_1)$ and the radius corresponding to the random values R (R_1, R_2, R_3,...,R_n) is shown in Eq. (4.12). After solving the Eq. (4.12) using quadratic equation, the two roots of the circle-line intersection coordinates are generated as $Q(x_e, y_e)$ or $Q(-x_e, -y_e)$.

$$(x_e - x_1)^2 + (y_e - y_1)^2 = (R)^2 \, , R = R_1, R_2, R_3, ..., R_n \tag{4.12}$$

To choose the valid root either $Q(x_e, y_e)$ or $Q(-x_e, -y_e)$, e sensor node calculates the euclidean distance between $P(x_m, y_m)$ and $Q(\pm x_e,\pm y_e)$ as E_p and E_n. Based on the comparison between E_p and E_n as $(E_p < E_n)?(-x_e, -y_e) : (x_e, y_e)$, the sensor node selects the root which is nearer to $P(x_m, y_m)$, as shown in Fig. 4.3(c). Let $Q(x_e, y_e)$ be the circle-line intersection coordinate.

To find the other intersection coordinates $F(\pm x_t,\pm y_t)$ on a radical line JK, let relabel the input coefficients of Eq. (4.12) as x_e to x_t. After rebelling the coefficients, the circle line intersection points $F(\pm x_t,\pm y_t)$ are calculated using quadratic equation. The generated two roots $F(\pm x_e,\pm y_e)$ are shown in Fig. 4.3(b). The mid point of the line segment between $Q(x_e, y_e)$ and $F(x_t, y_t)$, and $Q(x_e, y_e)$ and $F(-x_t, -y_t)$ are $L(x_{mid1} = \frac{xe+x_t}{2}, y_{mid1} = \frac{ye-x_t}{2})$ and $M(x_{mid2} = \frac{xe+x_t}{2}, y_{mid2} = \frac{ye-x_t}{2})$ respectively, as shown in Fig. 4.3(c). The

slope m_{LM} and intercept c_{LM} of the line segment between the points $L(x_{mid1}, y_{mid1})$ and $M(x_{mid2}, y_{mid2})$ are used to approximate the point on the circumference of the assumed circle, as shown in Fig. 4.3(d). The euclidean distance between the mid point $T(mid_x, mid_y)$ of the line segment LM and beacon point $B(x_1, y_1)$ estimates the half chord length E_{xy} as follows:

$$E_{xy} = \sqrt{(x_1 - mid_x)^2 + (y_1 - mid_y)^2} \tag{4.13}$$

4.2.3 Approximation of Sagitta

This is the third phase of the proposed MBBRFLS-OBPS. In this phase, we have used all the earlier estimate parameters to approximate the Sagitta of an arc. From the previous calculation, we have half chord length E_{xy}, the midpoint of the chord $T(mid_x, mid_y)$, and the radius corresponding to each random values R. All the approximated parameters are used to estimate the Sagitta of an arc. The Sagitta [73] is the vertical line from the midpoint of the chord to the arc itself, as shown in Fig. 4.4. The half chord length, Sagitta, and radius of the arc are inter-related, and if we know any two parameters, then we calculate the other parameter. Each generated random values of R and measured half chord length E_{xy} are used

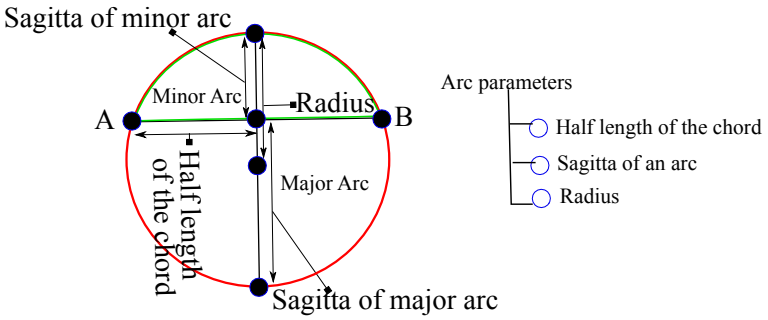

Figure 4.4: Arc of the circle.

to calculate the Sagitta of an arc as follows:

$$H = \left(\frac{\sum_{i=1}^{k} R(i)}{k}\right) \pm \sqrt{\left(\frac{\sum_{i=1}^{k} R(i)}{k}\right) - E_{xy}^2}, \tag{4.14}$$

where H represent the Sagitta of an arc, R denotes the radius of the assumed circle, E_{xy} denote the half chord length, and k denotes the number random radius corresponding to R. In this work, we have considered the Sagitta of minor arc for projecting the points on the assumed circle. Let, $N(\pm\, x_{c(1)}(k), \pm\, y_{c(1)}(k))$ are the valid projected points on the assumed circle.

4.2.4 Position Estimation and Differentiation

This is the final phase of the proposed MBBRFLS-OBPS. In this phase, we have estimated the valid position of the sensor node using the perpendicular bisector of the chord and the

approximated radius. Each generated root N($\pm x_v$,$\pm\ y_v$) corresponding to the H of an minor arc are shown in Fig. 4.5(a). Table. 4.1, shows all combination of the points N($\pm x_v$,$\pm y_v$) and B(x_1,y_1). Let combination of beacon points B(x_1,y_1) and N(x_v,y_v) generates a chord

Table 4.1: Combination of generated chord points

All combination of chord points	
Chord Point 1	**Chord Point 2**
B(x_1,y_1)	N(x_v,y_v)
B(x_1,y_1)	N($-x_v$,$-y_v$)

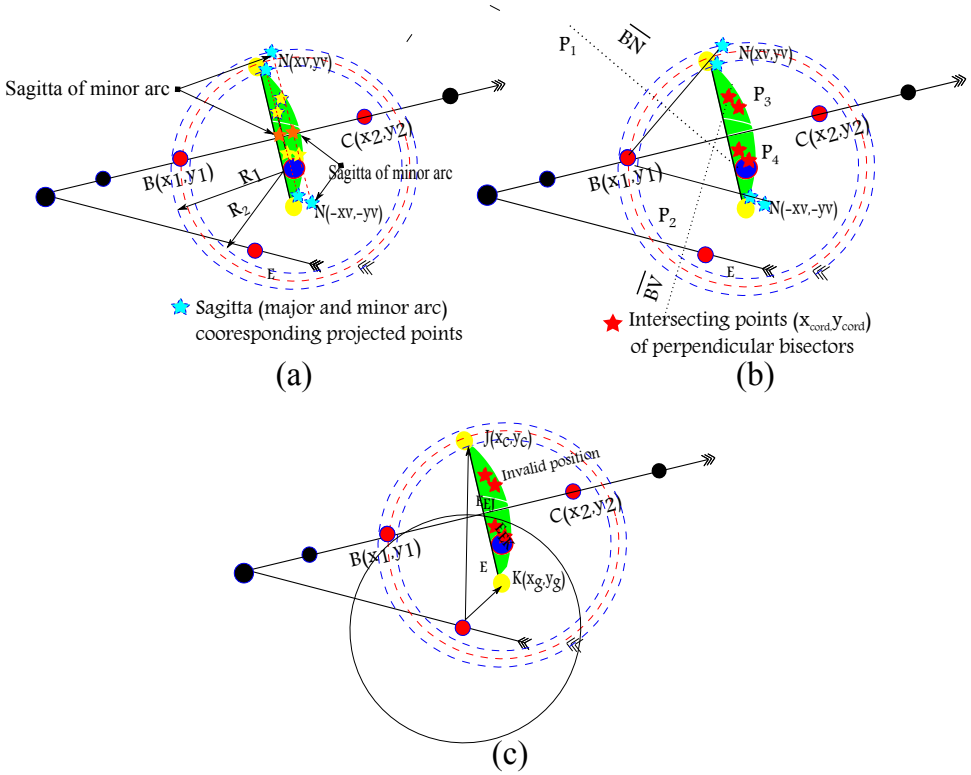

Figure 4.5: Final position estimation and differentiation. (a) Sagitta of minor arc corresponding projected points on the assumed circle. (b) Perpendicular bisector of chords $\overline{BN}$ and $\overline{BV}$ corresponding candidate positions of the sensor node. (c) Identify the valid candidate position using the third beacon point of the selected list.

$\overline{BN}$, and B(x_1,y_1) and N(-x_v,-y_v) generates a chord $\overline{BV}$, as shown in Fig. 4.5(b). Each individual random values R is considered as the radius r of the assumed circle. Sensor node decides the valid combination of beacon points B(x_1,y_1) with N(x_v,y_v) or N(-x_v,-y_v) based on the third beacon point M(x_3,y_3).

To differentiate the valid combination of beacon points B(x_1,y_1) with N(x_v,y_v) or N(-x_v,-y_v), the sensor node measures the euclidean distance E_{MJ} and E_{MK} between the third beacon point M(x_3,y_3) and the end point of radical line J(x_c,y_c) and K(x_g,y_g). Based on the comparison of estimated euclidean distance E_{MJ} and E_{MK}, the sensor node further redefine its residence area, which is near to the third beacon point M(x_3,y_3). The new residence area

of the sensor node belongs to the major arc of the assumed circle, as shown in Fig. 4.5(b). The previous comparison of euclidean distances E_{MJ} and E_{MK} differentiates the major arc and minor arc of the assumed circle. To differentiate the valid projected points N($\pm x_v$,$\pm y_v$), the sensor node further calculates the euclidean distance between the approximated points N($\pm x_v$,$\pm y_v$) and the end points of the radical line J(x_c,y_c) and K(x_g,y_g). The comparison of euclidean distance E_{MJ} and E_{MK} generates two conditions for selection of the valid point either N(x_v,y_v) or N(-x_v,-y_v) as follows:

$$IF\ E_{MJ} < E_{MK}: \tag{4.15}$$

$$E_{JN} = \sqrt{(x_c - x_v)^2 + (y_c - y_v)^2} \tag{4.16}$$

$$E_{JV} = \sqrt{(x_c + x_v)^2 + (y_c + y_v)^2} \tag{4.17}$$

$$(E_{JN} > E_{JV})?(x_v, y_v) : (-x_v, -y_v) \tag{4.18}$$

$$ELSE: \tag{4.19}$$

$$E_{KN} = \sqrt{(x_g - x_v)^2 + (y_c - y_v)^2} \tag{4.20}$$

$$E_{KV} = \sqrt{(x_g + x_v)^2 + (y_c + y_v)^2} \tag{4.21}$$

$$(E_{KN} < E_{KV})?(x_v, y_v) : (-x_v, -y_v) \tag{4.22}$$

$$END \tag{4.23}$$

Based on the above comparison sensor node is able to select the valid point either N(x_v,y_v) or N(-x_v,-y_v). After identification of the valid point, sensor node estimates its position. Let N(x_v,y_v) be the valid point in combination with the beacon point B(x_1,y_1), and the radius corresponding to each R.

$$Q = \sqrt{(x_1 - x_v)^2 + (y_1 - y_v)^2} \tag{4.24}$$

$$Mid_x = (x_1 + x_v)/2 \tag{4.25}$$

$$Mid_y = (y_1 + y_v)/2 \tag{4.26}$$

$$x_{pos1} = Mid_x + \sqrt{(R^2 - (Q/2)^2)} * (y_1 - y_v)/Q \tag{4.27}$$

$$y_{pos1} = Mid_y + \sqrt{(R^2 - (Q/2)^2)} * (x_1 - x_v)/Q \tag{4.28}$$

$$x_{pos2} = Mid_x - \sqrt{(R^2 - (Q/2)^2)} * (y_1 - y_v)/Q \tag{4.29}$$

$$y_{pos2} = Mid_y - \sqrt{(R^2 - (Q/2)^2)} * (x_1 - x_v)/Q, \tag{4.30}$$

where Q is the chord length of the assumed circle between the beacon points B(x_1,y_1) and N(x_v,y_v), and (Mid_x,Mid_y) is the mid point of the chord $\overline{BN}$. Each random value R corresponding to the radius estimates the position (x_{pos1},y_{pos1}) and (x_{pos2},y_{pos2}). Sensor node applies the polygon test for identification of its valid position either (x_{pos1},y_{pos1})

or (x_{pos2},y_{pos2}). Whichever coordinate either (x_{pos1},y_{pos1}) or (x_{pos2},y_{pos2}) lies within the residence area, sensor node identifies its position with that coordinate, as shown in Fig. 4.5 (c). The final position of the sensor node is considered as the average of the all the estimation positions corresponding to the random value R. Let the estimated positions are (x_{pos1},y_{pos1}). Then the average of these positions are store in x_p and y_p as $x_p = \left(\frac{\sum_{i=1}^{k} x_{pos1}(i)}{k}\right)$ and $y_p = \left(\frac{\sum_{i=1}^{k} y_{pos1}(i)}{k}\right)$.

4.3 Simulation And Results

The performance of the proposed MBBRFLS-OBPS is evaluated using MATLAB R2013a (8.1.0.604). Table. 4.2 shows the simulation parameters and values. For performance

Table 4.2: Simulation Parameters

Parameters	Values
Network size (m^2)	100x100
Number of sensor nodes (n)	100, 200, 300
Communication range (r)	20, 30, 40
DOI	0, 0.01, 0.02, 0.03, 0.04, 0.05
Number of mobile beacon	1
Beacon broadcasting intervals	3 m, 5 m, 7 m

evaluation, the sensor nodes are randomly deployed in an area of size 100×100 m^2, where a mobile beacon traverses the network in the predefined trajectories [66–68] such as HILBERT, CIRCLE, S-CURVE, and SPIRAL. In the first set, we have evaluated the performance by considering various influencing factors such as communication range, sensor deployment density, and radio propagation irregularity. In the second set, we have evaluated the performance at four different trajectories under same simulation parameters. In the third set, we have compared the simulation outcome of each trajectory and its impact on localization accuracy. Finally, we have compared the performance of the proposed MBBRFLS-OBPS with Ssu [38], Galstyan [40], and Singh [44] schemes.

4.3.1 Performance At Varying DOI

In this section, we evaluate the performance of the proposed MBBRFLS-OBPS at varying degree of irregularity, where DOI defines the path loss per unit degree change in direction. The radio irregularity model (RIM) [25] is used to represent the various irregularity in radio propagation, which is defined as follows:

$$K_i = \begin{cases} 1, & i = 0, \\ K_{i-1} \pm Rand * DOI, & 0 < i < 360, i \in N, \end{cases} \tag{4.31}$$

where $|K_0 - K_{359}| \leq DOI$, K_i represents the coefficient of path loss for per unit degree change in direction(0 to 360 degree). In Fig. 4.6, we have shown the different DOI corresponding irregular communication patterns. To evaluate the performance, we have

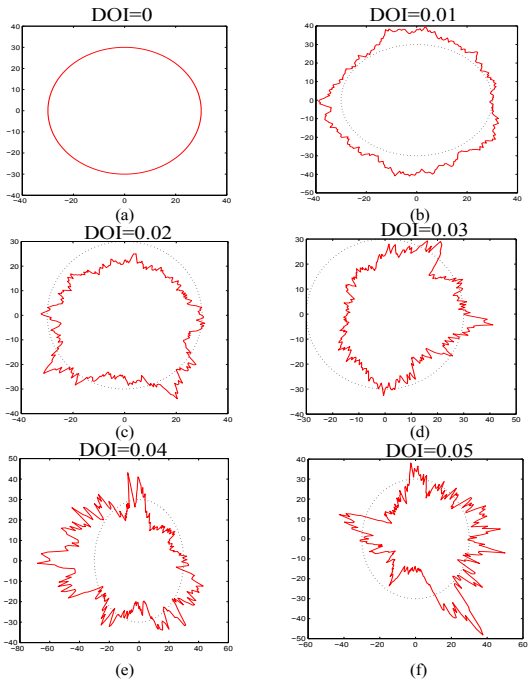

Figure 4.6: Radio propagation pattern at different values of DOI.

set the simulation with the beacon broadcasting interval of 5 m, communication range of 20 m, and varying DOI (0 to 0.05). From Fig. 4.7, it is observed that as DOI is increased

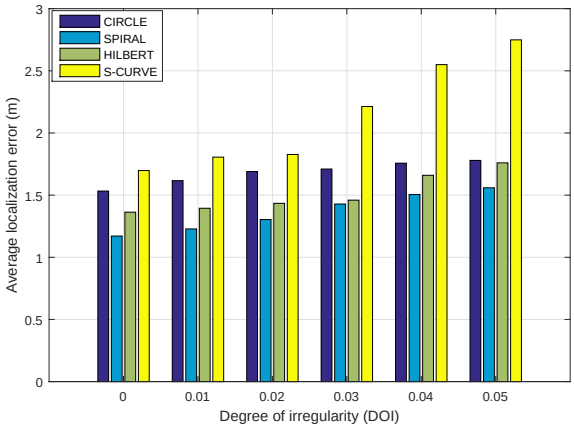

Figure 4.7: Performance evaluation at varying DOI versus average localization error.

the localization error also increased. In CIRCLE, SPIRAL, and S-CURVE trajectories of a mobile beacon, it is observed that the sensor nodes which reside at the corners of the network have a significant position estimation error as compared to the nodes lying near the center area of the network. The DOI affects the homogeneity of radio propagation, resulting the sensor nodes lies at the corner of the network receives less number of beacon points.

The less number of beacon points reduces the options for the sensor nodes to minimize its residence area, which leads to high localization error. In HILBERT trajectories, the mobile beacon uniformly cover the entire network, which improves the beacon points options for the sensor nodes. However, the linear movement of a mobile beacon using HILBERT trajectory shows 10.05 % high localization error than SPIRAL trajectory. Besides, a mobile beacon on SPIRAL trajectory shows 18.96 %, 10.05 %, 34.88 % less localization error than CIRCLE, HILBERT, and S-CURVE trajectory, respectively. The average localization error at DOI of 0.05 for CIRCLE, SPIRAL, HILBERT, and S-CURVE trajectories are 2.3 m, 2.4 m, 2.2 m, and 2.3 m, respectively.

4.3.2 Performance At Varying Communication Range

The communication range has great significance to improve the covering of the network with less mobility. The simulation is performed on each trajectory using varying communication range, beacon broadcasting interval of 5 m, and DOI of 0.05. From Fig. 4.8, it is observed

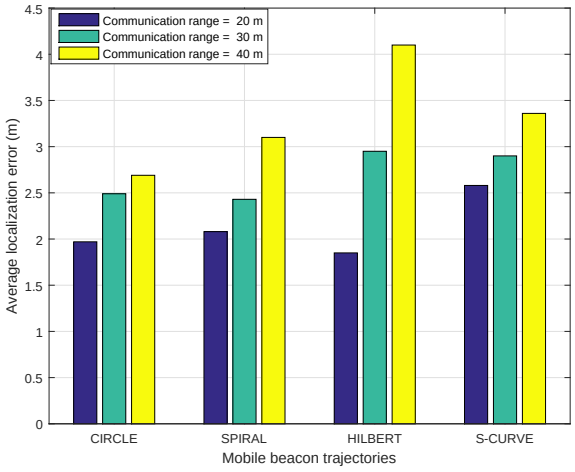

Figure 4.8: Performance evaluation at varying communication range versus average localization error

that HILBERT trajectory at the communication range of 40 m shows high localization error as compared to other trajectories of a mobile beacon. The mobile beacon using HILBERT trajectory generates large quantity the linear beacon points, which influence the minimization of the initial residence area of the sensor node. The longer communication range and less number of non-linear beacon points degrade the localization accuracy. Besides, the mobile beacon using CIRCLE, SPIRAL and S-CURVE trajectories generates the enough quantity of non-linear beacon points, which provides the sufficient options for the sensor nodes to minimize its residence area. Therefore, the mobile beacon at longer communication range and using CIRCLE, SPIRAL, and S-CURVE trajectories shows less localization error. However, the non-linear movement of trajectories usually inefficient to cover the entire network, which leads the few sensor node to shows high localization error. The

mobile beacon using HILBERT trajectory and communication range of 40 m shows 34.3 %, 24.3%, and 18 % high localization error than CIRCLE, SPIRAL, and S-CURVE trajectory, respectively. Besides, the mobile beacon using CIRCLE trajectory and communication range of 40 m shows 13.2 %, 34.3 %, and 19.9 % less localization error than SPIRAL, HILBERT, and S-CURVE trajectory, respectively. The mobile beacon using CIRCLE, SPIRAL, S-CURVE, and HILBERT trajectories along with varying communication, shows the average localization error less than 2.5 m, 2.6 m, 3 m, and 2.1 m respectively.

4.3.3 Performance At Varying Deployed Density

The performance of the proposed MBBRFLS-OBPS is evaluated at varying deployment density of the sensor nodes. The simulation is performed using beacon broadcasting interval of 5 m, DOI of 0.05, and communication range of 20 m. From Fig. 4.9, It is observed that

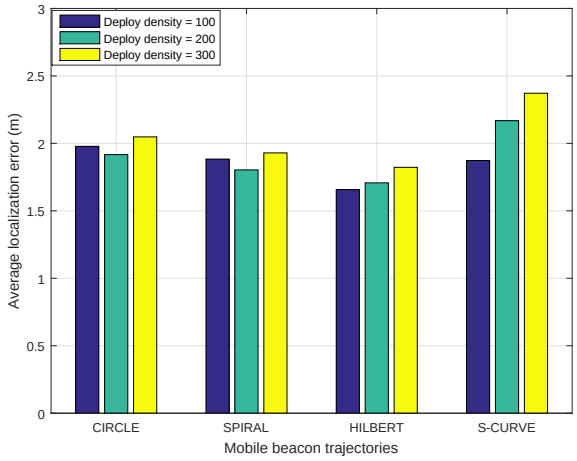

Figure 4.9: Performance evaluation at different deployed density versus average localization error

the mobile beacon using HILBERT trajectory on the deployment density of 100 shows 18.7 %, 12.3 %, and 11.7 % less localization error, than using CIRCLE, SPIRAL, and S-CURVE trajectories. Similarly, at the deployment density of 300, the mobile beacon using HILBERT trajectory shows 22.1 %, 5.2 %, and 11.9 % less localization error than CIRCLE, SPIRAL, and S-CURVE trajectories respectively. The varying deployment density of the sensor node has the minor impact on the localization accuracy. Rather, the density of the beacon points impact the localization accuracy. At high density of the beacon points, the sensor node has enough choices to minimize its residence area. The mobile beacon using different trajectory on different deployment density, the average localization error is below 2 m.

4.3.4 Performance At Varying Beacon Broadcasting Interval

In any mobile beacon based localization schemes, the beacon broadcasting interval has a significant impact on the localization accuracy. To evaluate the performance at

varying beacon broadcasting interval, the simulation is performed using the DOI of 0.05, communication range of 20 m, and different trajectories of mobile beacon. From Fig. 4.10,

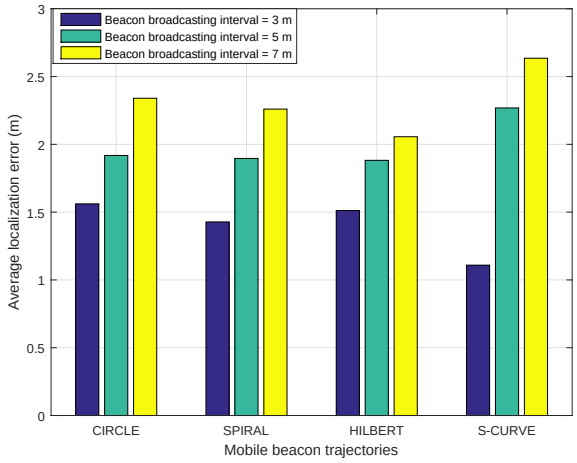

Figure 4.10: Performance evaluation at different beacon broadcasting interval versus average localization error

it is observed that as the beacon broadcasting interval is increased the localization error is also increased. The longer beacon broadcasting interval reduces the density of the beacon points, resulting few sensor node has less options to minimize its residence area. Therefore, sensor node shows high localization error on the longer beacon broadcasting interval of the mobile beacon. The mobile beacon using S-CURVE trajectory and the beacon broadcasting interval of 3 m shows 28.9 %, 22.3 %, and 26.6 % less localization error than CIRCLE, SPIRAL, and HILBERT respectively. Similarly, the mobile beacon using the HILBERT trajectory and the beacon broadcasting interval of 7 m shows 12.1 %, 9.2 %, and 4 % less localization error than CIRCLE, SPIRAL, and S-CURVE trajectories respectively. The average localization error at all the beacon broadcasting intervals using CIRCLE, SPIRAL, S-CURVE, and HILBERT trajectories are 2.2 m, 1.89 m, 1.69 m, and 1.5 m respectively.

4.3.5 Simulation on CIRCLE, SPIRAL, S-CURVE and HILBERT Trajectory

The performance of the proposed MBBRFLS-OBPS has been evaluated using different trajectories of a mobile beacon with beacon broadcasting interval of 5 m, communication range of 20 m, and DOI of 0.05. Each trajectory has a unique shape and ability to cover the entire network. The simulation outcome of the proposed MBBRFLS-OBPS using CIRCLE, SPIRAL, HILBERT, and S-CURVE trajectories are shown in Fig. 4.11. The average localization error using the CIRCLE, SPIRAL, HILBERT, and S-CURVE trajectories are 1.8 m, 1.9 m, 1.95 m, and 2 m respectively.

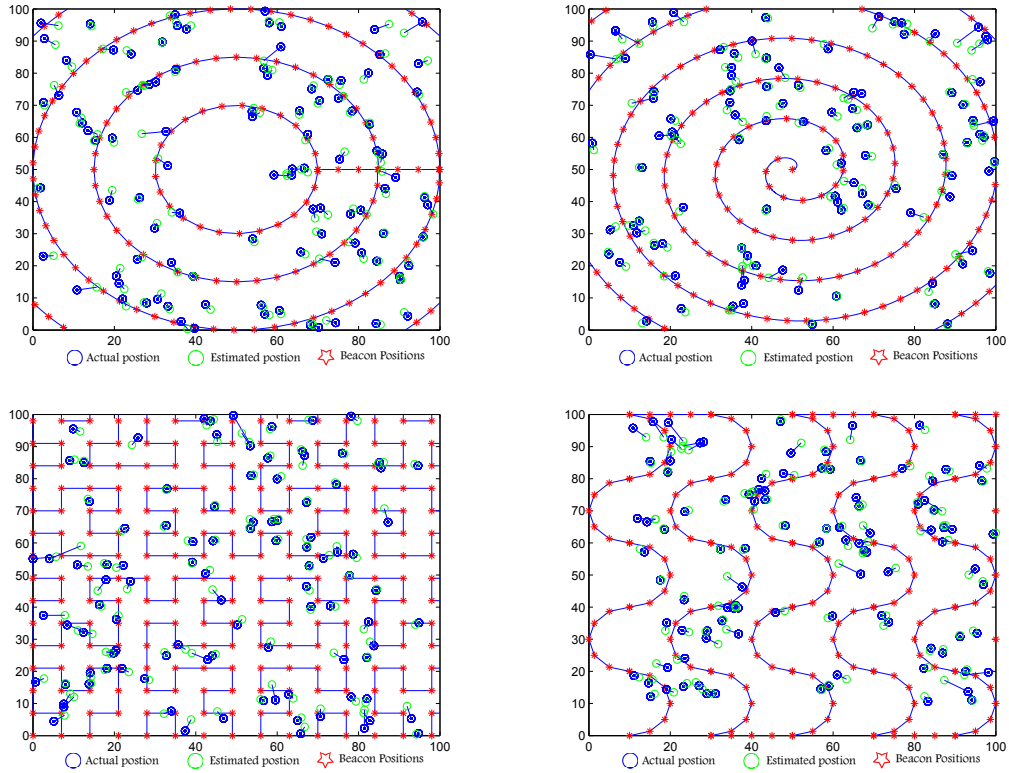

Figure 4.11: Simulation outcome of the proposed MBBRFLS-OBPS using CIRCLE, SPIRAL, HILBERT, and S-CURVE trajectories

4.3.6 Performance Comparison of MBBRFLS-OBPS

In this section, we have performed the simulation comparison of the proposed MBBRFLS-OBPS with Ssu [38], Galstyan [40], and Singh [44] schemes. The performance is evaluated using different trajectories of a mobile beacon with beacon broadcasting interval of 5 m, communication range of 20 m, and varying DOI from 0 to 0.05. From Fig. 4.12 (a), it is observed that the MBBRFLS-OBPS, Singh, Ssu, and Galystan schemes using the CIRCLE trajectory with DOI of 0.05 shows average localization error of 1.7794 m, 6.89 m, 9.56 m, and 8.35 m respectively. In Fig. 4.12 (b), the proposed MBBRFLS-OBPS, Singh, Ssu, and Galystan schemes using the SPIRAL trajectory with DOI of 0.05 shows 1.3993 m, 6.19 m, 9.356 m, and 8.565 m respectively. In Fig. 4.12 (c),the proposed MBBRFLS-OBPS, Singh, Ssu, and Galystan schemes using the HILBERT trajectory with DOI of 0.05 shows 1.7993 m, 7.358 m, 9.856 m, and 8.865 m respectively. Finally, the proposed MBBRFLS-OBPS, Singh, Ssu, and Galystan schemes using the S-CURVE trajectory with DOI of 0.05 shows 2.690 m, 7.758 m,10.156 m, and 9.865 m respectively. From the results, it is observed that Ssu scheme at DOI of 0.05 shows high localization error than the proposed MBBRFLS-OBPS, Singh, and Galystan schemes. The high DOI influence the uniformity of the radio propagation, resulting the sensor nodes are failed to identity the near far relationship among the received beacon points. In Ssu scheme, the localization is performed using the perpendicular bisector

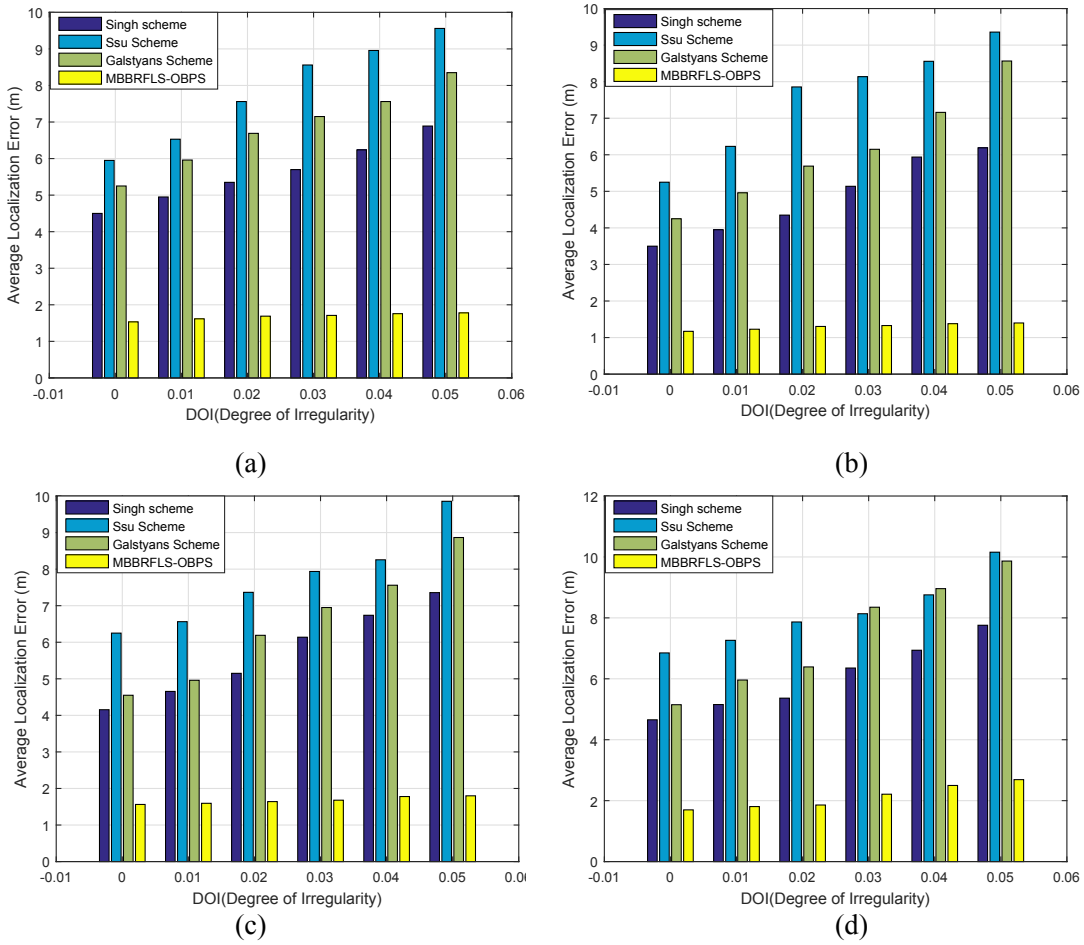

Figure 4.12: Simulation comparison of the proposed MBBRFLS-OBPS with Ssu [38], Galstyan [40], and Singh [44] schemes using CIRCLE, SPIRAL, HILBERT, and S-CURVE trajectories respectively.

of the chords (the line segment between the selected beacon points). Due to DOI, the selected beacon points are not exactly resides at the boundary of the sensor node communication range. Therefore, the perpendicular bisector of the chords between the selected anchor points leads the Ssu scheme to show high localization error. Similarly, the Singh scheme use the beacon points to create the residence area of the sensor node. Later, the residence area is used to approximate the arc parameters (radius, half length of the chord and Sagitta of an arc). The approximated arc parameters are used to generate the chords on the assumed circle of the sensor node. Later, the perpendicular bisector of the chord determines the position of the sensor node. Therefore, the inappropriate selection of the beacon points influence the approximation accuracy, which leads the Singh scheme to shows high localization error. Besides, Singh scheme has the lack of differentiation capability to identity the valid estimated position of the sensor node. In Galystan scheme, the sensor node uses the less number of the beacon points to create its residence area. Therefore, the less number of delimit area corresponding to the inappropriate beacon points leads the Galystan scheme to show high localization error. On the other hand, the proposed MBBRFLS-OBPS even at the inappropriate selection of beacon points is able to shows less localization error than

Ssu, Galystan, and Singh scheme. In the proposed MBBRFLS-OBPS, the inappropriate beacon points increases the size of the residence area, which degrade the approximation accuracy. However, even at the lager size of the residence area the large quantity of the sensor nodes improves the approximation accuracy by generating more number of random points. The average localization error of the proposed MBBRFLS-OBPS using CIRCLE, SPIRAL, HILBERT and S-CURVE trajectories are 1.7794 m, 1.3993 m, 1.7993 m, and 2.690 m respectively.

4.4 Comparative Strength And Weakness

In this section, we have further taken the overhead to compare the strength and weakness of the proposed MBBRFLS-OBPS scheme with other schemes. The performance comparison of the proposed MBBRFLS-OBPS with other schemes is given in Table. 4.3. Where N

Table 4.3: Comparative strength and weakness

Performance parameters	MBBRFLS-OBPS	Singh [44]	Ssu [38]	Galystan [40]
Accuracy	Good	Fair	Fair	Fair
Node Density	>0	>0	>0	>0
Beacon Heard	>2	>2	>3	>3
DOI	Good	Good	Fair	Fair
GPS error	Good	Good	Good	Good
Scalability	Good	Fair	Good	Fair
Communication Overhead	N	N	N	N
Time Complexity	O(N^2)	O(N^2)	O(N^2)	O(N^2)
Energy efficiency	Good	Good	Good	Good

designate the total number of the beacon points.

4.5 Analysis of Robustness and Efficiency

To analyze the robustness and efficiency of the proposed scheme with other schemes, we have taken the worst case scenarios of performance evaluating parameters. The worst scenarios of performance parameters are longer beacon broadcasting interval of 9 m, longer communication range of 50 m, and radio propagation irregularity of 0.05. Besides, that we have also consider the mobile trajectories and its impact on localization accuracy. In proposed MBBRFLS-OBPS, the localization is begins through optimized selection of beacon points, that gives smaller size of the constraint area. The smaller size of constraint area further reduce the maximum localization error within the constraint limit. Besides, the optimized selection of the beacon points easily identify the correct candidate position of the sensor node. Hence, the failure of correct identification due to RSSI based differentiation has been avoided in proposed MBBRFLS-OBPS. Therefore, the uncertainty in identification of candidate position can not further increases the average localization error in proposed scheme

MBBRFLS-OBPS. The robustness and efficiency analysis as discussed in Chapter 3 under Section 3.7 is same applicable for proposed MBBRFLS-OBPS.

The comparative results of worst case scenarios are given in the Table. 4.4. From

Table 4.4: Comparative result in worst case scenarios

Mobile Beacon Trajectories	Proposed MBBRFLS-OBPS		Ssu [38]		Galstyan [40]		Singh [44]	
	Average Location Error (m)	Average Localized (%)	Average Location Error (m)	Average Localized (%)	Average Location Error (m)	Average Localized (%)	Average Location error	Average Localized (%)
CIRCLE	<2.5 & >2	>96	<10 & >9	>95	<9 & >8	>95	<7 & >6	>95
SPIRAL	<2 & >1.5	>99	<10 & >9	>98	<10 & >9	>99	<6 & >5	>99
HILBERT	<2 & >1.6	>98	<10 & >9	>93	<9 & >8	>95	<8 & >7	>98
S-CURVE	<2.5 & >2	>95	<10 & >9	>92	<10 & >9	>96	<7 & >6	>97

the result, it is observed that the proposed MBBRFLS-OBPS scheme provide the less localization error than others schemes in worst case scenarios of performance parameters.

4.6 Summary

In this chapter, we have proposed a mobile beacon based range free localization scheme (MBBRFLS) using an optimized beacon points selection (OBPS). The proposed MBBRFLS-OBPS scheme create the differentiating residence area using the optimized beacon points. Therefore, the increased localization error using the logarithmic path loss model in the MBBRFLS is further reduced in the proposed MBBRFLS-OBPS. The proposed MBBRFLS-OBPS localizes the sensor nodes using the perpendicular bisector of the chord and the approximated radius. In this scheme, the chord is generated corresponding to the Sagitta of the minor arc. Therefore, the complexity of geometric calculation is reduced in the proposed MBBRFLS-OBPS. The performance of the proposed scheme is evaluated using the simulation. The metric used for performance evaluation are communication range, beacon broadcasting interval, degree of irregularity, and various trajectories of mobile beacon. To further improve the localization accuracy, we have proposed an another mobile beacon based range free localization scheme (MBBRFLS) using an optimized residence area formation (ORAF).

Chapter 5

MBBRFLS Using Optimized Residence Area Formation (ORAF)

In this chapter, we have proposed a mobile beacon based range free localization scheme (MBBRFLS) using an optimized residence area formation (ORAF). The proposed MBBRFLS-ORAF improved the approximation accuracy of the arc parameters, using the adaptive mechanism. The adaptive mechanism defines the number of the variant types of random points required for different size of the constraint area. Therefore, the complexity of geometric calculation using constant number of random points is further reduced in the proposed MBBRFLS-ORAF. The performance of the proposed MBBRFLS-ORAF is evaluated using the simulation as well as the experimental validation.

5.1 Introduction

The traditional constraint area based localization schemes are not adaptive according to the different size of the constraint area. Therefore, the larger size of the constraint area degrade the localization accuracy [25–28]. The adaptive mechanism in the proposed MBBRFLS-ORAF defines the number of the random points required for different size of the constraint area. The proposed MBBRFLS-ORAF use the constraint area for approximation of the arc parameters. To enhance the approximation accuracy at different size of the constraint area, we have used the adaptive mechanism. The adaptive mechanism is useful for the sensor nodes which have less options of the beacon points to minimize its residence area. This mechanism enabled the proposed MBBRFLS-ORAF to localize the sensor node even in the sparse network with less localization error. Besides, the proposed MBBRFLS-ORAF minimized the constraint area using the three non-collinear beacon points, which further improves the approximation accuracy. In the previous proposed MBBRFLS-OBPS, the primary residence area of two distance beacon points is used for approximation. Therefore, the larger size of the constraint area degrade the localization accuracy. The proposed MBBRFLS-ORAF use the similar mechanisms as proposed in the MBBRFLS-OBPS, where the perpendicular bisector of the chords and the approximated radius are used for localization. The performance of the proposed MBBRFLS-ORAF is evaluated using the simulation as well as experimental validation.

The remaining part of this chapter are as follows. Section 5.2, presents MBBRFLS using optimized residence area formation. Section 5.3, presents simulation and results. Section 5.4, presents the experiment using prototype test bench. Section 5.5, presents the conclusion.

5.2 MBBRFLS-ORAF Based On Analytical Geometry

The proposed MBBRFLS-ORAF is based on the analytical geometry , where arc is used as the primitive geometric shape. Our mechanism use a mobile beacon to assist other sensor nodes to perform its localization.

The proposed MBBRFLS-ORAF has been divided into five phases as follows:

- Beacon points selection
- Sensor node constraint area formation
- Random approximation of arc parameters
- Approximate the Sagitta (height) of the minor arc.
- Localization performed using the approximated arc parameters.

5.2.1 Beacon Points Selection

In the proposed MBBRFLS-ORAF, the mobile beacon traverses the sensing field using the random way-point mobility (RWP) model [71]. The mobile beacon periodically broadcast the beacon messages, while the static sensor collects the beacon messages. From the collected beacon information, the sensor node identify the beacon points (location coordinates) and the communication range of the mobile beacon. From the collected beacon points, the sensor node choose the three non-collinear beacon points. The selections of the beacon points are based on the larger perimeter of their combination. Fig. 5.1(a) shows the sensor node selects the three beacon points $B_1(x_1, y_1)$, $B_2(x_2, y_2)$, and $B_3(x_3, y_3)$. The sum of the euclidean distances measured between the beacon points B_1B_2, B_1B_3, and B_2B_3 gives the perimeter of their combination. If greater the perimeter of their combination, than smaller the constraint area of the sensor node. The constraint area is created using the communication range of the selected beacon points.

5.2.2 Sensor Node Residential Area Formation

From the selected beacon points $B_1(x_1, y_1)$, $B_2(x_2, y_2)$, and $B_3(x_3, y_3)$, the sensor node initially choose two distant beacon points. For simplicity of analysis, we consider $B_1(x_1, y_1)$ and $B_3(x_3, y_3)$ as the selected beacon points. The intersection of the selected beacon points

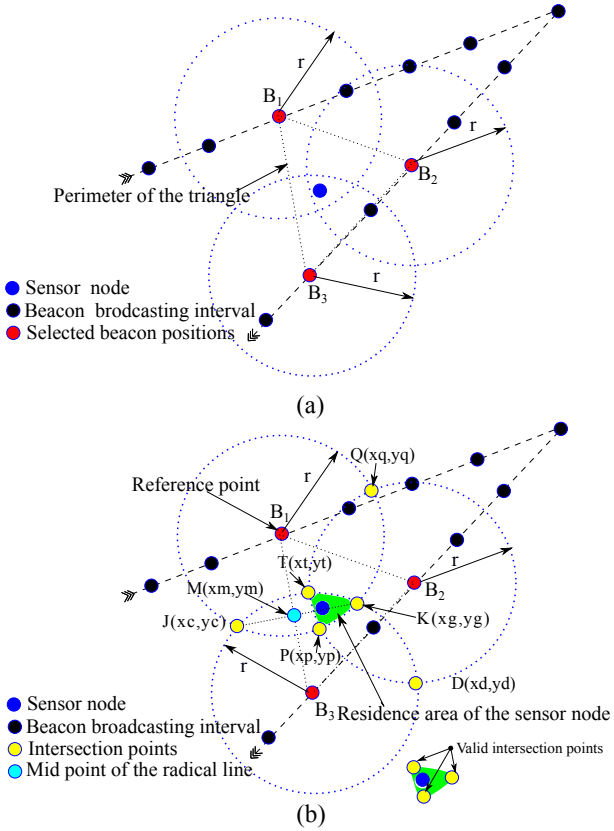

Figure 5.1: Constraint area formation. (a) Beacon points selection based on the perimeter of their combination. (b) Identification of the valid intersection vertex.

creates the initial constraint area of the sensor node. The intersection area of the two circles with center $B_1(x_1, y_1)$, $B_3(x_3, y_3)$, and equal radii r can be represented as:

$$(x - x_1)^2 + (y - y_1)^2 \leq r^2 \tag{5.1}$$

$$(x - x_2)^2 + (y - y_2)^2 \leq r^2 \tag{5.2}$$

The generated intersection area has two vertices named as $J(x_c, y_c)$ and $K(x_g, y_g)$, as shown in Fig. 5.1(b). To identify which one is the valid intersection vertex, the sensor node calculates the euclidean distance with the beacon point $B_2(x_2, y_2)$. The lesser distance corresponding vertex is the valid vertex of the constraint area. From Fig. 5.1(b), we can see $K(x_g, y_g)$ as the valid intersection vertex.

Later, the intersection of the beacon point $B_2(x_2, y_2)$ further minimizes the initial residence area of the sensor node. During the minimization of the initial residence area, the sensor node performs two intersections between the circles. The first intersection is performed between the circles with center $B_2(x_2, y_2)$ and $B_1(x_1, y_1)$ with equal radii r. The generated intersection area has two vertices named as $P(x_p, y_p)$ and $Q(x_q, y_q)$. To find which one is the valid vertex, the sensor node calculates the euclidean distance with the mid point $M(x_m = (x_c + x_g)/2, y_m = (y_c + y_g)/2)$ of the radical line between $J(x_c, y_c)$ and $K(x_g, y_g)$. The lesser distance corresponding vertex either $P(x_p, y_p)$ or $Q(x_q, y_q)$ is the valid vertex of

the constraint area. Similarly, the sensor node perform other intersections between the circles with center $B_2(x_2, y_2)$ and $B_3(x_3, y_3)$ with equal radii r. To identify the valid intersection vertices between $T(x_t, y_t)$ and $D(x_d, y_d)$, the sensor node apply the same procedure. From Fig. 5.1(b), the valid intersection vertices of the constraint area are $P(x_p, y_p)$ and $T(x_t, y_t)$.

5.2.3 Random Approximation of Radius and Half Chord Length

To approximate the arc parameters, the sensor node select one of the beacon point (from the selected beacon points) as the reference point. The selection is made randomly between the two distant beacon points $B_1(x_1, y_1)$ or $B_3(x_3, y_3)$. From Fig 5.2(a), we can see $B_1(x_1, y_1)$ as the selected reference point. After selecting the reference point, the sensor node assumes a circle whose circumference passes through the selected reference point. The line segment between the beacon point $B_1(x_1, y_1)$ and $B_3(x_3, y_3)$ divides the assumed circle into two halves called major arc and minor arc. In fact, the line segment is not a complete chord of the assumed circle, but it has the enough length to be used to approximate the half chord length and the radius of the assumed circle. For the approximation, the sensor node generate few (3 or 5) random points on the line segment connecting the beacon point $B_1(x_1, y_1)$ and mid point $I(x_u = (x_p + x_g)/2, y_u = (y_p + y_g)/2)$ of the valid intersection vertices $P(x_p, y_p)$ and $K(x_g, y_g)$, as shown in Fig. 5.2(b). To ensure that the generated random points reside within the constraint area, the sensor node set the random approximation ranges. The approximation range is derived using the following input parameters.

1. The slope $m_{B_1B_3} = \frac{y_1 - y_3}{x_1 - x_3}$ and intercept $c_{B_1B_3} = -(m_{B_1B_3} * x_1) + y_1$ of the line segment between $B_1(x_1, y_1)$ and $B_3(x_3, y_3)$.

2. The mid point $M(x_m = (x_c + x_g)/2, y_m = (y_c + y_g)/2)$ of the line segment between $J(x_c, y_c)$ and $K(x_g, y_g)$.

3. The slope $m_{B_1I} = \frac{y_1 - y_u}{x_1 - x_u}$ and intercept $c_{B_1I} = -(m_{B_1I} * x_1) + y_1$ of the line segment between the B_1 and I.

4. The circle line intersection point $C(x_s, y_s)$ is generated using the circle with center B_3 and communication radius r that intersect the line segment between B_1 and the mid point of the valid intersection point I. The intersection point $C(x_s, y_s)$ is calculated as:

$$(x_s - x_3)^2 + (y_s - y_3)^2 = r^2 \tag{5.3}$$

Firstly, we substitute the equation of line $c_{B_1I} = -(m_{B_1I} * x_1) + y_1$ in Eq. (5.3), and we get:

$$(x_s - x_3)^2 + (y_s - m_{B_1I} * x_1 - c_{B_1I})^2 = r^2 \tag{5.4}$$

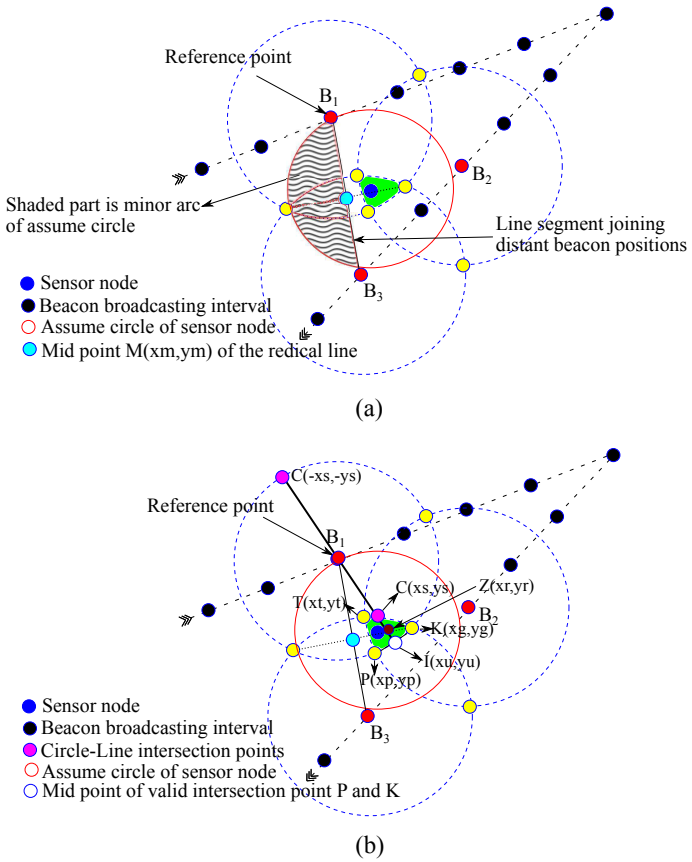

Figure 5.2: Parameters for approximation. (a) Reference point selection for approximation of arc parameters (radius and half chord length). (b) Setting the random approximation range for the arc parameters.

Simplifying the above equation we get:

$$\begin{aligned}(m_{B_1I}^2+1)*x_s^2+2*(m_{B_1I}*c_{B_1I}-m_{B_1I}*y_1-x_1)\\ x_s+(y_1^2-r^2+x_1^2-2*c_{B_1I}*y_1+c_{B_1I}^2)=0\end{aligned} \tag{5.5}$$

Eq. (5.5) can be expressed in standard form of quadratic equation as Ax_s^2+Bx_s+C=0, which can be solved using quadratic formula as follows:

$$x_s=\frac{-b\pm\sqrt{B^2-4*A*C}}{2*A} \tag{5.6}$$

$$y_s=m_{B_1I}*\pm x_s+c_{B_1I} \tag{5.7}$$

The above expression of the quadratic formula generates two roots $C(\pm x_s,\pm y_s)$, as shown in Fig. 5.2(b). To choose the valid root either $C(x_s,y_s)$ or $C(\text{-}x_s,\text{-}y_s)$, sensor node calculates the distances between $M(x_m,y_m)$ and $C(\pm x_i,\pm y_i)$ as E_p and E_n respectively. Based on the comparison between E_p and E_n as $(E_p<E_n)?(-x_s,-y_s):(x_s,y_s)$, the root which is nearer to the midpoint $M(x_m,y_m)$ is selected as the circle-line intersection point ($C(x_s,y_i)$ or $C(\text{-}x_s,\text{-}y_s)$).

5. The midpoint $Z(x_r = (x_s + x_u), y_r = (y_s + y_u))$ of the line segment between $C(x_s,y_s)$ and $I(x_u, y_u)$.

6. The euclidean distances E_{MI}, E_{MZ}, and E_{B_1Z} between the earlier estimated points $M(x_m,y_m)$, $I(x_u, y_u)$, and $Z(x_r,y_r)$.

7. The slope $m_{JK} = \frac{y_c - y_g}{x_c - x_g}$ and intercept $c_{JK} = -(m_{JK} * x_c) + y_c$ of the line segment between $J(x_c,y_c)$ and $K(x_g,y_g)$.

In this scheme, we have used the adaptive mechanism to generate the varying quantity of random points corresponding to varying size of the constraint area. The traditional constraint area based localization schemes are not adaptive according to the different size of the constraint area. Therefore, the larger size of the constraint area leads the schemes to high localization error. To minimize the localization error, we have proposed an adaptive mechanism to enhance the approximation accuracy. The functionality of the adaptive mechanism is represented in Fig. 5.3(a) and Fig. 5.3(b). In Fig. 5.3(a), we have shown that if the constraint area size cannot cross the midpoint of the minimum two radical lines, then less variant type of random points are generated. Besides, if the constraint area size crossed the midpoint of the minimum two radical lines, then we will generate more variant types of random points, as shown in Fig. 5.3(b). At the larger size of the constraint area, it is difficult to exactly predict the sensor node position. Therefore, the more variant type of random points are required to generate the variant positions of the sensor node within the constraint area. Later, the average of all the generated positions predicts the nearly approximated position of the sensor node. The localization performed using the constraint area averaging may not provide such accuracy. The distances between the reference point $B_1(x_1, y_1)$ and generated variant random points are used to represent the variant radius and half chord length of the virtual circle.

Each estimated parameters are successively used to approximate the radius and half chord length. Initially, we approximate the radius with reference to $B_1(x_1, y_1)$. The relation given below randomly estimate the radius within the approximation range:

$$r_1 = E_{B_1Z} + E_{MI} \tag{5.8}$$

$$r_2 = E_{B_1Z} - E_{MZ} \tag{5.9}$$

$$R = (r_2 - r_1) * rand(k, 1) + r_1,\ k = 1, 2, ..., n, \tag{5.10}$$

where r_1 and r_2 are the random approximation range with reference to $B_1(x_1, y_1)$, k is the number of variant type of random points, and R is the random point generating function. Each random value $R = (R_1, R_2, R_3, ..., R_k)$ within the range r_1 and r_2 are considered as the radius, as shown in Fig. 5.4(a). From the reference point $B_1(x_1, y_1)$ to the randomly generated points, the sensor node calculates the distances. Each calculated distance is considered as the radius of the assumed circle. Later, each radius corresponding drawn

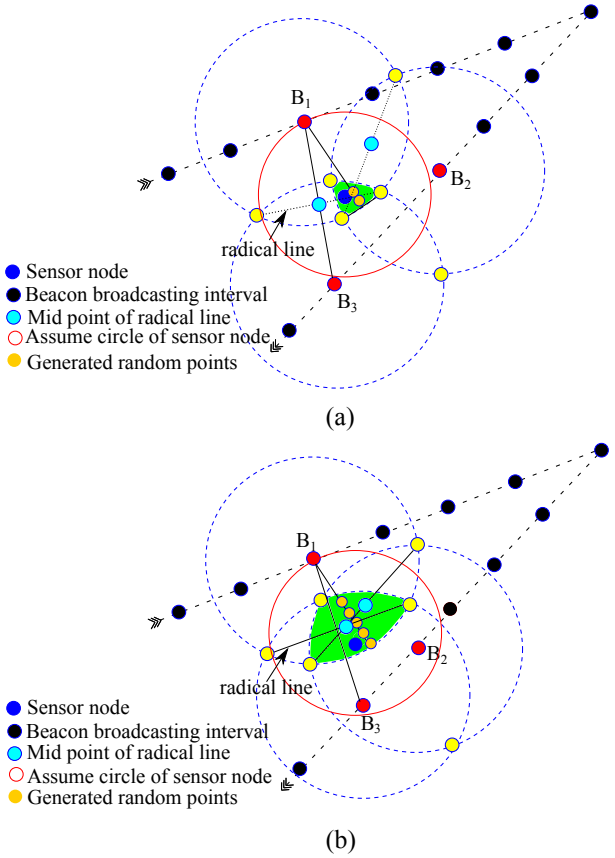

Figure 5.3: Adaptive mechanism. (a) Less variant random points for smaller size of the constraint area. (b) More variant random points for larger size of the constraint area.

circle with center B_1, intersects the line segment between $B_1(x_1, y_1)$ and $B_3(x_3, y_3)$. The intersection point is designated as $Q(\pm x_e, \pm y_e)$, which is later used to approximate the half chord length.

Each random value corresponding drawn circle with center $B_1(x_1, y_1)$ and radius corresponding to each generated random values is shown in Eq. (5.11) as follows:

$$(x_e - x_1)^2 + (y_e - y_1)^2 = (R)^2,\ R = (R_1, R_2, R_3, ..., R_k) \tag{5.11}$$

The above circle generated in Eq. (5.11) intersects the line segment $c_{B_1B_3} = -(m_{B_1B_3} * x_1) + y_1$, as shown in Eq. (5.12).

$$(x_e - x_1)^2 + (y_e - m_{B_1B_3} * x_1 - c_{B_1B_3})^2 = (R)^2 \tag{5.12}$$

Simplifying the above equation we get:

$$\begin{aligned}(m_{B_1B_3}^2 + 1) * x_e^2 + 2 * (m_{B_1B_3} * c_{B_1B_3} - m_{B_1B_3} * y_1 - x_1) \\ x_e + (y_1^2 - R^2)^2 + x_1^2 - 2 * c_{B_1B_3} * y_1 + c_{B_1B_3}^2) = 0\end{aligned} \tag{5.13}$$

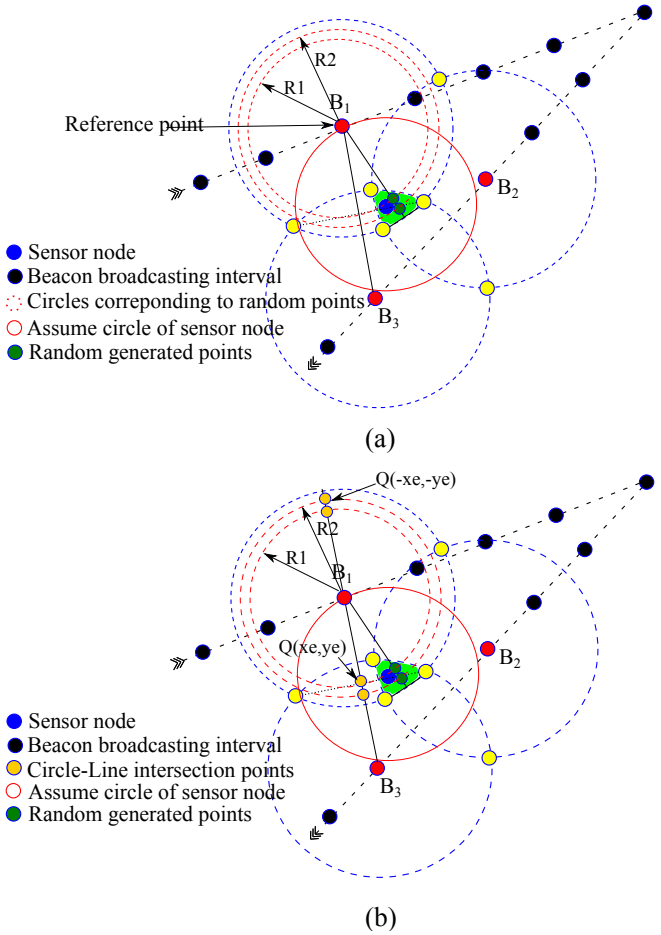

Figure 5.4: Random approximation of radius and half chord length. (a) Generated random points with reference to $B_1(x_1, y_1)$ (radius). (b) Each radius corresponding drawn circle-line intersection points with reference to $B_1(x_1, y_1)$ (half chord length).

Eq. (5.13) can be expressed in standard form of quadratic equation as Ax_e^2+Bx_e+C=0, which can be solved using quadratic formula as follows:

$$x_e = \frac{-B \pm \sqrt{B^2 - 4 * A * C}}{2 * A} \tag{5.14}$$

$$y_e = m_{B_1B_3} * \pm x_e + c_{B_1B_3} \tag{5.15}$$

The above expression of quadratic formula generates two roots $Q(\pm x_e,\pm y_e)$, as shown in Fig. 5.4(b). To choose the valid root either $Q(x_e,y_e)$ or Q(-x_e,-y_e), the sensor node measures the distance between $M(x_m,y_m)$ and $Q(\pm x_e,\pm y_e)$ as E_p and E_n respectively. Based on the comparison between E_p and E_n as $(E_p < E_n)?(-x_e, -y_e) : (x_e, y_e)$, the root which is nearer to the midpoint $M(x_m, y_m)$ is selected as the circle-line intersection point ($Q(x_e, y_e)$ or Q(-x_e,- y_e)), as shown in Fig. 5.4(b).

Sensor node measures the distance E_{xy} between the reference point $B_1(x_1, y_1)$ and each valid intersection point $Q(x_e,y_e)$ corresponding to each random value $R = (R_1, R_2, R_3, ..., R_k)$. Each measured distance is considered as half chord length, as shown in Eq. (5.16). However, the selection of the approximated half chord length is based on a

condition that, the half chord length can be equal to the radius or less than the radius (Eq. (5.17)).

$$E_{xy} = \sqrt{(x_1 - x_e)^2 + (y_1 - y_e)^2} \tag{5.16}$$

$$E_{xy} <= R_1, R_2, R_3, ..., R_k \tag{5.17}$$

5.2.4 Approximation of Sagitta H of An Arc

Sagitta [73] of an arc is a vertical line from the mid point of the chord to the arc itself, as shown in Fig. 5.5. The half chord length, radius, and sagitta of an arc are inter-related, if any two of them are known, than we can easily calculate the other. For approximation of sagitta H of minor arc, we have radius corresponding to each random values of R, and half chord length E_{xy}. In this paper, we only consider the sagitta H of minor arc, which is calculated by taking the average of all radius corresponding to each random value R, and it is calculated as follows:

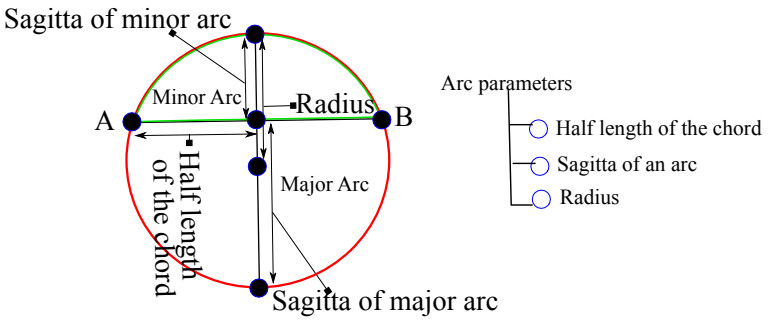

Figure 5.5: Arc of the circle.

$$H = \left(\frac{\sum_{i=1}^{k} R(i)}{k}\right) - \sqrt{\left(\frac{\sum_{i=1}^{k} R(i)}{k}\right) - E_{xy}^2)} \tag{5.18}$$

Using sagitta H of minor arc, sensor node project a point on the circumference of the assumed circle. To project the point on the circumference of the assumed circle, sensor node derives the equation using the slope $m_{JK} = \frac{y_c - y_g}{x_c - x_g}$ and intercept $c_{JK} = -(m_{JK} * x_c) + y_c$ of the line segment connecting $J(x_c,y_c)$ and $K(x_g,y_g)$, mid point of the chord $Q(x_e, y_e)$, and sagitta of an arc H. The projected point $N(x_v,y_v)$ is calculated as follows:

$$(m_{JK}^2 + 1) * x_v^2 + 2 * (m_{JK} * c_{JK} - m_{JK} * y_e - x_e) * x_v + (y_e^2 - H^2 + x_e^2 - 2 * c_{JK} * y_e + c_{JK}^2) = 0 \tag{5.19}$$

Eq. (5.19) can be expressed in standard form of quadratic equation as Ax_v^2+Bx_v+C=0, which can be solved using quadratic formula as follows:

$$x_v = \frac{-B \pm \sqrt{B^2 - 4 * A * C}}{2 * A} \tag{5.20}$$

$$y_v = m_{JK} * \pm x_v + c_{JK} \tag{5.21}$$

Eq. (5.20) and Eq. (5.21) generates two roots $N(x_v, y_v)$ and $N(-x_v, -y_v)$.

5.2.5 Position Estimation

For position estimation, sensor node has to identify the valid projected point from $N(x_v, y_v)$ or $N(-x_v, -y_v)$. To differentiate the valid point among $N(x_v, y_v)$ or $N(-x_v, -y_v)$, sensor node measures the distance between $B_2(x_2, y_2)$ and $N(\pm x_v, \pm y_v)$ as E_p and E_n respectively. Based on the comparison between E_p and E_n as $(E_p < E_n)?(-x_e, -y_e) : (x_e, y_e)$, sensor node selects the root which is farther from $B_2(x_2, y_2)$, as shown in Fig. 5.6(a). From Fig 5.6(b), the valid projected point on the circumference of the assumed circle is $N(x_v, y_v)$. The combination of reference points $B_1(x_1, y_1)$ with valid projected point $N(x_v, y_v)$ generates a chord $\overline{BN}$.

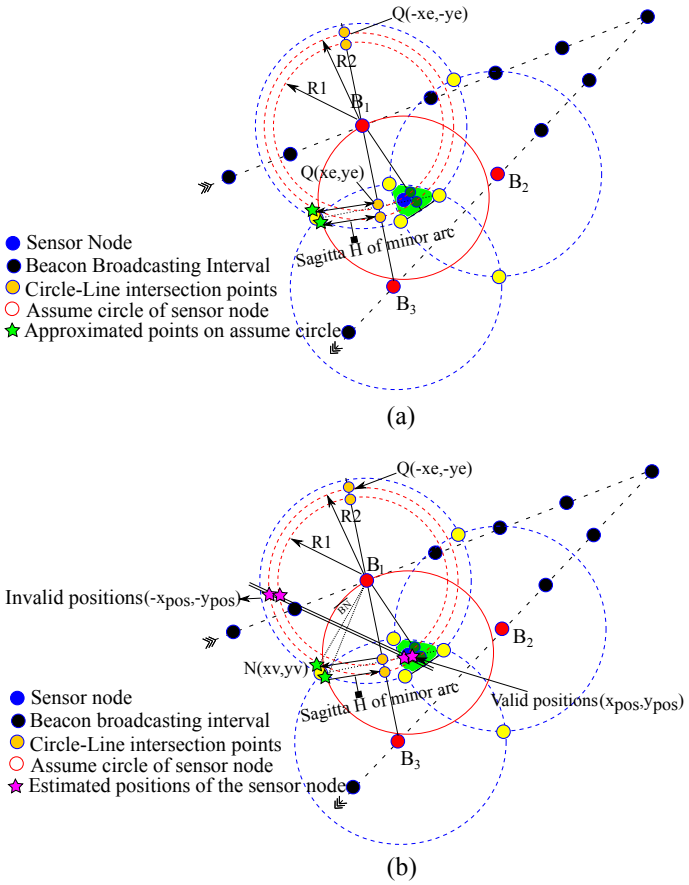

Figure 5.6: Position estimation. (a) Approximated arc radius and half chord length derives the sagitta H of minor arc. (b) Perpendicular bisector of the chord $\overline{BN}$ generates the positions of the sensor node.

Using the valid projected point $N(x_v, y_v)$ and reference point $B_1(x_1, y_1)$ with radius corresponding to each random value $R = (R_1, R_2, R_3, ..., R_k)$, sensor node approximate its position through the perpendicular bisector of the chord $\overline{BN}$. The position is approximated as follows:

$$B_1N = \sqrt{(x_1 - x_v)^2 + (y_1 - y_v)^2} \tag{5.22}$$

$$Mid_x = (x_1 + x_v)/2 \tag{5.23}$$

$$Mid_y = (y_1 + y_v)/2 \tag{5.24}$$

$$x_{pos} = Mid_x \pm \sqrt{(R^2 - (B_1N/2)^2)} * (y_1 - y_v)/B_1N \tag{5.25}$$

$$y_{pos} = Mid_y \pm \sqrt{(R^2 - (B_1N/2)^2)} * (x_1 - x_v)/B_1N, \tag{5.26}$$

where B_1N is the chord length of the assumed circle between B_1(x_1,y_1) and $N(x_v, y_v)$. x_e and y_e are the mid points of the chord $\overline{B_1N}$. Each radius corresponding to the random value $R = (R_1, R_2, R_3, ..., R_k)$ estimates the position as ($\pm x_{pos}$,$\pm y_{pos}$). Sensor node identify its valid position among (x_{pos}, y_{pos}) or $(-x_{pos}, -y_{pos})$. The coordinate (x_{pos}, y_{pos}) or $(-x_{pos}, -y_{pos})$ which lies within the residence area is selected as the valid position of the sensor node, as shown in Fig. 5.6(b). The final position of the sensor node is estimated using the average of all positions lying within the residence area of the sensor node corresponding to the random value $R = (R_1, R_2, R_3, ..., R_k)$. Let the estimated positions are (($x_{pos(1)}$,$y_{pos(1)}$), ($x_{pos(2)}$,$y_{pos(2)}$), ($x_{pos(3)}$,$y_{pos(3)}$),...., ($x_{pos(k)}$,$y_{pos(k)}$)). Then the average of these positions are stored in x_p and y_p as follows:

$$x_p = \left(\frac{\sum_{i=1}^{k} x_{pos(i)}}{k} \right) \tag{5.27}$$

$$y_p = \left(\frac{\sum_{i=1}^{k} y_{pos(i)}}{k} \right), \tag{5.28}$$

where k is the number of the generated random values $R = (R_1, R_2, R_3, ..., R_k)$.

5.3 Simulation And Results

The simulation is performed using MATLAB R2015a (8.5.0.197613). Table. 5.1 shows the simulation environment. The simulation is performed in an area of size 100×100 m^2, where

Table 5.1: Simulation environment

Parameters	Values
Network size (m^2)	100x100
Number of unknown nodes	100
Number of the mobile node	1
Beacon broadcasting intervals	3, 5, 7, 9, 11, 13
Signal propagation range (m)	10, 20, 30, 40, 50, 60
DOI	0, 0.01,0.02,0.03,0.04,0.05
Number of simulation runs	100

the sensor nodes are randomly deployed with a mobile beacon. Mobile beacon traverses the network using non deterministic trajectory called RWP [71]. Simulation is performed by considering various influencing parameters such as signal propagation range of the mobile

beacon, beacon broadcasting interval, and radio propagation irregularity. We have also performed the comparison of the proposed MBBRFLS-ORAF with other well known range free localization schemes such as Ssu [38], Xiao [41], Lee [39], and Singh [21]. All the results presented in this paper are the average of 100 simulation runs.

5.3.1 Performance Evaluation At Varying DOI

In the real environment, the radio signal suffers from various environmental noise such as diffraction, multipath, reflection, refraction, and diffusion. To simulate these impacts, we have used the radio propagation irregularity model [25] as follows:

$$K_i = \begin{cases} 1, & i = 0, \\ K_{i-1} \pm Rand * DOI, & 0 < i < 360, i \in N, \end{cases} \tag{5.29}$$

where $|K_0 - K_{359}| \leq DOI$, K_i represent the path-loss per unit degree change in the direction, DOI defines the degree of irregularity. The model has no information about the angle corresponding to the radio propagation irregularity. Hence, it is very difficult to use this model. To simplify the model, we adopt a model proposed in [41], and it is presented as follows:

$$\begin{aligned} RSS = VSP\ Adjusted\ Sending\ Power - \\ DOI\ Adjusted\ Path\ Loss + Fading \end{aligned} \tag{5.30}$$

$$\begin{aligned} VSP\ Adjusted\ Sending\ Power = Sending\ Power \\ *(1 + NormalRand * VSP), \end{aligned} \tag{5.31}$$

$$DOI\ Adjusted\ Path\ Loss = Path\ loss * (1 \pm Rand \times DOI), \tag{5.32}$$

where, $Rand$ follows the $Weibull$ distribution that represent the variance of path loss, $Received\ Signal\ Strength\ (RSS)$, $Variance\ of\ Sending\ Power\ (VSP)$, and $Fading$ is zero-mean Gaussian random variable.

To compare the performance of the proposed MBBRFLS-ORAF with Ssu, Xiao, Lee, and Singh schemes, we set the communication range to 20 m, beacon broadcasting interval of 5 m, and the varying degree of irregularity (0 to 0.05). The varying DOI generates the non-uniform distribution of the radio signal, resulting the sensor nodes receive less number of mobile beacons. The unpredictability in radio distribution divides the sensing area into two zones called high zone and low zone. The high zone corresponding sensor nodes receive more number of the beacon points, while the low zone corresponding sensor nodes receive less number of the beacon points. This unpredictability influence the constraint area of the sensor node. The low zone corresponding beacon points are more nearer to the sensor node, while high zone corresponding beacon points may or may not be nearer to the sensor node. Hence, this unpredictability corresponding selected beacon points create large size of the

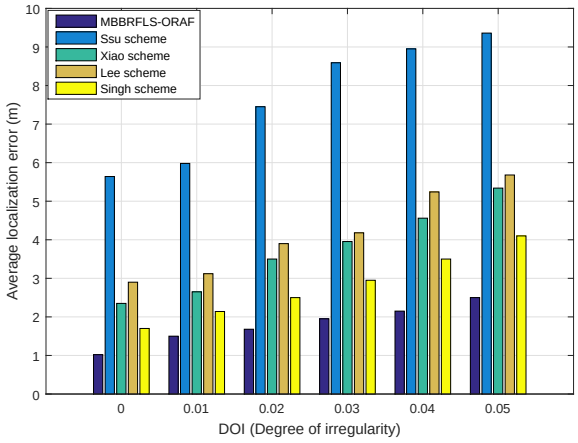

Figure 5.7: Performance comparison at varying DOI versus average localization error.

constraint area.

From Fig. 5.7, we can see the impact of varying DOI on the localization accuracy. From the results, it is observed that the proposed MBBRFLS-ORAF even at high DOI shows less localization error than Ssu, Xiao, Lee, and Singh schemes. The unpredictability of radio distribution affects the best selection of the beacon points. In Ssu scheme, the selected beacon points are not exactly resides on the communication range of the sensor node. Hence, the localization using the perpendicular bisector of the chords gives high localization error. Besides, Xiao scheme create the overlapping areas of the sensor node using the mobile beacon points. In fact, the high DOI corresponding selected beacon points fail to minimize the generated overlapping areas. Hence, the localization using the averaging of valid overlapping area gives high estimation error. Similarly, Lee scheme uses the communication range of the mobile beacon to constraint the position of the sensor node. Due to high DOI, the selected beacon points corresponding constraint area has larger size. Therefore, the localization using the constraint area averaging fails to minimize the localization error. In Singh scheme, the constraint area of the sensor node is used to approximate the arc parameters. Due to high DOI, the selection of the beacon points are inappropriate which creates larger size of the constraint area. The larger size of the constraint area degrades the approximation accuracy of the arc parameters, which leads to high localization error. From Fig. 5.7, it is observed that the proposed MBBRFLS-ORAF shows less localization error as compared to other localization schemes. The average localization error at DOI of 0.05 for the proposed MBBRFLS-ORAF, Ssu, Xiao, Lee, and Singh schemes are 2.5 m, 12.54 m, 5 m, 7.1 m, and 4.1 m respectively.

5.3.2 Performance Evaluation At Varying Communication Range

The communication range of the mobile beacon has a significant impact on the localization accuracy and the covering of the network. However, the longer communication range with

less option of beacon points may increase the localization error. The longer communication range along with high DOI affects the size of the constraint area. The high DOI affects the best selection of the beacon points. Besides, the communication range without the best selection of beacon points creates larger size of constraint area. For performance comparison of the proposed MBBRFLA-ORAF with Ssu, Xiao, Lee, and Singh schemes, we set the communication range varying from 10-60 m, beacon broadcasting period of 5 m, and DOI of 0.05. From Fig. 5.8, it is observed that, as the communication range increases, the localization error also increases. In the proposed MBBRFLS-ORAF, only few sensor nodes show high localization error at longer communication range. Ssu scheme produces high localization error as compared to proposed MBBRFLS-OBRAF, Xiao, Lee, and Singh schemes. The average localization error at DOI of 0.05 for MBBRFLS-ORAF scheme, Ssu, Xiao, Lee, and Singh schemes are 1.5 m, 8.43 m, 2.4 m, 3.5 m, and 1.9 m respectively.

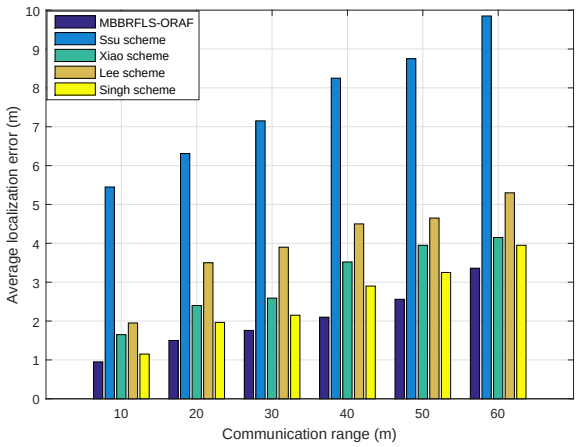

Figure 5.8: Performance comparison at varying communication range versus average localization error.

5.3.3 Performance Evaluation At Varying Beacon Broadcasting Interval

The beacon broadcasting interval has a major impact on the localization error. If the beacon broadcasting interval is longer, then the quantity of the beacon points is lesser. The less quantity of the beacon points influence the size of the constraint area. The longer beacon broadcasting interval along with high DOI reduces the best options of the beacon points for the sensor nodes to minimize the constraint area. Therefore, the localization error increases. The proposed MBBRFLS-ORAF shows better performance even at longer beacon broadcasting interval. In the Ssu scheme, the longer beacon broadcasting interval influence the best selection of the mobile beacon points. Hence, the localization using the perpendicular bisector of the chords (line segment between the selected mobile beacon points) gives high localization error. In the Xiao localization scheme, the longer beacon

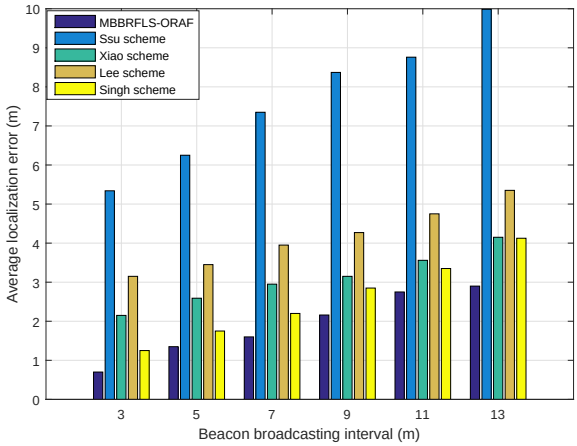

Figure 5.9: Performance comparison at varying beacon broadcasting interval versus average localization error.

broadcasting interval affects the best selection of the beacon points. Hence, the selected beacon points corresponding overlapping region gives high localization error. Besides, the Lee scheme at longer beacon broadcasting intervals fails to minimize the constraint area of the sensor node. Therefore, the localization using the constraint area averaging gives high localization error. Similarly, Singh scheme use the constraint area for approximation of the arc parameters. The constraint area with larger size degrades the approximation accuracy of the arc parameters, which leads to high localization error. To compare the performance of the MBBRFLS-ORAF with Ssu, Xiao, Lee, and Singh schemes, we set the beacon broadcasting interval from 3-13 m, communication range of 20 m, and DOI of 0.05. From Fig. 5.9, it is observed that at a beacon broadcasting interval of 7 m, the average localization error for proposed MBBRFLS-ORAF, Ssu, Xiao, Lee, and Singh schemes are 1.6 m, 12.25 m, 2.95 m, 3.86 m, and 2.2 m respectively.

5.4 Experiments Validation

In the experimental validation, we have used the logarithmic regression model to map the RSSI-distance relationship. The proposed MBBRFLS-ORAF is based on the geometric constraint, where the communication range of the mobile beacon is used to create the constraint area. In the experimental validation, the communication range of the mobile beacon is derived from the logarithmic regression model of RSSI-distance relationship. The entire experimental validation has been divided into four phases:

- Logarithmic regression model
- Experimental setup
- Functionality of the nodes (sensor, anchor, and gateway)

- Experimental validation

5.4.1 Logarithmic Regression Model

The radio propagation irregularity is a major problem that affects the symmetric distribution of the radio signal. The symmetric distribution of the radio signal is not realistic and it does not hold in practice. To understand its behavior, we have used MRF24J40MA radio transceiver. In the initial experiment, we have testify the radio propagation pattern of MRF24J40MA. The experiment is performed using two sensor nodes (one act as a transmitter and another as a receiver). The transmitter at 0 dBm send the 100 packets at a rate of 1 packet/sec, and the receiver at 2 m recorded the RSSI from four different directions (North, South, West, and East), as shown in Fig. 5.10. The MRF24J40MA generates the decimal values of the RSSI, which is converted into dBm using the Eq. (5.33).

$$RSSI = (0.1977 * rssi_{dec} - 87.626), \tag{5.33}$$

where $RSSI$ gives the signal strength in dBm and $rssi_{dec}$ represents the signal strength in decimal. From the result, it is proved that MRF24J40MA has a asymmetric distribution of

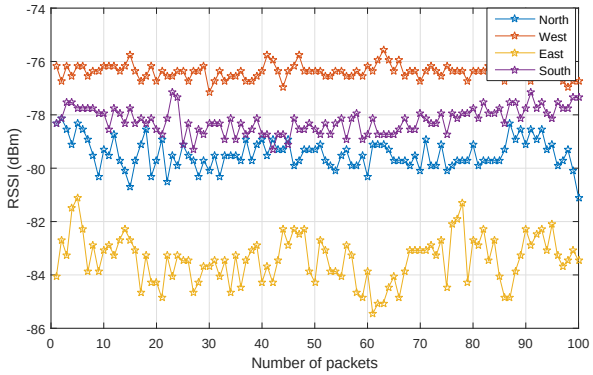

Figure 5.10: MRF24J40MA transceiver antenna radio propagation measured in four direction.

radio signal. Hence, it is very difficult to predict the nearly approximated distance using RSSI. To minimize the distance estimation error using RSSI, at the beginning we map the RSSI-distance relationship using the logarithmic regression model. The RSSI-distance mapping is performed in an indoor room of size 6.4 m $\times$ 4.2 m $\times$ 4.5 m, where transmitter and receiver are placed at a height of 1 m. The transmitter operates at 0 dBm power level, and the receiver receives the packet when the RSSI is greater than a threshold of -80 dBm. Then, 100 records of RSSI measurements are taken at individually at every 0.1 m till 3.5 m. The recorded RSSI-distance relationship is fitted with a logarithmic regression curve $y = -7.3623ln(x) - 65.5326$ with coefficient of determination R^2 = 0.8336. The scatter plot and root mean square error (RMSE) for every measurements at different locations are shown in Fig. 5.11(a) and Fig. 5.11(b), respectively. From the experimental results, it is

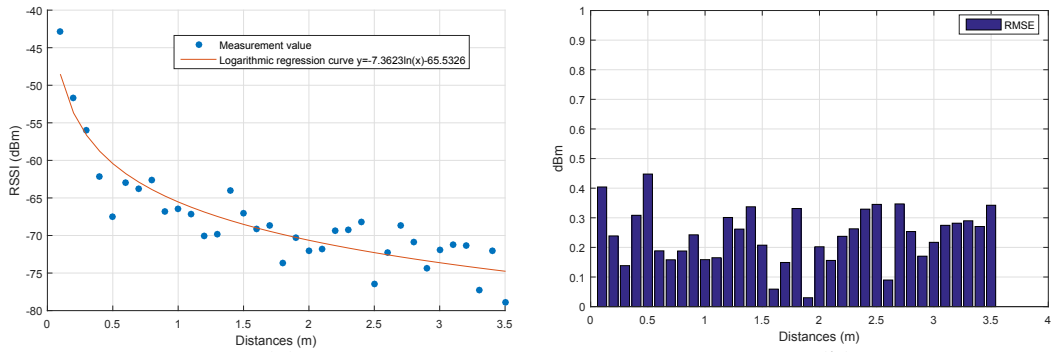

(a) (b)

Figure 5.11: (a) Logarithmic regression curve of RSSI-distance relationship. (b) RMSE.

verified that beyond 1.5 m the RMSE is greater. The greater RMSE represents the greater regression error. Hence, the distance estimation beyond that range is erroneous. In the experiment, the estimated distances are used to represent the communication range of the mobile beacon. Later, the intersection of their communication range are used to create the constraint area of the sensor node. To ensure the intersection, we have selected the mobile beacons with maximum RSSI. The mobile beacon with maximum RSSI has the greater chance that the sensor node resides within its communication range. Hence, we can use its communication range as the threshold for other beacon points (with less chances). Fig. 5.12 shows the threshold of the circle extension. The estimated distance from the beacon point with maximum RSSI is calculated using Eq. (5.34).

$$d = e^{\frac{RSSI+\delta}{\gamma}}, \tag{5.34}$$

where d is the estimated distance, δ represents the offset quantity, and γ represents the adjusting coefficient. The quantity $\delta = -65.5326$ and $\gamma = -7.3623$ are derived from the logarithmic regression curve, as shown in Fig. 5.11(a)

5.4.2 Experiments Setup

In our experimental validation, sensors are designed using 8-bit ATmega Microcontroller and MRF24J40MA radio transceiver. The entire setup is powered using 2000 mAh lithium ion battery. Fig. 5.12 shows the designed sensor node and mobile robot. The maximum transmit power level of MRF24J40MA is 0 dBm, which supports communication range of 40 m in indoor and 120 m in outdoor environment [75]. The packet format of transmitter and receiver are shown in Fig. 5.13 (a) and 5.13 (b), respectively. Table 5.2 shows the experimental environment. Due to the memory limitation and processing delay of the microcontroller, the localization is performed at the computationally powerful base station. Therefore, the received information of the mobile beacon from the sensor node is further delivered to a gateway node. The gateway node is connected with a computationally powerful base

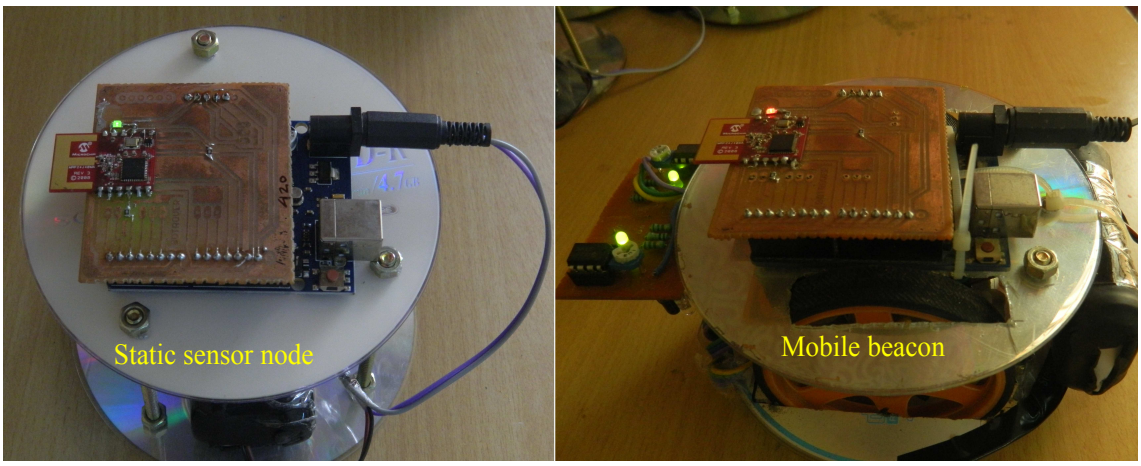

Figure 5.12: Static sensor node and mobile beacon.

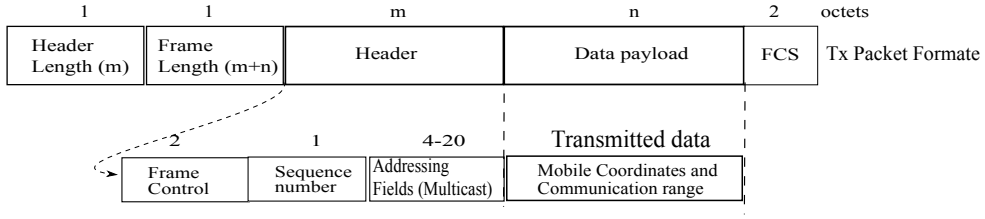

(a)

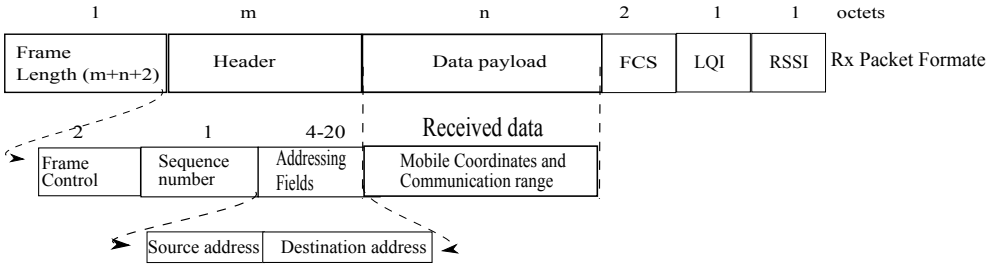

(b)

Figure 5.13: Packet format. (a) Transmitted packet format. (b) Received packet format

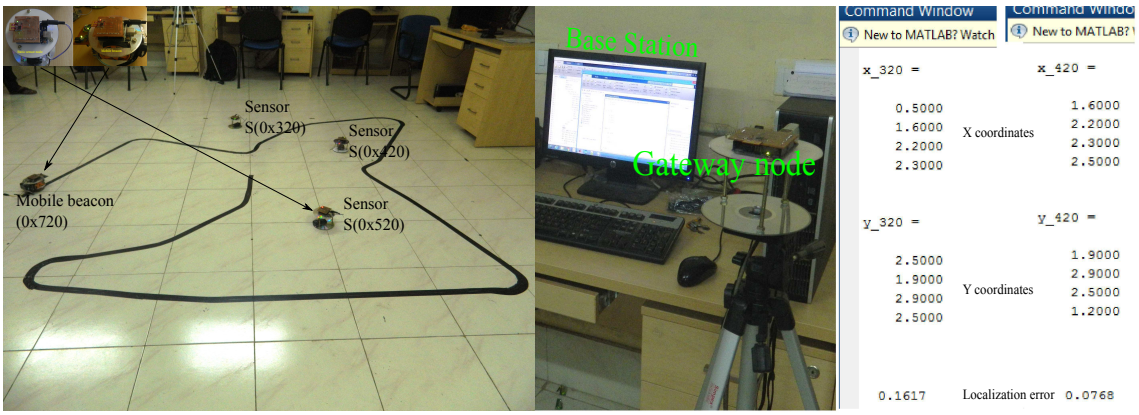

(a) (b)

Figure 5.14: Experimental setup. (a) Sensor deployment area. (b) Gateway node connected with the computer to localize the sensor node.

Table 5.2: Experimental environment

Parameters	Values
Transceiver module (dBm)	MRF24J40MA
IEEE Standard	802.15.4
Operating frequency (GHz)	2.405-2.48
Selected channel frequency (GHz)	2.405
Transmit power (dBm)	-20
Receiver sensitivity (dBm)	-90
Network size (m^2)	3×3
Maximum communication range (m)	2
Number of sensor node	5
Trajectory of mobile robot	Random
Packet receiving threshold (dBm)	-80
Number of experimental runs	10

station. All the computation for localization is performed at the base station. The sensor node deployment along with a mobile robot is shown in Fig. 5.14 (a), while the gateway node connected with a base station is shown Fig. 5.14(b).

5.4.3 Functionality of Different Nodes

In this experiment, we have used three types of nodes (anchor, sensor, and gateway node) to perform the localization. The action performed by the each node in the experiment is demonstrated using the flow graph, as shown in Fig. 5.15.

Mobile anchor

Mobile anchor broadcast its manually assigned 12 different location coordinates. Due to less number of static sensor nodes in the experimental scenario, we have used multicast addressing. At each broadcasting interval , mobile beacon transmit the location coordinates to all the multicast addresses of the sensor nodes.

Sensor node

Sensor node collects the location coordinates of the mobile beacon. From the signal strength of the received beacon, the sensor node estimate its distance from the mobile beacon using the logarithmic regression model. The sensor node verify the intersection of its estimated distances using the intersection threshold. Later, the verified estimated distances along with the mobile beacon location coordinates are further delivered to a gateway node.

Gateway node

Gateway node is connected with a computationally powerful base station, that performs the localization of the sensor node. The received information of the sensor node is further

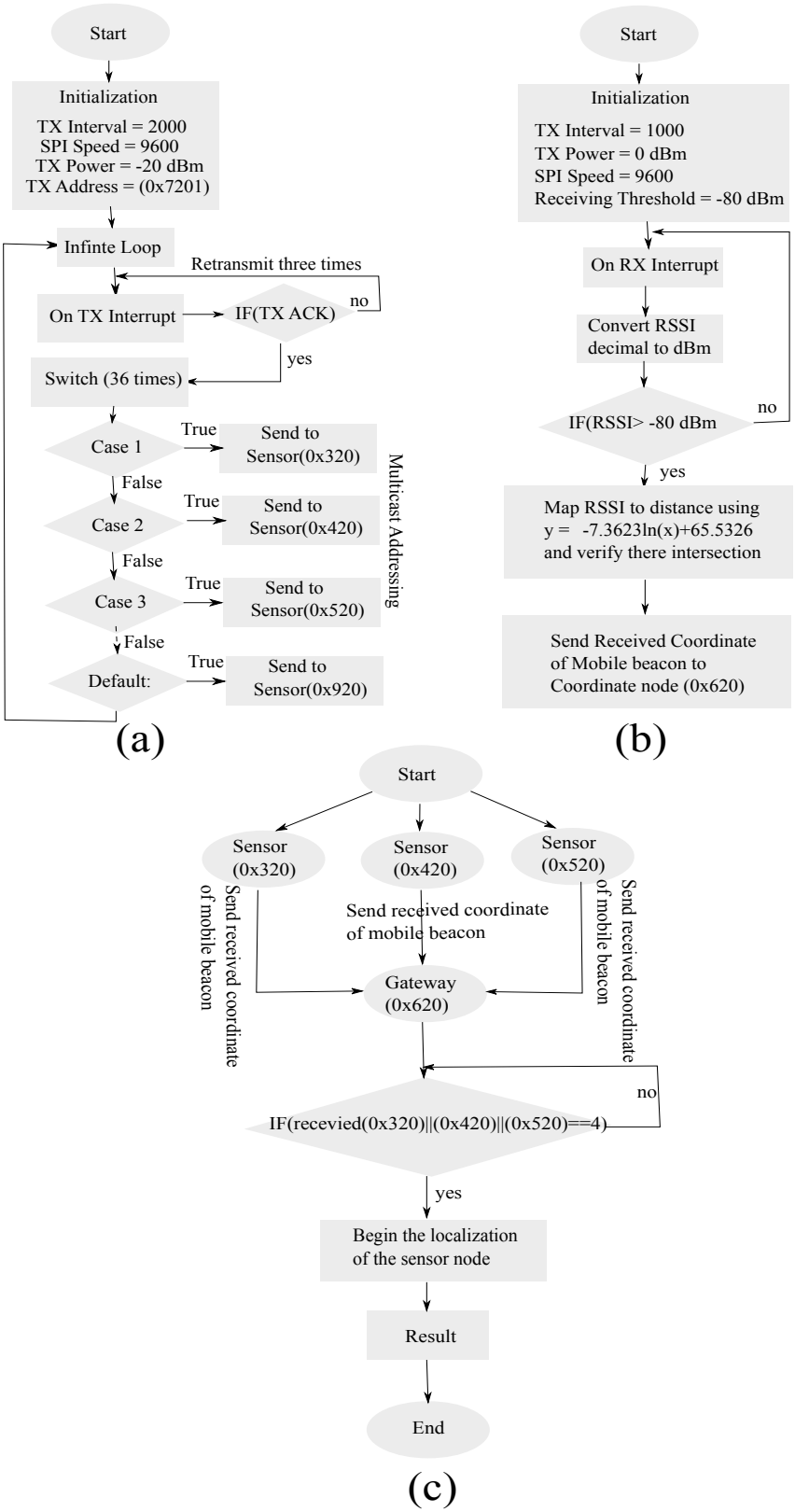

Figure 5.15: Experimental flow-graph: (a) Mobile anchor as a transmitter. (b) Sensor node as a coordinator. (c) Gateway node as a receiver.

delivered into the MATLAB environment.

5.4.4 Experimental Validation

To perform the experiment, we use the network area of size $3 \times 3\ m^2$. The mobile robot moves on a predefined trajectory and periodically transmits its manually assigned 12 different location coordinates. At every 1 m of interval, the mobile beacon broadcast the assigned

Table 5.3: Mobile broadcasting locations

S.No	Mobile broadcasting locations (x,y)
1	(0.2,0.5)
2	(0.5,1.45)
3	(1.3,1.3)
4	(1.4,2.3)
5	(2.2,2.7)
6	(3,2.9)
7	(2.5,2)
8	(2.8,1.1)
9	(2.9,0.2)
10	(2,0.1)
11	(1,0.3)
12	(1.5,0.7)

location coordinate to the multicast addresses of the sensor nodes, as shown in Fig. 5.16(a). The transmitting interval is calculated using the wheel speed, motor revolution per minute (RPM), and wheel diameter of the mobile robot. Later, the estimated travel time to cover the one meter along with marginal error is set for the transmitting interval. All the static sensor nodes collect the beacon messages under the threshold range of -80 dBm. From the signal strength of three different beacon messages, the sensor node estimate three distances using the logarithmic regression model of the RSSI-distance relationship. The estimate distances represent the communication range of the selected mobile beacon points. The estimated distances along with location coordinates of selected beacon points are further delivered to a gateway node. The gateway node is connected with a computationally powerful base station, where localization process begins to localize the sensor node.

Table 5.4: Experimental result at a beacon broadcasting interval of 1 m

Sensor ID	Sensor actual locations S(x,y)	Sensor estimated location S(x',y')	Average Localization error (m)
S (0x320)	(2.2,0.7))	(2.27,0.51)	0.1913
S (0x420)	(2.1,2.2)	(1.95,2.19)	0.0320
S (0x520)	(0.9,1.9)	(1.01,1.82)	0.1402

The experiment is conducted at two different beacon broadcasting intervals (1 m and 2 m). For broadcast purpose, the manually assigned location coordinates for the mobile beacon

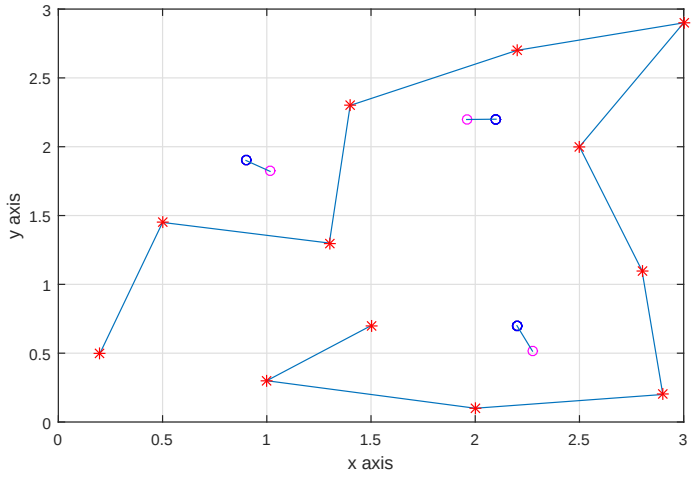

Figure 5.16: Experimental outcome at a beacon broadcasting interval of 1 m.

are given in Table . 5.3. Fig. 5.16 and Fig. 5.17 shows the experimental outcome at two different beacon broadcasting interval. From the results given in Table. 5.4 and Table. 5.5, its is observed that the quantity of the beacon points influence the localization accuracy. At the beacon broadcasting interval of 1 m and 2 m, the average localization errors are 0.12 m and 0.25 m respectively.

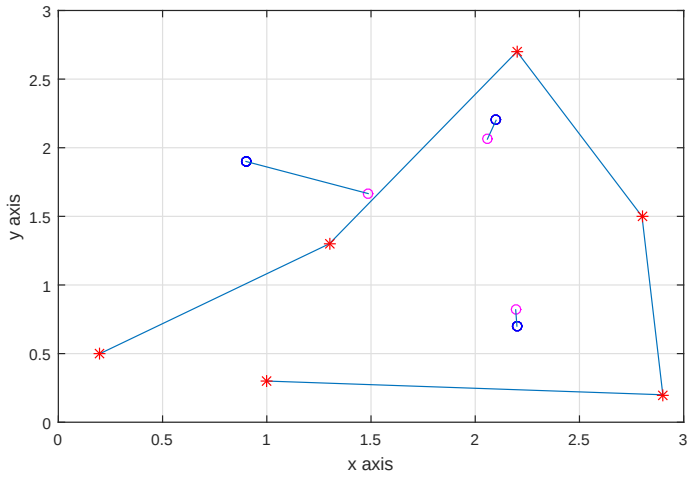

Figure 5.17: Experimental outcome at a beacon broadcasting interval of 2 m.

Table 5.5: Experimental outcome at a beacon broadcasting interval of 2 m

Sensor ID	Sensor actual locations S(x,y)	Sensor estimated location S(x',y')	Average Localization error (m)
S (0x320)	(2.2,0.7))	(2.1,0.81)	0.117
S (0x420)	(2.1,2.2)	(2.05,2.06)	0.053
S (0x520)	(0.9,1.9)	(1.48,1.65)	0.59

5.5 Comparative Strength And Weakness

The comparative strength and weakness of the proposed MBBRFLS-ORAF is compared with the other schemes under various types of overhead. The comparative results are given in Table. 5.6, where N denotes the number of beacon points.

Table 5.6: Comparative strength and weakness

Performance parameters	MBBRFLS-ORAF	Singh [21]	Lee [39]	Ssu [38]	Xiao [41]
Accuracy	Good	Good	Good	Fair	Good
Node Density	>0	>0	>0	>0	>0
Beacon Heard	>2	>2	>2	>3	>3
DOI	Good	Good	Fair	Fair	Fair
GPS error	Good	Good	Good	Good	Good
Scalability	Good	Fair	Good	Good	Fair
Communication Overhead	N	N	N	N	N
Time Complexity	O(N^2)	O(N^2)	O(N^2)	O(N^2)	O(N^2)
Energy efficiency	Fair	Fair	Good	Good	Fair

5.6 Analysis of Robustness and Efficiency

To analyse the robustness and efficiency of proposed scheme MBBRFLS-ORAF with other schemes, we have taken the similar performance evaluating parameters such as longer beacon broadcasting interval (LBBI) of 13 m, longer communication range (LCR) of 60 m, and degree of irregularity (DOI) of 0.05. The robustness and efficiency analysis are same applicable for proposed MBBRFLS-ORAF as discussed in Chapter 3 under Section 3.7. Besides, the adaptive mechanism for different size of constraint area futher improves the localization accuracy in proposed MBBRFLS-ORAF. The adaptive mechanism generate more number of variant random points specific for the bigger constraint area, which results the approximation accuracy is improved. Hence, the average localization error in proposed MBBRFLS-ORAF is further reduced than Singh [21], Lee [39], Ssu [38], and Xiao [41] schemes . The adaptive mechanism is regarded as the robustness of the proposed MBBRFLS-ORAF, while minimize the localization error for the sensor with bigger constraint area is regarded as the efficiency of the proposed scheme. The comparison results of worst performance evaluating parameters are given in Table. 5.7. From the results, it is

Table 5.7: Comparison results in worst case scenarios

Comparative Parameters	Proposed MBBRFLS-ORAF		Ssu [38]		Xiao [41]		Singh [44]		Lee [39]	
	Average Location Error (m)	Average Localized (%)	Average Location Error (m)	Average Localized (%)	Average Location Error (m)	Average Localized (%)	Average Location Error (m)	Average Localized (%)	Average Location Error (m)	Average Localized (%)
LBBIl	<2.2 & >2	>95	<10.5 & >11	>95	<4.5 & >4	>95	<4.5 & >4	>95	<6 & >5.5	>90
LCR	<3.5 & >3	>99	<10 & >9	>98	<4.5 & >4	>99	<4.5 & >3.5	>99	<5.5 & >5	>98
DOI	<2 & >1.8	>95	<10 & >9	>93	<6 & >5	>95	<8 & >7	>98	<6 &>5.5	>95

observed that the proposed MBBRFLS-ORAF scheme shows higher localization accuracy than the other schemes.

5.7 Summary

In this chapter, we have proposed a adaptive mechanism for different size of the constraint area. The adaptive mechanism generate the random points based on the size of the constraint area. Therefore, the approximation accuracy of the arc parameters is improved even at the larger size of the constraint area, which leads the proposed MBBRFLS-ORAF to high localization accuracy. The mechanism is useful for the sensor node with less option of the beacon points for minimization of its residence area. From the simulation results, it is observed that the proposed MBBRFLS-ORAF localize the sensor node even in sparse network. To validate the proposed MBBRFLS-ORAF for real environment, we have designed a prototyped experimental test-bed. In the experimental test-bed, we have used the real sensors enabled with communication modules. The deployment scenario have a mobile robot and the static sensors. The mobile robot traverses the sensing field and broadcast the manually assigned localization coordinate at the particular intervals. From the received information of mobile robot, the sensor node performs its localization. The experiment is conducted in indoor environment at two different beacon broadcasting interval. From the simulation and experimental results, it is observed that the proposed MBBRFLS-ORAF provides less localization error. In the next chapter, we have proposed a localization scheme for an unpredictable environment (LSURE), where the radio propagation irregularity and its impact on localization accuracy is demonstrated using an experimental test-bed.

Chapter 6

Localization Scheme in Unpredictable Radio Environment (LSURE) for WSNs

In this chapter, we have proposed a range free localization scheme for unpredictable radio environment (LSURE). The proposed LSURE localizes the sensor node even in the unpredictable radio environment. To validate the proposed LSURE, we have designed the various scenarios of radio propagation irregularity using the experimental testbed. The scenarios are modeled using the additional error in the estimated distances from the selected anchors, and the different placement of the anchors. The proposed scheme use the dynamic circle expansion technique to localize the sensor node even in worst scenario of radio propagation irregularity. The impact of generated scenarios are represented on the constraint area of the sensor node.

6.1 Introduction

Research has revealed the significance of ranging techniques for accurate localization of WSNs. Among all types of ranging, the received signal strength indicator (RSSI) based ranging is widely preferred, due to its simplicity and readily availability in most of the radio transceivers [57–61]. However, RSSI based distance estimation is unpredictable in nature, and it is easily affected by environmental obstruction and noise. Therefore, the localization schemes based on the RSSI technique generally shows high localization error in real indoor environments. In the proposed LSURE, we have used the dynamic circle expansion technique to localize the sensor node even in worst scenario of radio propagation irregularity. The proposed scheme localize the sensor node even without knowing the accurate distances. The method is based on the analytical geometry, where arc is used as a primitive geometric shape. The localization process begins with approximation of arc parameters such as radius, half chord length, and Sagitta of an arc. Later, the approximated parameters are used to generate the chord. Th perpendicular bisector of the chord and the approximated radius are used to localize the sensor node. For the performance evaluation, we have designed an experimental platform for indoor environment. In this platform various

scenarios of unpredictable radio environment are modeled to validate the proposed LSURE. From the experimental results, it is observed that the proposed LSURE provides a better localization accuracy than APIT scheme and Weighted Centroid (WC) scheme.

The remaining part of this chapter are as follows. Section 6.2, presents the proposed LSURE. Section 6.3, presents experimental validation. Section 6.4, presents simulation comparison. Section 6.5, presents the summary.

6.2 Proposed Localization Scheme

In this section, we have proposed a range free localization scheme for unpredictability environment. To understand the working methodology of the proposed LSURE, we initially assume that the communication range of the anchor node is r. Later, we will derive the communication range using the logarithmic regression model of RSSI-distance relationship. The proposed localization scheme is divided into four phases:

- Selection of anchor nodes for constraint area formation.
- Approximation of arc parameters.
- Chord point projection corresponding to the Sagitta.
- Final position estimation and differentiation.

6.2.1 Anchor Points Selection and Residence Area Formation

The anchor nodes periodically broadcast beacon messages, while sensor nodes receives the beacon messages. Sensor node perform its localization when it acquires minimum three non-collinear anchor points. The triangular area enclosed within the selected anchor points determines the accuracy of localization. If larger the enclosed area than smaller the intersection area of their communication range. The intersection area of the selected anchor points is the residence area of the sensor node, as shown in Fig. 6.1. In the entire method, the communication range r of all the anchor nodes are symmetric. For simplicity of analysis, we assume that the anchor node positions are $a_1(0,0)$, $a_2(1,0)$, and $a_3(0.5,\sqrt{0.75})$ with communication radius r. The distance between the anchor nodes a_1 and a_2, a_1 and a_3, and a_2 and a_3 are d_1, d_2, and d_3 respectively. The intersection area of their communication range can be represented as:

$$x^2 + y^2 < r^2 \tag{6.1}$$

$$(x-1)^2 + y^2 < (r-d_1)^2 \tag{6.2}$$

$$x^2 + y^2 < (r-d_2)^2 \tag{6.3}$$

$$(x-0.5)^2 + (y-\sqrt{0.75})^2 < r^2 \tag{6.4}$$

$$(x-1)^2 + y^2 < r^2 \tag{6.5}$$

$$(x-0.5)^2 + (y-\sqrt{0.75})^2 < (r-d_3)^2 \tag{6.6}$$

Sensor node selects two distant anchor points a_1 and a_3 to minimize its initial intersection area. The initial intersection area of two rings with center a_1 and a_3 and radii r and $r - d_2$ is shown in Eq. (6.3) and Eq. (6.4). It has two intersection points P_3 and Q_3. Similarly, Eq. (6.1) and Eq. (6.2), and Eq. (6.5) and Eq. (6.6) have the intersection points P_1 and Q_1, and P_2 and Q_2 respectively. The potential position of the sensor node resides within these intersection areas A_Q and A_P with vertices Q_1, Q_2, and Q_3, and vertices Q_1, Q_2, and P_3, respectively.

To differentiate the valid subarea from A_Q and A_P, the sensor node use the anchor point a_2 and mid point P_m of P_3 and Q_3. Initially, the sensor node differentiate the valid intersection point from P_3 and Q_3 with reference to a_2. If distance between a_2 and P_3 is smaller than a_2 and Q_3, then P_3 is the valid intersection point, otherwise Q_3. Similarly, for other valid intersection points, sensor node perform the distance estimation with reference to P_m. If distance between P_m and P_1 is smaller than P_m and Q_1, then P_1 is the valid intersection point, otherwise Q_1. Likewise, if distance between P_m and P_2 is smaller than P_m and Q_2, then P_2 is the valid intersection points otherwise Q_2.

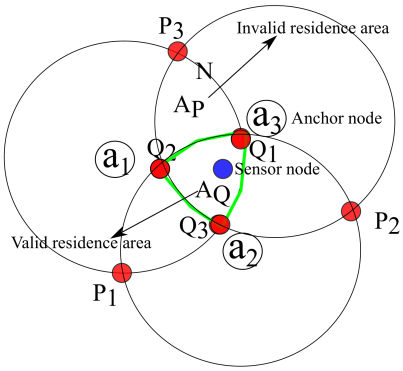

Figure 6.1: Sensor node residence area formation

6.2.2 Random Approximation of Radius and Half Chord Length

After differentiating the valid intersection area of the sensor node, we begin the approximation of the arc parameters (radius, half chord length, and Sagitta of an arc). The arc belongs to the assumed circle of the sensor node, which is created by the line segment connecting the two distant anchor nodes a_1 and a_3. However, the line segment is not a complete chord of the assumed circle but, it has a enough length to be used to approximate the half chord length. The approximation begins with the selection of any one anchor node (a_1 or a_3) on the circumference of the assumed circle. All the approximations are taken

with reference to the selected anchor point. From Fig. 6.2, we can see a_1 is the selected reference point. The line segment connecting a_1 and the mid point Q_m of Q_1 and Q_3, are used to calculate the radius of the assumed circle. For approximation, sensor node generates the few (3-5) random points $R = \{r_1, r_2, r_3, ..., r_k\}$ on the line segment between Q_m and a_1. All the generated random points are resides within the residence area A_Q. The euclidean distances $E = \{e_1, e_2, e_3, ..., e_k\}$ between each generated points and a_1, are considered as the radius of the assumed circle, as shown in Fig. 6.2. Each circle with center a_1 and radii

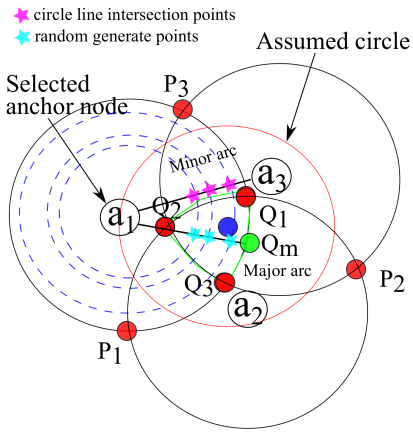

Figure 6.2: Approximation of radius and half chord length of assumed circle

corresponding to euclidean distances $E = \{e_1, e_2, e_3, ..., e_k\}$, intersects the line segment between a_1 and a_3. The distances between the intersection points $I = \{i_1, i_2, i_3, ..., i_k\}$ and a_1 are considered as the half chord length C. Among all the approximated radius and half chord lengths, sensor node made the selections based on a relation. The relation says that the radius should be greater than or equal to the half chord length. In the proposed LSURE, we have considered that the line segment between the anchor nodes a_1 and a_3 divides the assumed circle into two halves called major arc and minor arc.

6.2.3 Approximation of Sagitta H of Minor Arc

In this work, we have considered the minor arc of the assumed circle. The approximated radius and half chord length is used to estimate the Sagitta of an arc. Sagitta [73] is a vertical line from the mid point of the chord to the arc itself, as show in Fig. 6.3. The Sagitta H of minor arc is calculated using the relation between radius (average of all random points $R = \{r_1, r_2, r_3, ..., r_k\}$) and the half chord length C. Eq. (6.7) shows the calculation of Sagitta H.

$$H = \left(\frac{\sum_{i=1}^{k} R(i)}{k}\right) - \sqrt{\left(\frac{\sum_{i=1}^{k} R(i)}{k}\right) - C^2)} \tag{6.7}$$

Later, the approximated H of the minor arc is used to project the points on the boundary of the assumed circle, as shown in Fig. 6.4. To differentiate the valid projected points, we have

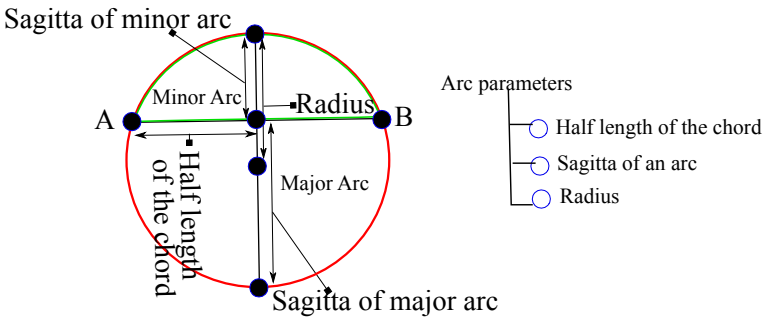

Figure 6.3: Sagitta of an arc

measured the distance between the projected point N and a_2, and V and a_2. Whichever has the larger distance from a_2, sensor node concludes that projected point (N or V) as the valid projection.

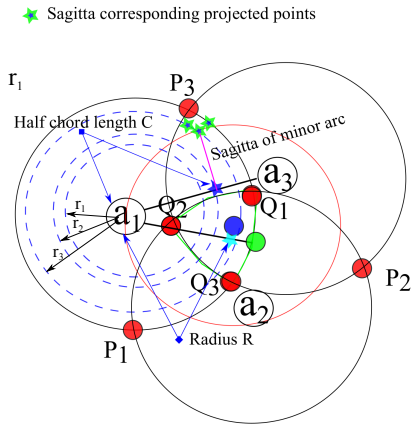

Figure 6.4: Approximation of Sagitta of minor arc

6.2.4 Sensor Node Position Estimation and Differentiation

According to the analytical geometry, if any two points on the circumference of the circle and radius are known, than its center coordinates can be easily determined, as shown in Fig. 6.5. From the above calculations, we have two points $a_1(x_1, y_1)$ and a valid projected point $N(x_n, y_n)$, where the radius corresponds to each random point $R = \{r_1, r_2, r_3, ..., r_k\}$. The position of the sensor node is estimated as follows:

$$a_1N = \sqrt{(x_1 - x_n)^2 + (y_1 - y_n)^2} \tag{6.8}$$

$$Mid_x = (x_1 + x_n)/2 \tag{6.9}$$

$$Mid_y = (y_1 + y_n)/2 \tag{6.10}$$

$$x_p(i) = Mid_x \pm \sqrt{(R(i)^2 - (a_1N/2)^2)} * (y_1 - y_n)/a_1N \tag{6.11}$$

$$y_p(i) = Mid_y \pm \sqrt{(R(i)^2 - (a_1N/2)^2)} * (x_1 - x_n)/a_1N, \tag{6.12}$$

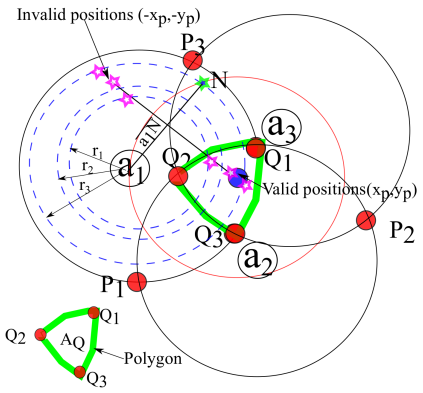

Figure 6.5: Sensor node position estimation

where a_1N is the chord length of the assumed circle between a_1 and $N(x_n, y_n)$, (Mid_x,Mid_y) is the mid point coordinate of the chord $\overline{B_1N}$, and (x_p,y_p) is the position coordinate of the sensor node. Each radius corresponding to $R = \{r_1, r_2, r_3, ..., r_k\}$ estimates the position of the sensor node, which have two different locations ($\pm x_p$,$\pm y_p$). Sensor node identify the valid position using *point in polygon test* of area A_Q. The estimated position whichever resides ((x_p, y_p) or $(-x_p, -y_p)$) within the area A_Q, sensor node selects that coordinate as its valid position. The final position of the sensor node is taken as the average of all positions resides within the area A_Q. Let the estimated positions are ($(x_{p(1)}$,$y_{p(1)})$, ($x_{p(2)}$,$y_{p(2)}$), ($x_{p(3)}$,$y_{p(3)}$),.... ,($x_{p(k)}$,$y_{p(k)}$)). Then the average of these positions are stored in x_a and y_a as follows:

$$x_a = \left(\frac{\sum_{i=1}^{k} x_{p(i)}}{k} \right) \tag{6.13}$$

$$y_a = \left(\frac{\sum_{i=1}^{k} y_{p(i)}}{k} \right), \tag{6.14}$$

where k is the number of the generated random values $R = \{r_1, r_2, r_3, ..., r_k\}$.

6.3 Experimental Validation

In the experimental validation, we have used the logarithmic regression model to map the RSSI-distance relationship. The proposed LSURE is based on the geometric constraint, where the communication range of the anchor nodes are used to create the constraint area. In the experimental validation, the communication range of the anchor node is derived from the logarithmic regression model of RSSI-distance relationship. The entire experimental validation has been divided into four phases:

- Logarithmic regression model

- Experimental setup
- Functionality of the nodes (sensor, anchor, and gateway)
- Experimental validation on different scenarios

6.3.1 Logarithmic Regression Model

The radio propagation irregularity is a major problem that affects the symmetric distribution of the radio signal. The symmetric distribution of the radio signal is not realistic and it does not hold in practice. To understand its behavior, we have used MRF24J40MA radio transceiver. In the initial experiment, we have testify the radio propagation pattern of MRF24J40MA. The experiment is performed using two sensor nodes (one act as a transmitter and another as a receiver). The transmitter at 0 dBm send 100 packets at a rate of 1 packet/sec, and receiver at 2 m recorded the RSSI from four different directions (North, South, West, and East), as shown in Fig. 6.6. The MRF24J40MA generates the decimal values of the RSSI, which is converted into dBm using the Eq. (6.15).

$$RSSI = (0.1977 * rssi_{dec} - 87.626), \tag{6.15}$$

where $RSSI$ gives the signal strength in dBm and $rssi_{dec}$ represents the signal strength in decimal. From the result, it is proved that MRF24J40MA has a asymmetric distribution of

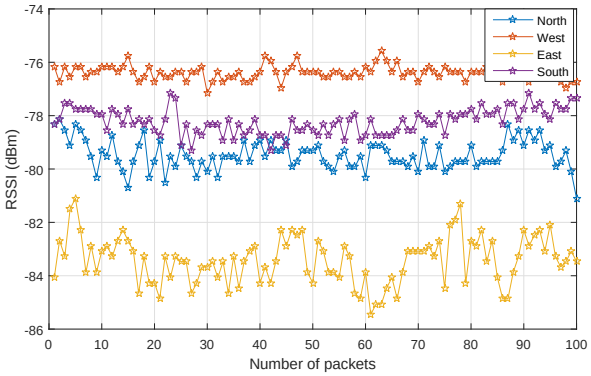

Figure 6.6: MRF24J40MA transceiver antenna radio propagation measure in four direction.

radio signal. Hence, it is very difficult to predict the nearly approximated distance using RSSI. To minimize the distance estimation error using RSSI, at the beginning we map the RSSI-distance relationship using the logarithmic regression model. The RSSI-distance mapping is performed in an indoor room of size 6.4 m $\times$ 4. 2 m $\times$ 4.5 m, where transmitter and receiver are placed at a height of 1 m. The transmitter is operates at 0 dBm power level, and the receiver receives the packet when the RSSI is greater than the threshold of -80 dBm. Then, 100 records of RSSI measurements taken at individually at every 0.1 m till 3.5 m. The recorded RSSI-distance relationship is fitted with a logarithmic regression curve

$y = -7.3623ln(x) - 65.5326$ with coefficient of determination R^2 = 0.8336. The scatter plot and root mean square error (RMSE) for every measurements at different locations are shown in Fig. 6.7(a) and 6.7(b), respectively. From the experimental results, it is verified

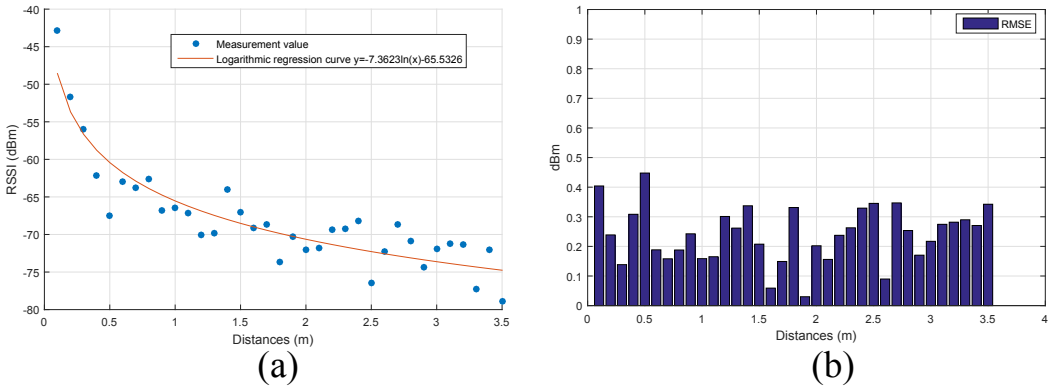

Figure 6.7: (a) Logarithmic regression curve of RSSI-distance relationship. (b) RMSE.

that beyond 1.5 m the RMSE is greater. The greater RMSE represents the greater regression error. Hence, the distance estimation beyond that range is erroneous. In the experiment, the estimated distances are used to represent the communication range of the anchor nodes. Later, the intersection of their communication range are used to create the constraint area of the sensor node. To ensure the intersection, we have selected the anchor nodes with maximum RSSI. The anchor node with maximum RSSI has the greater chance that the sensor node resides within its communication range. Hence, we can use its communication range as the threshold for other anchor nodes (with less chances). Fig. 6.8 shows the threshold of the circle extension. The estimated distance from the anchor node with maximum RSSI is calculated using Eq. (6.16).

$$d = e^{\frac{RSSI+\delta}{\gamma}}, \tag{6.16}$$

where d is the estimated distance, δ represents the offset quantity, and γ represents the

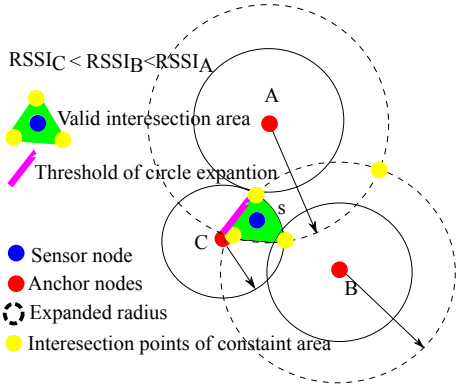

Figure 6.8: Example of circle extension for constraint area formation.

adjusting coefficient. The quantity $\delta = -65.5326$ and $\gamma = -7.3623$ are derived from the logarithmic regression curve, as shown in Fig. 6.7(a). To create a valid residence area,

we have extended the communication range for those anchors which have a less chance. The valid residence area ensures that the sensor node resides within the intersection of the selected anchor nodes. The communication range is extended using Eq. (6.17).

$$d' = e^{\frac{RSSI+\delta}{\gamma}} + d/4, \tag{6.17}$$

where d' is the extended distance (communication range). The extension of the communication range is performed till the circle corresponding to radius d intersects the circle corresponding to radius d', as shown in Fig. 6.8. To say that the intersection is valid, we have set a threshold of $d/2$, that is validated by measuring the distance between every intersection points of their valid intersection area. The selected threshold improves the possibility of the sensor node to reside within the generated residence area.

6.3.2 Experimental Setup

In our experimental validation, sensors are designed using 8-bit ATmega Microcontroller and MRF24J40MA radio transceiver. The entire setup is powered using 2000 mAh lithium ion battery. Fig. 6.9 shows the designed sensor node. The maximum transmit power level of MRF24J40MA is 0 dBm, which supports communication range of 40 m in indoor and 120 m in outdoor environment [75]. Table 6.1 shows the experimental environment. The

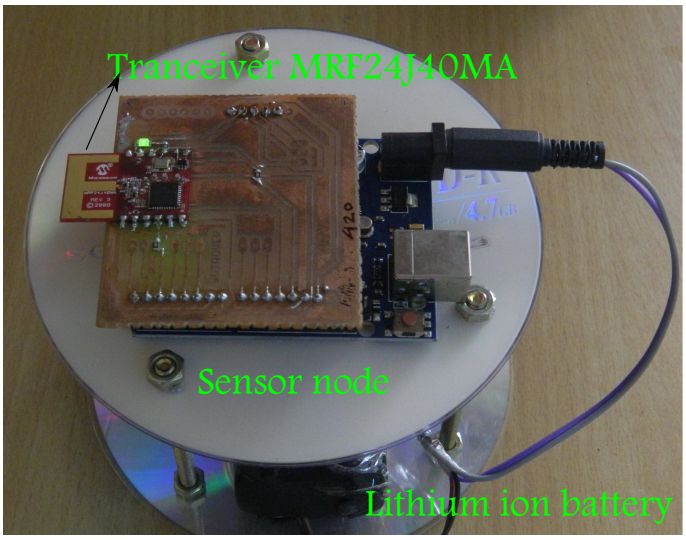

Figure 6.9: Sensor platform.

experiment is performed in indoor laboratory environment of size $3\times$ 3 m^2, where a sensor node is placed at a predetermined location while anchor nodes location are randomly selected at each experimental run, as shown in Fig. 6.10. The orientation of each anchor nodes are different at each experimental run. Due to memory limitation and processing delay of the microcontroller, we have delivered the received information of the anchor nodes from a sensor to a gateway node. The gateway node is connected with a computationally powerful

Table 6.1: Experimental environment

Parameters	Values
Transceiver module (dBm)	MRF24J40MA
IEEE Standard	802.15.4
Operating frequency (GHz)	2.405-2.48
Selected channel frequency (GHz)	2.405
Transmit power (dBm)	-20
Receiver sensitivity (dBm)	-90
Network size (m^2)	3×3
Maximum communication range (m)	2
Number of sensor node	5
Trajectory of mobile robot	Random
Packet receiving threshold (dBm)	-80
Number of experimental runs	10

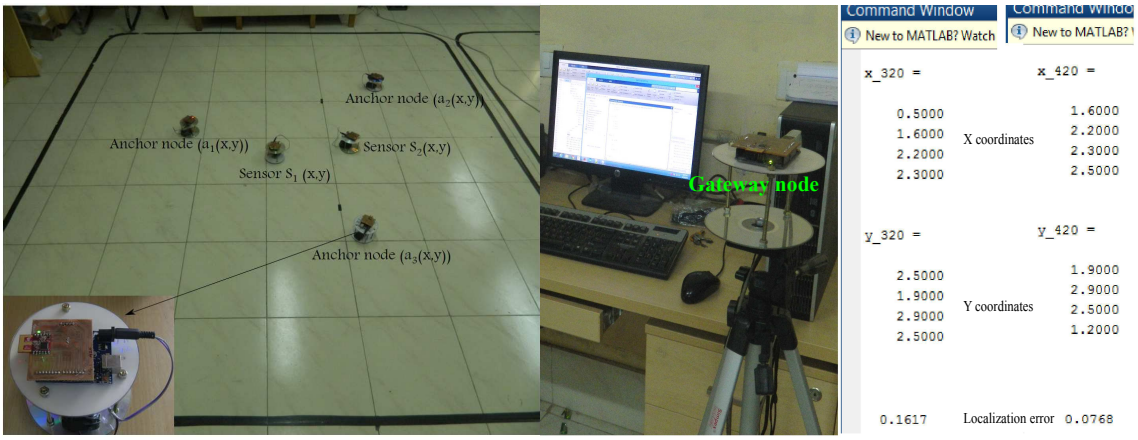

(a) (b)

Figure 6.10: Experimental setup. (a) Sensor deployment area. (b) Gateway node connected with the computer to localize the sensor node.

base station. All the computation for localization is performed at the base station. Fig. 6.10(b) shows the gateway node connected with the computer to localize the sensor node.

6.3.3 Functionality of Different Nodes

In this experiment, we have used three types of nodes (anchor, sensor, and gateway node) to perform the localization. The action performed by each node in the experiment is demonstrated using the flow graph, as shown in Fig. 6.11.

Anchor node

Anchor nodes broadcast their manually assigned location coordinates on demand. Due to less number of nodes in the experimental scenario, we have used the multicast addressing.

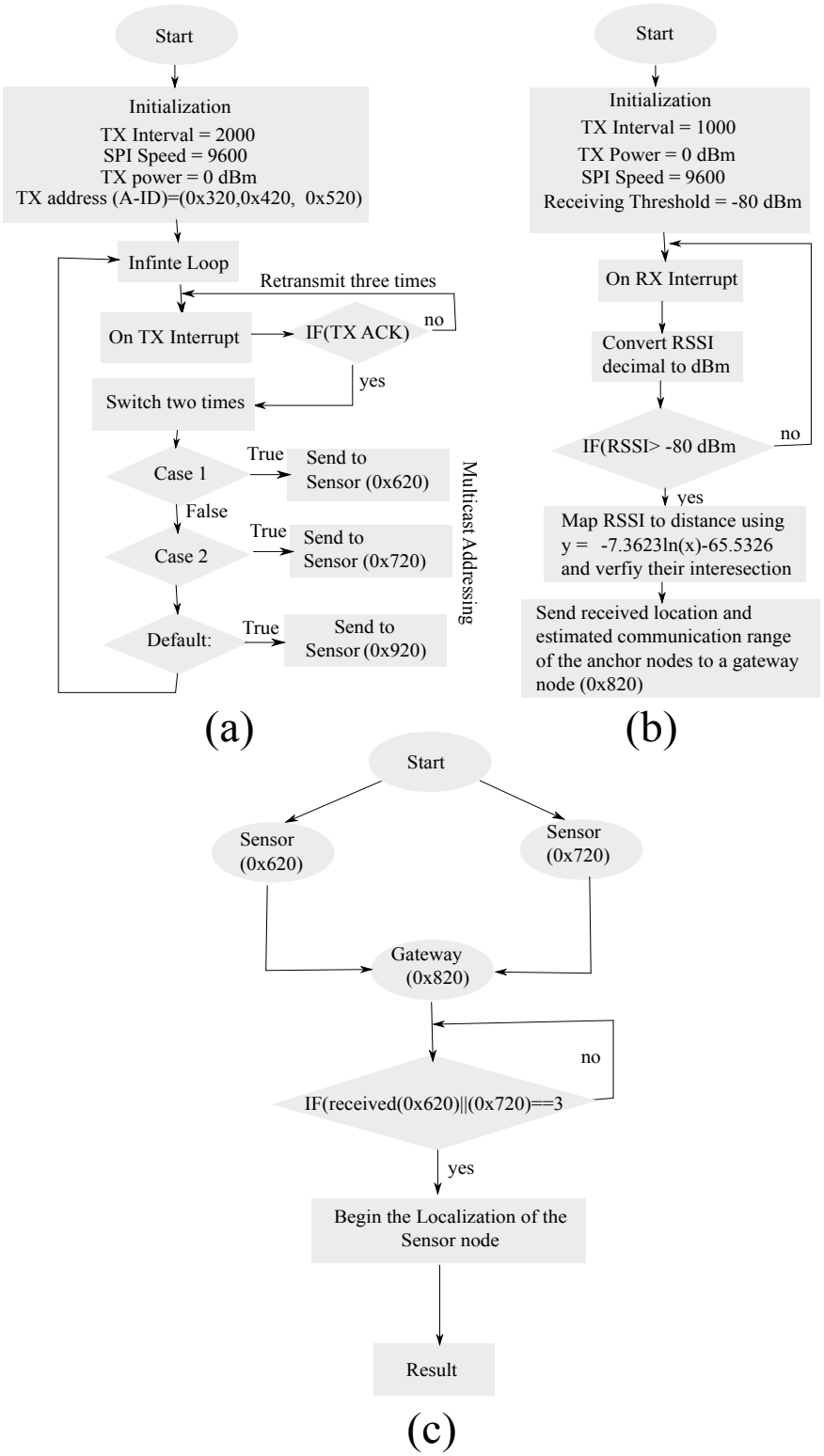

Figure 6.11: Experimental flow-graph: (a) Anchor nodes as a transmitter. (b) Sensor node as a coordinator. (c) Gateway node as a receiver.

Sensor node

Sensor node collects the location information of all the neighboring anchor nodes, and estimate the distances using logarithmic regression model. The sensor node verify the

intersection of the estimated distances along with the intersection threshold. Later, the verified estimated distances along with the anchor location coordinates are further delivered to the gateway node.

Gateway node

Gateway node is connected with a computationally powerful base station that performs the localization of the sensor node. The received information of the sensor node is further delivered into the MATLAB environment.

6.3.4 Experimental Validation On Various Scenarios

Most of the localization schemes neglect the effect of radio propagation irregularity, which doubted the applicability of their scheme in real environment. The effect of radio propagation irregularity is non uniform, in some direction the signal strength is maximum and in some direction it is minimum. Thus, sensor node using the RSSI fails to distinguish which anchor is nearer or farther. This unpredictability affects the localization schemes based on restricted area, where minimized restricted area defines their accuracy. To demonstrate its impact experimentally, we have designed various scenarios of radio propagation irregularity. These experiments demonstrate the different scenarios under which constraint area size gets larger. The generated scenarios are usually found in a network, where RSSI based unpredictability appears in the estimated distance. In this experiment, we have created the RSSI based unpredictability by incorporating the additional error on the estimated distance (derived from the logarithmic regression model). The aim of this experiment is to validate the proposed LSURE under different size of the constraint area, and to demonstrate its impact on the localization accuracy.

The additional error in the estimated distance of logarithmic regression is modeled using the normal random variable $X_\sigma \sim N(0, \sigma^2)$. In Eq. (6.18), X_σ is used to represent the noise of indoor environment with 0 mean and σ^2 variance, where σ is the standard deviation (we assumed $\sigma = 1dBm$).

$$RSSI_e = -7.3623ln(d) - 65.5326 + X_\sigma, \tag{6.18}$$

where $RSSI_e$ is estimated RSSI with additional error and d is the estimated distance.

First Experimental Scenario

In first experiment, we have changed the position of the anchor nodes to influence the residence area of the sensor node. When, the anchor nodes are placed nearer and its communication range is derived from additional error of the estimated distances, then their intersection creates a large size of the residence area. In the proposed LSURE, the size of the residence area affects the approximation accuracy of radius, half chord length, and Sagitta of

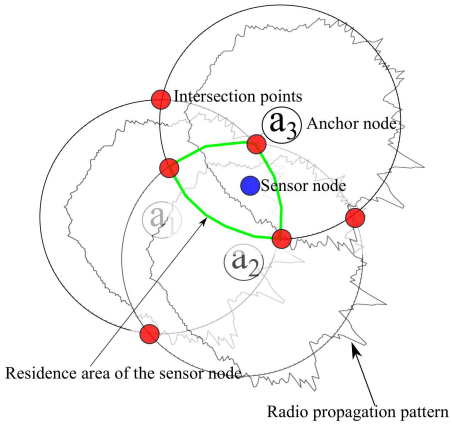

Figure 6.12: First scenario for radio propagation irregularity.

an arc. The inaccurate approximation may affect the localization accuracy of the proposed LSURE. To show its impact, we have performed couple of experiments by changing the positions of the anchor nodes, as shown in Fig. 6.12. Different size of residence areas are created by the combination of anchor nodes, as shown in Table 6.2. Table 6.3 shows the estimated distances from the selected anchor nodes. In this experiment, we fix the

Table 6.2: Different areas enclosed by the anchor nodes

Area enclosed (m^2) by the anchors a_1, a_2, and a_3	**Sensor (x,y)**	**Anchor a_1 (x,y)**	**Anchor a_2 (x,y)**	**Anchor a_3 (x,y)**
0.7450	(1.5,1.5)	(0.7,1.5)	(1.6,0.7)	(2,2)
0.5500	(1.5,1.5)	(1,1.5)	(1.6,0.7)	(2,2)
0.4400	(1.5,1.5)	(1.1,1.5)	(1.6,0.8)	(2,2)
0.3500	(1.5,1.5)	(1.1,1.5)	(1.6,1)	(2,2)
0.3000	(1.5,1.5)	(1.1,1.5)	(1.6,1)	(1.8,2)

Table 6.3: Estimated distances with error

Estimated distances from the anchor nodes (m)		Anchor ID		
Area enclosed by the anchor nodes (m^2)		a_1 (0x320)	a_2 (0x420)	a_3 (0x520)
	0.745	1.25 m	0.98 m	1.31 m
	0.550	1.1 m	1.12 m	1.51 m
	0.440	0.95 m	1.22 m	1.21 m
	0.350	0.78 m	0.96 m	1.32 m
	0.300	0.88 m	1.16 m	0.62 m

sensor position to (1.5,1.5), while anchors positions are changed. The localization error is an average of ten experimental runs at each area. From Fig. 6.13, it is observed that as the size of residence area increased localization error is also increased. At enclosed area of 0.7450 m^2, proposed LSURE shows 43.1 $\%$ less localization error than enclosed area of 0.3 m^2. The experimental outcome is shown in Fig. 6.14.

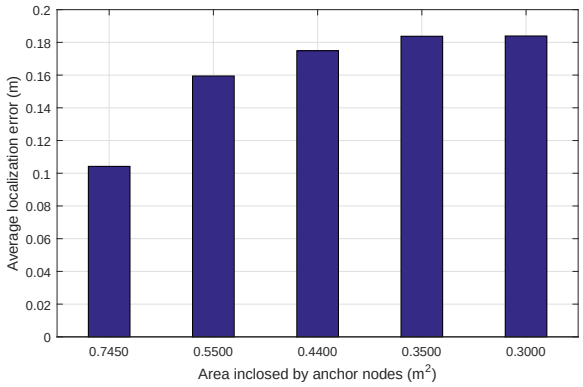

Figure 6.13: Average Localization error at different areas enclosed by the anchor nodes.

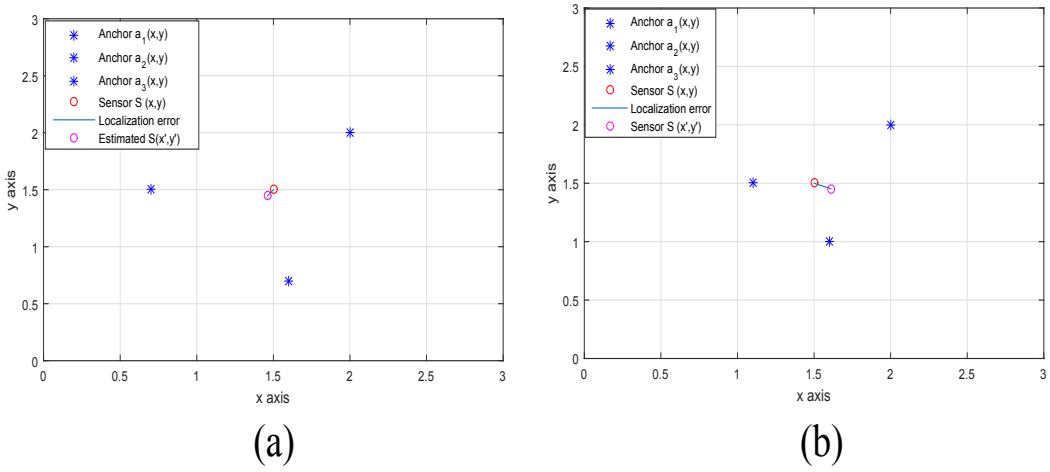

Figure 6.14: Experimental outcome at two different enclosed areas.

Second Experimental Scenario

In the second experiment, we have created another scenario by changing the positions of the anchors, as shown in Fig. 6.15. The existing geometric localization schemes requires

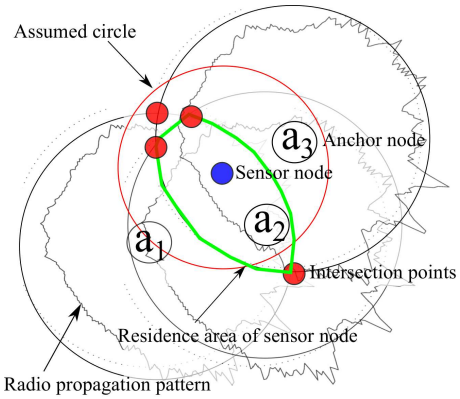

Figure 6.15: Second scenario for radio propagation irregularity.

minimum three non-collinear anchors to create the residence area of the sensor node. Later, the residence area is used to identify the estimated position of the sensor node. Similarly,

the proposed LSURE use the residence area to identify the estimated position along with the minor arc of the assumed circle. In this scenario, the sensor node fails to identity the minor arc of the assumed circle, which leads the proposed LSURE to high localization error. The experiment is performed using the different positions of the sensor and anchor nodes, as depicted in Table 6.4. Table 6.5 shows the estimated distances from the selected anchor nodes.

Table 6.4: Different areas enclosed by the anchor nodes

Area enclosed (m^2) by the anchors a_1, a_2, and a_3	Sensor (x,y)	Anchor a_1 (x,y)	Anchor a_2 (x,y)	Anchor a_3 (x,y)
0.2750	(1.5,2)	(0.7,1.5)	(1.8,1.5)	(2,2)
0.2000	(1.5,2)	(1,1.5)	(1.8,1.5)	(2,2)
0.1750	(1.5,2)	(1.1,1.5)	(1.8,1.5)	(2,2)
0.1250	(1.5,2)	(1.3,1.5)	(1.8,1.5)	(2,2)
0.0750	(1.5,2)	(1.5,1.5)	(1.8,1.5)	(2,2)

Table 6.5: Estimated distances with error

Estimated distances from the anchor nodes (m)		Anchor ID		
Area enclosed by the anchor nodes (m^2)		a_1 (0x320)	a_2 (0x420)	a_3 (0x520)
	0.275	1.45 m	0.98 m	1.33 m
	0.200	1.35 m	0.78 m	1.53 m
	0.175	0.127 m	0.93 m	1.32 m
	0.125	0.143 m	0.96 m	1.28 m
	0.0750	0.128 m	0.89 m	1.22 m

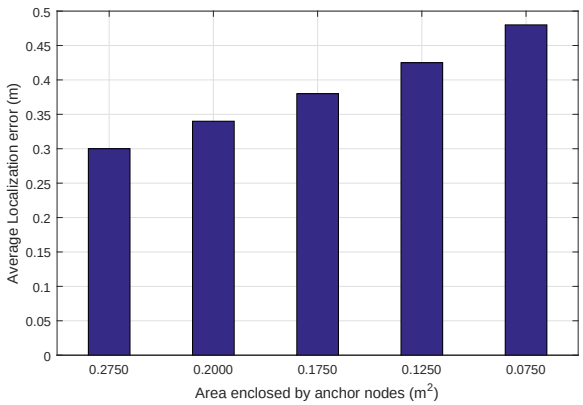

Figure 6.16: Average Localization error at different areas enclosed by the anchor nodes.

From Fig. 6.16, it is observed that proposed LSURE at an enclosed area of 0.2750 m^2 shows 37.5 $\%$ less localization error than the enclosed area of 0.0750 m^2. In this scenario, even through without knowing the valid side of minor arc, the average localization

error cannot go beyond the size of the residence area. In Fig. 6.17, we have shown the experimental outcome at two different areas enclosed by the anchor nodes.

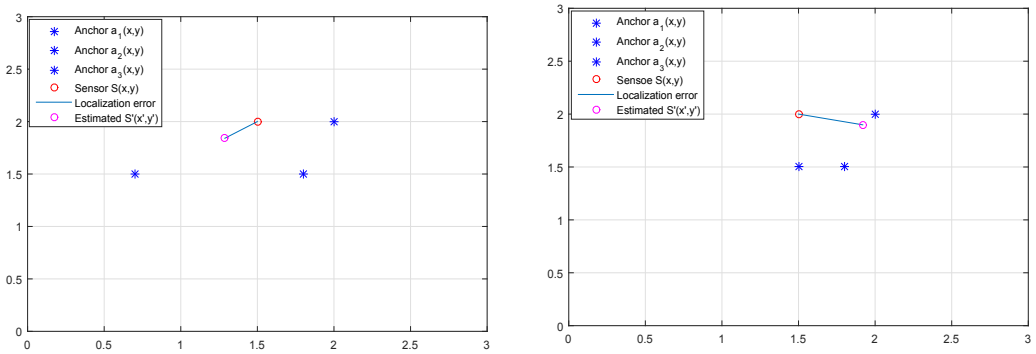

(a) (b)

Figure 6.17: Experimental outcome at two different enclosed areas.

Third Experimental Scenario

In this experiment, we have created a scenario where all the anchor nodes are distant from the sensor node, as shown in Fig. 6.18. The distant anchor nodes corresponding estimated distances have large estimation error, which leads to high localization error. The estimated distance along with the additional error further maximizes the residence area of the sensor node. The larger size of residence area degrades the approximation accuracy and it increases the localization error. The experiment is performed at two different areas enclosed by the

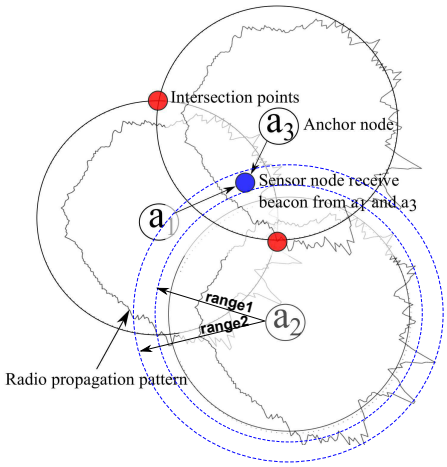

Figure 6.18: Third scenario for radio propagation irregularity.

anchor nodes, as depicted in Table 6.6. Table 6.7 shows the estimated distances from the selected anchor nodes.

At an an enclosed area of $1.0700m^2$, the average localization error of ten experiment runs along with different orientation of anchor nodes is 0.41 m. Similarly, at an enclosed

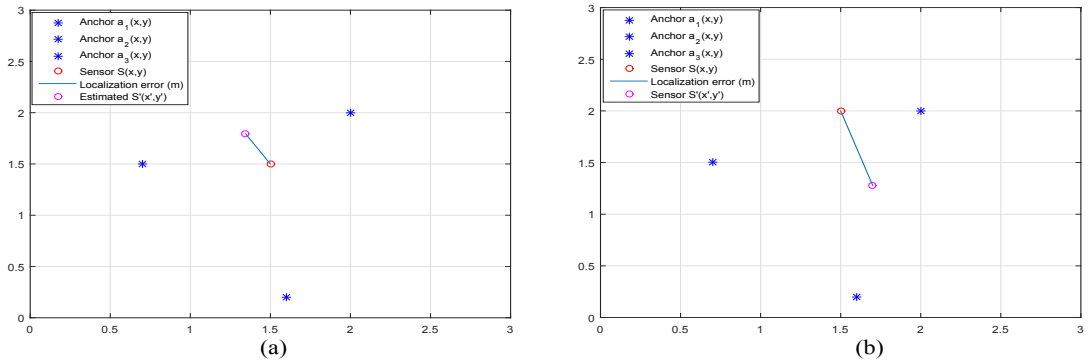

Figure 6.19: Experimental outcome at two different enclosed areas.

Table 6.6: Different areas enclosed by the anchor nodes

Area enclosed (m^2) by the anchors a_1, a_2, and a_3	**Sensor (x,y)**	**Anchor a_1(x,y)**	**Anchor a_2 (x,y)**	**Anchor a_3 (x,y)**
1.0700	(1.5,1.5)	(0.7,1.5)	(1.6,0.2)	(2,2)
1.095	(1.5,2)	(0.6,1.6)	(1.5,0.5)	(2.1,2.2)

Table 6.7: Estimated distances with error

Estimated distances from the anchor nodes (m)		Anchor ID		
Area enclosed by the anchor nodes (m^2)		a_1 (0x320)	a_2 (0x420)	a_3 (0x520)
	1.070	1.35 m	2.46 m	1.21 m
	1.095	2.69 m	2.88 m	2.54 m

area of $1.095m^2$, the average localization error is 0.49 m. Fig. 6.19 shows the experimental outcome at two different enclosed areas of the anchor nodes.

6.4 Comparison of proposed LSURE with APIT and Weighted Centroid

In this section, we compare the performance of the proposed LSURE with Weighted Centroid (WC) [76] and APIT [25] schemes. The APIT scheme uses the triangular geometry to constraint the sensor node within its area. The iterative triangle formation and received RSSI are used to predict the sensor node within the triangular region. Later, the average of the intersection points of the triangular area is used to localize the sensor node. Besides, the WC used the RSSI proximity to derive the weight for each anchor nodes. If the anchor node is nearer then its weight is more. Later, the received coordinates of the anchor nodes along with the measured weights are used to localize the sensor node. However, the APIT and WC schemes perform better in the dense network, where uncertainty of RSSI measurement has a minimal impact. For performance evaluation, we have add another anchor node along with three anchor nodes. The position of the fourth anchor node is fixed to (1,1). The experiment

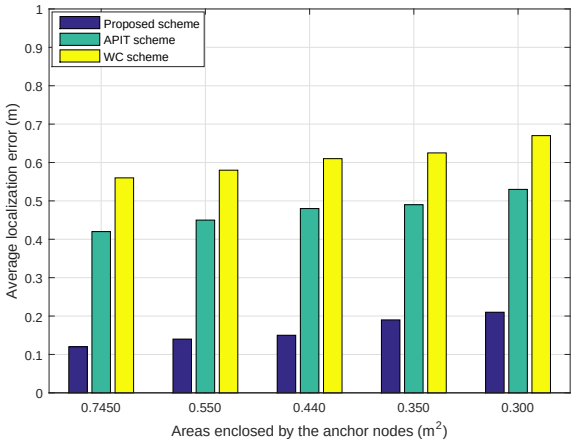

Figure 6.20: Localization error under different placement of the anchor nodes.

is performed using the similar scenario as depicted in Fig. 6.12, where the anchor nodes and sensor node positions are depicted in Table 6.2.

In APIT, the different positions of the anchor nodes create different triangular regions. The sensor node iteratively minimize the triangular region with best selection of the anchor nodes. However, the less number of the anchor nodes and erroneous estimated distances may not always provide minimized triangular region. This increases the average localization error. Besides, the calculated weights in WC scheme are affected by the erroneous estimated distances. Due to erroneous estimated distances, the sensor node fails to predict which anchor node is nearer or farther. Therefore, the estimated positions corresponding to the calculated weights increases the localization error. From Fig. 6.20, it is observed that the proposed LSURE shows less localization error than APIT and WC schemes. At the enclosed area of 0.3 m^2, the average localization error for proposed LSURE, APIT, and Weighted Centroid schemes are 0.21 m, 0.536 m, and 0.67 m, respectively.

6.5 Comparative Strength And Weakness

The proposed LSURE scheme for localization has been investigate on various scenarios of radio propagation irregularity. The scenarios are modelled using the different placement of the anchor nodes. In this chapter, we have consider the static sensors and static anchors deployment scenarios to understand the authenticity of the proposed scheme in static environment. The higher localization accuracy even at lesser number of deployed anchors regarded as the strength of the proposed LSURE, where APIT and WC schemes fails to achieve such accuracy. The comparative strength and weakness is given in Table. 6.8. Where N designate the total number of the anchor nodes.

Table 6.8: Comparative strength and weakness

Performance Parameters	WC [76]	APIT [25]	LSURE
Accuracy	Fair	Fair	Good
Node Density	>0	>6	>0
Anchor Heard	>10	>10	>2
DOI	Fair	Fair	Good
GPS error	Good	Good	Good
Scalability	Poor	Poor	Good
Communication Overhead	M+N	M+N	M
Time Complexity	O(N)	O(N^3)	O(N^2)
Energy efficiency	Fear	Fear	Good

6.6 Analysis of Robustness and Efficiency

To analyse the robustness and efficiency, we have taken the different placements scenarios of the anchor nodes. The comparative result in worst case of deployment scenarios is given in Fig. 6.20. The better localization accuracy in absence of appropriate anchor nodes is regarded as the robustness of the proposed scheme, while manage to localize even at wrong estimation of distance is regarded as the efficiency of the proposed scheme. In WC and APIT schemes, the localization accuracy is directly proportional to the density of anchor nodes. The wrong estimation of distance weight and less number of neighbouring anchor nodes leads the WC scheme to show high localization error. Besides, the APIT scheme with less number of anchor nodes fails to minimize the triangular intersection area, where the sensor node actually lies. Hence, the proposed LSURE is better than the WC and APIT schemes.

6.7 Summary

In this chapter, we have performed couple of experiments to demonstrate the impact of radio propagation irregularity. The proposed LSURE is based on dynamic circle expansion technique, where radio propagation irregularity is modelled using the erroneous estimated distances. For validation of the proposed LSURE, we have designed a prototype experimental platform for real indoor environment. In the experiment, we have used different types of nodes with independent functionality such as sensor node, anchor node, and gateway node. The prime objective of this experiment is two demonstrate the applicability of the proposed LSURE in real indoor environment. We have also compared the proposed LSURE with other state of art localization schemes such as APIT and WC. From the experimental results, it is observed that proposed LSURE provides a better localization accuracy even in worst scenarios of radio unpredictability.

Chapter 7
Conclusion and Future Work

7.1 Conclusion

The work in this thesis is based on analytical geometric, where an arc is used as a primitive geometric shape. To provide a simple, inexpensive, and energy efficient localization, we have proposed four distributed range free localization schemes namely MBBRFLS, MBBRFLS-OBPS, MBBRFLS-ORAF, and LSURE. The performance of the proposed schemes are evaluated using the simulation as well as experimental testbed. From the results, it is observed that the proposed schemes provides better localization accuracy even in the real environment.

First, we have proposed a MBBRFLS using an analytical geometry of an arc. The proposed scheme localizes the sensors using the geometric conjecture (perpendicular bisector of the chord). In this scheme, the localization begins with approximation of the arc parameters. Later, the approximated parameters are used to generate the chords. The perpendicular bisector of the chords generate the candidate positions of the sensor node. To identify the valid candidate position, the sensor node use the logarithmic path loss model. The performance of proposed scheme compared with Ssu and Galstyan schemes using various metrics such as communication range, beacon broadcasting interval, and DOI. From the results, it is observed that the proposed scheme at varying DOI shows 20.7% and 11.6% lesser localization error than Ssu and Galstyan schemes respectively. Similarly, at the varying beacon broadcasting interval the proposed scheme shows 18.8% and 8.3% lesser localization error than Ssu and Galstyan schemes respectively. Besides, at the varying communication range the proposed scheme shows 18% and 9.2% lesser localization error than Ssu and Galstyan schemes respectively.

To further improves the localization accuracy, we have proposed an another MBBRFLS using an optimized beacon points selection (OBPS). In this scheme, the constraint area corresponding to the optimized beacon points is used to differentiate the valid candidate position of the sensor node. For localization, the proposed MBBRFLS-OBPS use the perpendicular bisector of the chords and approximated radius. The proposed scheme reduces the complex geometric calculation by only considering the sagitta of minor arc for generating the chord. The performance of the proposed MBBRFLS-OBPS is compared with Ssu,

Galstyan and Singh schemes using the various trajectories of the mobile beacon. From the results, it is observed that the proposed scheme using CICRLE, SPIRAL, HILBERT, and S-CURVE trajectories shows 74.68%, 78.3%, 73.9%, and 70.3% less localization error than Ssu, Galstyan, and Singh schemes respectively.

Next, we have proposed a MBBRFLS using an optimized residence area formation (ORAF). In this scheme, we have used the adaptive mechanism for the different size of the constraint area. The adaptive mechanism is used to improve the approximation accuracy of the arc parameters for the specific size of the constraint area. The improved approximation accuracy along with minimized residence of three non-collinear beacon points further improves the localization accuracy of the proposed MBBRFLS-ORAF. For performance evaluation, we have used the simulation and experimental testbed. The performance of the proposed scheme is compared with Ssu, Lee, Xiao, and Singh schemes using communication range, beacon broadcasting interval, and DOI. From the results, it is observed that the proposed MBBRFLS-ORAF at varying communication range shows 73.2%, 48.7%, 33.2%, and 20.7% less localization error than Ssu, Lee, Xiao, and Singh schemes respectively. Similarly, at the varying beacon broadcasting intervals the proposed MBBRFLS-ORAF shows 75%, 53%, 38%, and 25% less localization error than Ssu, Lee, Xiao, and Singh schemes respectively. Besides, at the varying DOI the proposed MBBRFLS-ORAF shows 76.3%, 56.8%, 52%, and 35% less localization error than Ssu, Lee, Xiao, and Singh schemes respectively.

Finally, we have proposed a localization scheme for unpredictable radio environment (LSURE). In this scheme, we have used a dynamic circle expansion technique to create the constraint area. The performance of the proposed LSURE is evaluated using the experimental test bench, where three anchor nodes and a static sensor node is used. The various scenarios of radio propagation irregularity is modeled using the erroneous estimated distance, and the various deployment scenarios of anchor nodes. The impact of radio propagation irregularity is represented on the constraint area of the sensor node. In this scheme, the constraint area is created using the communication of the anchor nodes, which is derived using the logarithmic regression model of RSSI-distance relationship. The performance of the proposed LSURE is compared with APIT and Weighted Centroid schemes using the various deployment scenarios of the anchor nodes. From the results, it is observed that the proposed LSURE at various deployment scenarios shows 65.94% and 73.54% less localization error than APIT and Weighted Centroid schemes.

7.2 Future Scope

The future scope of the research is as follows:

- **Energy Efficient Localization** The most of the existing schemes are only focus on optimization of localization accuracy. A few work have done to improve the network

lifetime using localization. Therefore, the energy management is another interesting field for research.

- **Improve Ranging** The ranging technique is crucial for accurate localization of WSNs. Hence, there is a research scope to enhance the ranging techniques either using special antennas or by understanding the behaviour of signal propagation.
- **Radio Propagation Irregularity** The irregular radio propagation has a significant impact on localization accuracy of WSNs. A few work have done to improve the ranging techniques by understand the behaviour of radio propagation irregularity and its possible impacts.
- **Localization in 3-D** 3-D localization is an another exciting area for research in future. It has various applications in WSNs.
- **Real IoT Applications** Finally, we will implement the localization scheme to prevent the human life and improves the productivity in an unpredictable mining environment.

References

[1] I. F. Akyildiz, W. Su, Y. Sankarasubramaniam, and E. Cayirci, ‘‘Wireless sensor networks: a survey,’’ *Computer networks*, vol. 38, no. 4, pp. 393–422, 2002.

[2] J. Yick, B. Mukherjee, and D. Ghosal, ‘‘Wireless sensor network survey,’’ *Computer networks*, vol. 52, no. 12, pp. 2292–2330, 2008.

[3] J. A. Stankovic, ‘‘Research challenges for wireless sensor networks,’’ *ACM SIGBED Review*, vol. 1, no. 2, pp. 9–12, 2004.

[4] G. Mao, B. Fidan, and B. D. Anderson, ‘‘Wireless sensor network localization techniques,’’ *Computer networks*, vol. 51, no. 10, pp. 2529–2553, 2007.

[5] S. M. George, W. Zhou, H. Chenji, M. Won, Y. O. Lee, A. Pazarloglou, R. Stoleru, and P. Barooah, ‘‘Distressnet: a wireless ad hoc and sensor network architecture for situation management in disaster response,’’ *Communications Magazine, IEEE*, vol. 48, no. 3, pp. 128–136, 2010.

[6] D. Chen, Z. Liu, L. Wang, M. Dou, J. Chen, and H. Li, ‘‘Natural disaster monitoring with wireless sensor networks: a case study of data-intensive applications upon low-cost scalable systems,’’ *Mobile Networks and Applications*, vol. 18, no. 5, pp. 651–663, 2013.

[7] J. Aspnes, T. Eren, D. K. Goldenberg, A. S. Morse, W. Whiteley, Y. R. Yang, B. Anderson, and P. N. Belhumeur, ‘‘A theory of network localization,’’ *Mobile Computing, IEEE Transactions on*, vol. 5, no. 12, pp. 1663–1678, 2006.

[8] Y. Liu, Z. Yang, X. Wang, and L. Jian, ‘‘Location, localization, and localizability,’’ *Journal of Computer Science and Technology*, vol. 25, no. 2, pp. 274–297, 2010.

[9] W. Zhang and G. Cao, ‘‘Dctc: dynamic convoy tree-based collaboration for target tracking in sensor networks,’’ *Wireless Communications, IEEE Transactions on*, vol. 3, no. 5, pp. 1689–1701, 2004.

[10] L. Zhang, Q. Cheng, Y. Wang, and S. Zeadally, ‘‘A novel distributed sensor positioning system using the dual of target tracking,’’ *Computers, IEEE Transactions on*, vol. 57, no. 2, pp. 246–260, 2008.

[11] M. Hauswirth and L. Shu, ‘‘Geographic routing in wireless multimedia sensor networks,’’ 2008.

[12] F. Kuhn, R. Wattenhofer, Y. Zhang, and A. Zollinger, ‘‘Geometric ad-hoc routing: of theory and practice,’’ in *Proceedings of the twenty-second annual symposium on Principles of distributed computing*. ACM, pp. 63–72, 2003.

[13] G. Tan, M. Bertier, and A.-M. Kermarrec, ‘‘Visibility-graph-based shortest-path geographic routing in sensor networks,’’ in *INFOCOM 2009, IEEE*. IEEE, pp. 1719–1727, 2009.

[14] L. Hu and D. Evans, ‘‘Localization for mobile sensor networks,’’ in *Proceedings of the 10th annual international conference on Mobile computing and networking*. ACM, pp. 45–57, 2004.

[15] I. Amundson and X. D. Koutsoukos, ‘‘A survey on localization for mobile wireless sensor networks,’’ in *Mobile entity localization and tracking in GPS-less environnments*. Springer, pp. 235–254 , 2009.

[16] F. Hu and X. Cao, *Wireless sensor networks: principles and practice*. CRC Press, 2010.

[17] M. A. Perillo and W. B. Heinzelman, ‘‘Wireless sensor network protocols,’’ *Algorithms and Protocols for Wireless and Mobile Networks, Eds. A. Boukerche et al., CRC Hall Publishers*, 2004.

[18] S. Han, S. Lee, S. Lee, J. Park, and S. Park, ‘‘Node distribution-based localization for large-scale wireless sensor networks,’’ *Wireless Networks*, vol. 16, no. 5, pp. 1389–1406, 2010.

[19] N. Patwari, A. O. Hero III, M. Perkins, N. S. Correal, and R. J. O’dea, ‘‘Relative location estimation in wireless sensor networks,’’ *Signal Processing, IEEE Transactions on*, vol. 51, no. 8, pp. 2137–2148, 2003.

[20] N. Bulusu, J. Heidemann, and D. Estrin, ‘‘Gps-less low-cost outdoor localization for very small devices,’’ *Personal Communications, IEEE*, vol. 7, no. 5, pp. 28–34, 2000.

[21] M. Singh and P. M. Khilar, ‘‘An analytical geometric range free localization scheme based on mobile beacon points in wireless sensor network,’’ *Wireless Networks*, pp. 1–14, 2016.

[22] H. Chen, Q. Shi, R. Tan, H. V. Poor, and K. Sezaki, ‘‘Mobile element assisted cooperative localization for wireless sensor networks with obstacles,’’ *Wireless Communications, IEEE Transactions on*, vol. 9, no. 3, pp. 956–963, 2010.

[23] A. Galstyan, B. Krishnamachari, K. Lerman, and S. Pattem, ‘‘Distributed online localization in sensor networks using a moving target,’’ in *Information Processing in Sensor Networks, 2004. IPSN 2004. Third International Symposium on*. IEEE, pp. 61–70, 2004.

[24] A. Baggio and K. Langendoen, ‘‘Monte carlo localization for mobile wireless sensor networks,’’ *Ad Hoc Networks*, vol. 6, no. 5, pp. 718–733, 2008.

[25] T. He, C. Huang, B. M. Blum, J. A. Stankovic, and T. Abdelzaher, ‘‘Range-free localization schemes for large scale sensor networks,’’ in *Proceedings of the 9th annual international conference on Mobile computing and networking*. ACM, pp. 81–95, 2003.

[26] L. Doherty, K. S. Pister, and L. El Ghaoui, ‘‘Convex position estimation in wireless sensor networks,’’ in *INFOCOM 2001. Twentieth Annual Joint Conference of the IEEE Computer and Communications Societies. Proceedings. IEEE*, vol. 3. IEEE, pp. 1655–1663, 2001.

[27] V. Vivekanandan and V. W. Wong, ‘‘Concentric anchor beacon localization algorithm for wireless sensor networks,’’ *Vehicular Technology, IEEE Transactions on*, vol. 56, no. 5, pp. 2733–2744, 2007.

[28] C. Liu, T. Scott, K. Wu, and D. Hoffman, ‘‘Range-free sensor localisation with ring overlapping based on comparison of received signal strength indicator,’’ *International Journal of Sensor Networks*, vol. 2, no. 5-6, pp. 399–413, 2007.

[29] M. L. Sichitiu, V. Ramadurai, and P. Peddabachagari, ‘‘Simple algorithm for outdoor localization of wireless sensor networks with inaccurate range measurements.’’ in *International Conference on Wireless Networks*, vol. 2003, 2003.

[30] C. Liu, K. Wu, and T. He, ‘‘Sensor localization with ring overlapping based on comparison of received signal strength indicator,’’ in *Mobile Ad-hoc and Sensor Systems, 2004 IEEE International Conference on*. IEEE, pp. 516–518, 2004.

[31] C. Liu and K. Wu, ‘‘Performance evaluation of range-free localization methods for wireless sensor networks,’’ in *Performance, Computing, and Communications Conference, 2005. IPCCC 2005. 24th IEEE International*. IEEE, pp. 59–66, 2005.

[32] J.-P. Sheu, P.-C. Chen, and C.-S. Hsu, ‘‘A distributed localization scheme for wireless sensor networks with improved grid-scan and vector-based refinement,’’ *Mobile Computing, IEEE Transactions on*, vol. 7, no. 9, pp. 1110–1123, 2008.

[33] T. Kim, M. Shon, W. Choi, M. Song, and H. Choo, ‘‘Low-cost two-hop anchor node-based distributed range-free localization in wireless sensor networks,’’ in *Computational Science and Its Applications–ICCSA 2010*. Springer, pp. 129–141, 2010.

[34] P. Bahl and V. N. Padmanabhan, ''Radar: An in-building rf-based user location and tracking system,'' in *INFOCOM 2000. Nineteenth Annual Joint Conference of the IEEE Computer and Communications Societies. Proceedings. IEEE*, vol. 2, IEEE, pp. 775–784, 2000.

[35] R. C. Luo, O. Chen, and S. H. Pan, ''Mobile user localization in wireless sensor network using grey prediction method,'' in *Industrial Electronics Society, 2005. IECON 2005. 31st Annual Conference of IEEE*. IEEE, pp. 6–pp, 2005.

[36] M. Stella, M. Russo, and D. Begusic, ''Location determination in indoor environment based on rss fingerprinting and artificial neural network,'' in *Telecommunications, 2007. ConTel 2007. 9th International Conference on*. IEEE, pp. 301–306, 2007.

[37] M. Gholami, N. Cai, and R. Brennan, ''An artificial neural network approach to the problem of wireless sensors network localization,'' *Robotics and Computer-Integrated Manufacturing*, vol. 29, no. 1, pp. 96–109, 2013.

[38] K.-F. Ssu, C.-H. Ou, and H. C. Jiau, ''Localization with mobile anchor points in wireless sensor networks,'' *Vehicular Technology, IEEE Transactions on*, vol. 54, no. 3, pp. 1187–1197, 2005.

[39] S. Lee, E. Kim, C. Kim, and K. Kim, ''Localization with a mobile beacon based on geometric constraints in wireless sensor networks,'' *Wireless Communications, IEEE Transactions on*, vol. 8, no. 12, pp. 5801–5805, 2009.

[40] A. Galstyan, B. Krishnamachari, K. Lerman, and S. Pattem, ''Distributed online localization in sensor networks using a moving target,'' in *Information Processing in Sensor Networks, 2004. IPSN 2004. Third International Symposium on*. IEEE, pp. 61–70, 2004.

[41] B. Xiao, H. Chen, and S. Zhou, ''Distributed localization using a moving beacon in wireless sensor networks,'' *Parallel and Distributed Systems, IEEE Transactions on*, vol. 19, no. 5, pp. 587–600, 2008.

[42] E. Guerrero, H. Xiong, Q. Gao, G. Cova, R. Ricardo, and J. Estévez, ''Adal: a distributed range-free localization algorithm based on a mobile beacon for wireless sensor networks,'' in *Ultra Modern Telecommunications & Workshops, 2009. ICUMT'09. International Conference on*. IEEE, pp. 1–7, 2009.

[43] L. Dong and F. L. Severance, ''Position estimation with moving beacons in wireless sensor networks,'' in *Wireless Communications and Networking Conference, 2007. WCNC 2007. IEEE*. IEEE, pp. 2317–2321, 2007.

[44] M. Singh and P. M. Khilar, ''Mobile beacon based range free localization method for wireless sensor networks,'' *Wireless Networks*, pp. 1–16, 2015.

[45] L. Oliveira, H. Li, L. Almeida, and T. E. Abrudan, ''Rssi-based relative localisation for mobile robots,'' *Ad Hoc Networks*, vol. 13, pp. 321–335, 2014.

[46] A. Uchiyama, S. Fujii, K. Maeda, T. Umedu, H. Yamaguchi, and T. Higashino, ''Ad-hoc localization in urban district,'' in *INFOCOM 2007. 26th IEEE International Conference on Computer Communications. IEEE*. IEEE, pp. 2306–2310, 2007.

[47] F. Mourad, H. Snoussi, F. Abdallah, and C. Richard, ''Anchor-based localization via interval analysis for mobile ad-hoc sensor networks,'' *Signal Processing, IEEE Transactions on*, vol. 57, no. 8, pp. 3226–3239, 2009.

[48] C. Di Franco, G. Franchino, and M. Marinoni, ''Data fusion for relative localization of wireless mobile nodes,'' in *Industrial Embedded Systems (SIES), 2014 9th IEEE International Symposium on*. IEEE, pp. 58–65, 2014.

[49] H. Chenji and R. Stoleru, ''Mobile sensor network localization in harsh environments,'' in *Distributed Computing in Sensor Systems*. Springer, pp. 244–257, 2010.

[50] S. K. Das, J. Wang, R. K. Ghosh, and R. Reiger, ''Algorithmic aspects of sensor localization,'' in *Theoretical aspects of distributed computing in sensor networks*. Springer, pp. 257–291, 2011.

[51] H. Chen, B. Liu, P. Huang, J. Liang, and Y. Gu, ''Mobility-assisted node localization based on toa measurements without time synchronization in wireless sensor networks,'' *Mobile Networks and Applications*, vol. 17, no. 1, pp. 90–99, 2012.

[52] M. Kushwaha, K. Molnár, J. Sallai, P. Völgyesi, M. Maróti, and A. Lédeczi, ''Sensor node localization using mobile acoustic beacons,'' in *Mobile Adhoc and Sensor Systems Conference, 2005. IEEE International Conference on*. IEEE, pp. 9–pp, 2005.

[53] C.-Y. Wen and F.-K. Chan, ''Adaptive aoa-aided toa self-positioning for mobile wireless sensor networks,'' *Sensors*, vol. 10, no. 11, pp. 9742–9770, 2010.

[54] F.-K. Chan and C.-Y. Wen, ''Aoa-aided toa distributed positioning for mobile wireless sensor networks,'' in *Industrial Electronics and Applications (ICIEA), 2010 the 5th IEEE Conference on*. IEEE, pp. 1774–1779, 2010.

[55] N. B. Priyantha, A. Chakraborty, and H. Balakrishnan, ''The cricket location-support system,'' in *Proceedings of the 6th annual international conference on Mobile computing and networking*. ACM, pp. 32–43, 2000.

[56] N. B. Priyantha, H. Balakrishnan, E. D. Demaine, and S. Teller, ''Mobile-assisted localization in wireless sensor networks,'' in *INFOCOM 2005. 24th Annual Joint Conference of the IEEE Computer and Communications Societies. Proceedings IEEE*, vol. 1. IEEE, pp. 172–183, 2005.

[57] Z. Guo, Y. Guo, F. Hong, Z. Jin, Y. He, Y. Feng, and Y. Liu, ''Perpendicular intersection: locating wireless sensors with mobile beacon,'' *Vehicular Technology, IEEE Transactions on*, vol. 59, no. 7, pp. 3501–3509, 2010.

[58] P. N. Pathirana, N. Bulusu, A. V. Savkin, and S. Jha, ''Node localization using mobile robots in delay-tolerant sensor networks,'' *Mobile Computing, IEEE Transactions on*, vol. 4, no. 3, pp. 285–296, 2005.

[59] J. Graefenstein, A. Albert, P. Biber, and A. Schilling, ''Wireless node localization based on rssi using a rotating antenna on a mobile robot,'' in *Positioning, Navigation and Communication, 2009. WPNC 2009. 6th Workshop on*. IEEE, pp. 253–259, 2009.

[60] R. Sumathi and R. Srinivasan, ''Rss-based location estimation in mobility assisted wireless sensor networks,'' in *Intelligent Data Acquisition and Advanced Computing Systems (IDAACS), 2011 IEEE 6th International Conference on*, vol. 2. IEEE, pp. 848–852, 2011.

[61] K. Kim and W. Lee, ''Mbal: A mobile beacon-assisted localization scheme for wireless sensor networks,'' in *Computer Communications and Networks, 2007. ICCCN 2007. Proceedings of 16th International Conference on*. IEEE, pp. 57–62, 2007.

[62] G. Yu, F. Yu, and L. Feng, ''A localization algorithm using a mobile anchor node under wireless channel,'' in *Robotics and Biomimetics, 2007. ROBIO 2007. IEEE International Conference on*. IEEE, pp. 1104–1108, 2007.

[63] Z. Guo, Y. Guo, F. Hong, Z. Jin, Y. He, Y. Feng, and Y. Liu, ''Perpendicular intersection: locating wireless sensors with mobile beacon,'' *IEEE Transactions on Vehicular Technology*, vol. 59, no. 7, pp. 3501–3509, 2010.

[64] C. Wang, K. Liu, and N. Xiao, ''A range free localization algorithm based on restricted-area for wireless sensor networks,'' in *Computing in the Global Information Technology, 2008. ICCGI'08. The Third International Multi-Conference on*. IEEE, pp. 97–101, 2008.

[65] Y.-L. Shen, Y. Zhang, Y.-P. Hu, and J. Zhang, ''A single chord localization algorithm for wireless sensor networks,'' *International Journal of Grid and Distributed Computing*, vol. 8, no. 1, pp. 1–10, 2015.

[66] J. Rezazadeh, M. Moradi, A. S. Ismail, and E. Dutkiewicz, ''Impact of static trajectories on localization in wireless sensor networks,'' *Wireless Networks*, vol. 21, no. 3, pp. 809–827, 2015.

[67] D. Koutsonikolas, S. M. Das, and Y. C. Hu, ‘‘Path planning of mobile landmarks for localization in wireless sensor networks,’’ *Computer Communications*, vol. 30, no. 13, pp. 2577–2592, 2007.

[68] R. Huang and G. V. Zaruba, ‘‘Static path planning for mobile beacons to localize sensor networks,’’ in *Pervasive Computing and Communications Workshops, 2007. PerCom Workshops' 07. Fifth Annual IEEE International Conference on*. IEEE, pp. 323–330, 2007.

[69] G. Han, H. Xu, J. Jiang, L. Shu, T. Hara, and S. Nishio, ‘‘Path planning using a mobile anchor node based on trilateration in wireless sensor networks,’’ *Wireless Communications and Mobile Computing*, vol. 13, no. 14, pp. 1324–1336, 2013.

[70] Z. Hu, D. Gu, Z. Song, and H. Li, ‘‘Localization in wireless sensor networks using a mobile anchor node,’’ in *Advanced Intelligent Mechatronics, 2008. AIM 2008. IEEE/ASME International Conference on*. IEEE, pp. 602–607, 2008.

[71] T. Camp, J. Boleng, and V. Daves, ‘‘A survey of mobility models for ad hoc network research,’’ *Wireless communications and mobile computing*, vol. 2, no. 5, pp. 483–502, 2002.

[72] Z. L. ZHONG, D.-Y. L. S.-Q. FAN, and X.-P. Q. Zhi-Hua11, ‘‘School of information science and engineering, central south university, changsha 410083, pr china; an adaptive localization approach for wireless sensor networks based on gauss-markov mobility model [j],’’ *Acta Automatica Sinica*, vol. 11, 2010.

[73] H. R. Jacobs, *Geometry*. San Francisco, CA: Freeman, 1987.

[74] C. Bo, D. Ren, S. Tang, X.-Y. Li, X. Mao, Q. Huang, L. Mo, Z. Jiang, Y. Sun, and Y. Liu, ‘‘Locating sensors in the forest: A case study in greenorbs,’’ in *INFOCOM, 2012 Proceedings IEEE*. IEEE, pp. 1026–1034, 2012.

[75] MRF24J40. Datasheet: ww1.microchip.com/downloads/en/devicedoc/39776a.pdf. [Online]. Available: ww1.microchip.com/downloads/en/DeviceDoc/39776a.pdf

[76] J. Blumenthal, R. Grossmann, F. Golatowski, and D. Timmermann, ‘‘Weighted centroid localization in zigbee-based sensor networks,’’ in *Intelligent Signal Processing, 2007. WISP 2007. IEEE International Symposium on*. IEEE, pp. 1–6, 2007.

Dissemination

Internationally indexed journals [1]

1. **Munesh Singh**, P. M. Khilar, ”An analytical geometric range free localization scheme based on mobile beacon points in Wireless Sensor Network,” **Published**: *Wireless Networks, Springer,1-14, 2015*

2. **Munesh Singh**, P. M. Khilar, ”Mobile beacon based range free localization method for wireless sensor networks,” **Published**: *Wireless Networks, Springer,1-16, 2016*

3. S. K. Bhoi, P. M. Khilar, **Munesh Singh** ”A path selection based routing protocol for urban vehicular ad hoc network (UVAN) environment,” **Published**: *Wireless Networks, Springer,1-12, 2015*

4. **Munesh Singh**, P.M Khillar. (2015). A Range Free Geometric Technique for Localization of Wireless Sensor Network (WSN) based on Controlled Communication Range. **Published**: *Wireless Personal Communications, Springer Publisher*, 2016.

5. **Munesh Singh.**, S.K Bhoi., P.M Khilar (2016). Omnidirectional Radio Propagation Antenna Using Organized Grouping of Monopole Antennas. *National Academy Science Letters, Springer*, 2016. **Accepted**

6. **Munesh Singh.**, S.K Bhoi., P.M Khilar., ‘Geometric Constraint Based Range Free Localization Scheme for Wireless Sensor Networks’, **IEEE Sensors**, 2017, **Minor Revision Submitted**

Conference accepted [2]

1. **Singh, M.**, Bhoi, S. K., & Khilar, P. M. (2016). Short Range Frequency Modulated Continuous Wave (FMCW) Radar Using Universal Software Defined Radio Peripheral (USRP). *Advances in Intelligent Systems and Computing, Springer*, NIT, Rourkela, India, Sep. 22-24, 2016.

2. Bhoi, S. K., **Singh, M.**, & Khilar, P. M. (2016). A Theoretical Model for Vehicular Communication System to Predict Link Failure Using Link Existence Diagram.

[1] Articles already published, in press, or formally accepted for publication.
[2] Accepted.

Advances in Intelligent Systems and Computing, Springer, NIT, Rourkela, India, Sep. 22-24, 2016.

Article under preparation [3]

1. **Singh, M.**, Bhoi, S. K., & Khilar, P. M. (2016). Localization Scheme For Wireless sensor Networks (WSNs) in Unpredictable Radio Propagation Environment. *IJCS Wileyl*, 2016.

2. **Singh, M.**, Bhoi, S. K., & Khilar, P. M. (2016). Geometric Constraint Based Range Free Localization Scheme for Wireless Sensor Networks. *IEEE Sensor Journal*, 2016.

3. Bhoi, S. K., **Singh, M.**, & Khilar, P. M. (2016). A Routing Protocol for Urban Vehicular Networks to Support Sellers and Buyers On Wheels. *IEEE Transactions on Intelligent Transportation Systems, IEEE*, 2016.

4. Bhoi, S. K., **Singh, M.**, & Khilar, P. M. (2016). High CO_2 Zone Localization in a City Area Using an Efficient Urban VANET Routing Protocol: An Experimental Approach. *IEEE Region 10 Symposium*, 2017.

5. Bhoi, S. K., **Singh, M.**, & Khilar, P. M. (2016). Gaming in Parking Lots: A New Application Using Urban Vehicular Ad Hoc Network *IJCS, Wiley*, 2016.

6. Bhoi, S. K., **Singh, M.**, & Khilar, P. M. (2017), & Rashmi Ranjan Sahoo & Rakesh Ranjan Swain. A Routing Scheme for Urban Vehicular Communication System Using Local Traffic Information *Arabian Journal for Science and Engineering*, 2017

[3] Articles under review, communicated, or to be communicated.